Optimized Perturbation Theory at Finite Temperature

Suenori CHIKU

A dissertation submitted to the Doctoral Program
in Physics, the University of Tsukuba
in partial fulfillment of the requirements for the
degree of Doctor of Philosophy (Physics)

January, 2000

Abstract

The naive perturbation theory is known to break down at high temperature (T). This is because higher order terms are enhanced by the powers of T and eventually exceed the lower order terms even if the expansion parameter in the perturbation is small. These large terms at high T are called the hard thermal loops (HTLs). Therefore, we need to resum HTLs to obtain sensible results at high T.

So far, several methods have been proposed to carry out this resummation. As one of the promising candidates, self-consistent resummation method has been studied for a long time. However, it was found that the method has difficulties in the renormalization at finite T and in the proof of the Nambu-Goldstone theorem at finite T.

In this thesis, we develop an optimized perturbation theory (OPT) at finite temperature in the $O(N)$ ϕ^4 theory, which can resum higher order terms at finite T without the problems mentioned above. It has the following features:

1. Hard thermal loops are correctly resummed at high T.

2. The renormalization of the ultra-violet divergences can be carried out systematically in any given order of OPT.

3. The Nambu-Goldstone theorem is fulfilled for arbitrary N and the any given order of OPT.

After presenting the general features of OPT, we first apply OPT to $\lambda\phi^4$ theory to check whether it can describe the correct qualitative features of the phase transition. In the leading order analyses in the self-consistent methods proposed so far, it is known that the phase transition becomes first order, which has apparent contradiction to the second order transition predicted in the renormalization group and the lattice QCD analyses. This situation is similar in OPT in the leading order. However, in the next-to-leading order analyses in OPT, we found that correct second order behavior is obtained although the critical exponent β stays in the mean-field value.

As an phenomenological application of OPT to physical system, we study the $O(4)$ linear σ model. This model, which is described by π and σ meson fields, can be regarded as a low energy effective theory of QCD with two flavors. The π fields are regarded as Nambe-Goldstone modes associated with the chiral symmetry breaking in QCD. The σ meson (chiral partner of the pion) is recently appeared in the Particle Data Table with a mass 400-1200 MeV and a width 300-500 MeV. Our main purpose is to study spectral functions of the soft modes at finite T by taking into account the mode couplings between σ and π.

Thanks to OPT, the physical threshold of the spectrum in the σ channel, which is determined by the tree level pion mass, is obtained in the one-loop approximation. The threshold enhancement of the spectral function at finite T in the σ channel is shown to be a typical signal of the partial restoration of the chiral symmetry. To study the detectability of the threshold enhancement, the diphoton decay $\sigma \to 2\gamma$ from the hot plasma is examined. In a relatively narrow window of T and the invariant mass of the diphoton, the enhancement is shown to appear over the thermal background $\pi^+\pi^- \to 2\gamma$.

Contents

Chapter 1

Introduction

1.1 Quantum Chromodynamics at finite temperature

It is widely accepted that Quantum Chromodynamics (QCD) [1] describes the dynamics of quarks and gluons. At high energies, the interactions among the quarks and gluons become weak, which is known as the asymptotic freedom [2]. This is the reason why the perturbation theory works well at high energy, which has been tested experimentally in the deep inelastic scatting and the e^+e^--annihilations. According to the asymptotic freedom, it is expected that there exists a phase at high energy density in which quarks and gluons behave as free particles. This phase is called the quark-gluon plasma (QGP) [3].

At low energies, however, quarks and gluons form baryons and mesons as the interactions become strong. Namely the confined phase is realized. This implies that there will be a confinement-deconfinement phase transition as temperature (T) or the energy density raises. The phase diagram expected at finite temperature and/or density is shown in Fig.1.1 [4].

Besides the deconfinement at high T, it is also believed that the chiral symmetry in QCD is recovered at high T. This symmetry corresponds to the invariance under the transformation

$$q_i \to q_i + i\alpha^a \frac{\lambda^a_{ij}}{2} q_j, \quad q_i \to q_i + i\beta^a \frac{\lambda^a_{ij}}{2} \gamma_5 q_j, \quad (\alpha^a, \beta^a \ll 1) \tag{1.1}$$

where q_i is quark fields and λ^a is the $N_f^2 - 1$ Gell-Mann matrices for $SU(N_f)$-flavors. This symmetry is broken spontaneously in the vacuum where we live in, and it explains why the pion is much lighter than other mesons. The results of the numerical simulations on the lattice at finite T [5] shows that chiral symmetry restoration takes place at almost the same temperature with the deconfinement temperature.

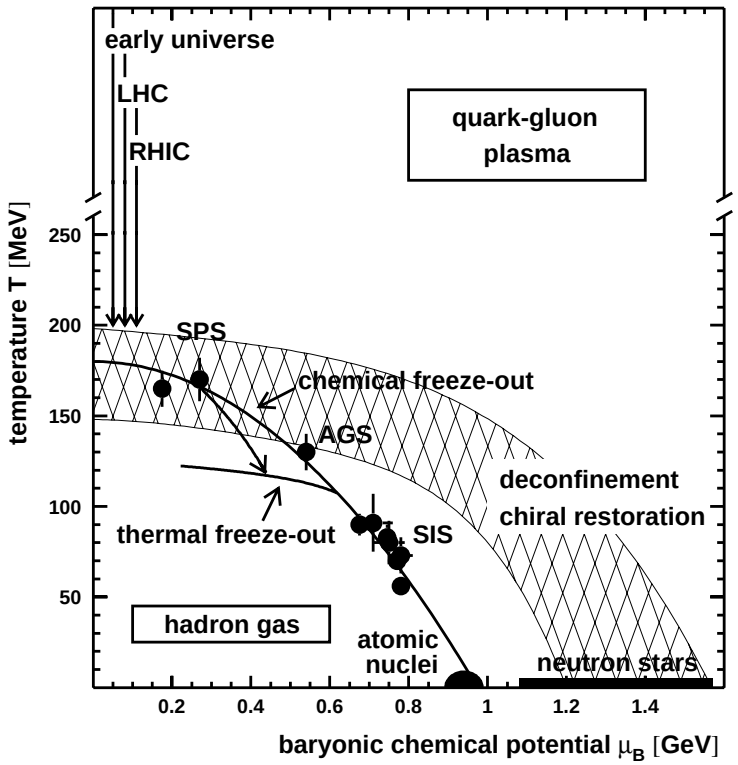

Figure 1.1: Typical phase diagram for QGP and hadron. Figure from [4].

According to the big bang theory [6], the early universe was a very hot and high density state. The present universe is realized as a result of cooling and expansion of this hot and high density state. The thermal equilibrium has been achieved at least after the era of the electroweak phase transition, because the reaction rates of particles became much larger than the expansion rate after that time. The universe had experienced various phases during the process of the expansion. It is believed that the quark-gluon plasma (QGP) phase in which deconfinement and the chiral symmetry restoration occur has also been realized as one of the phases in the early universe. Therefore, understanding QCD at finite T is essential for studying such phase in the early universe.

Experiments for aiming at reproducing the QGP phase in the laboratory is planned at Brookhaven National Laboratory (Relativistic Heavy Ion Collider (RHIC)) and at European Laboratory for Particle Physics (Large Hadron Collider (LHC)) [3]. The regions which these experiments (RHIC and LHC) cover are also shown in Fig.1.1. QGP, which is a deconfined phase in early universe, is going to be studied experimentally.

Also, if the chiral symmetry restoration is of second order (continuous) or weakly first order, long range fluctuations of the order parameter exist. This is known as soft modes, and it has been studied as a probe of second order phase transitions in

the condensed matter physics [7]. Whether this mode is observed in QCD or not is an interesting question.

Thus, to understand QCD at such high temperature is one of the most interesting subjects in hadron physics.

1.2 Theoretical tools in QCD at finite T

At present, there are two major calculational methods in QCD at finite T:

- Numerical simulation in lattice QCD [5].
- Hard thermal loops resummation scheme (HTLRS) [8].

Numerical simulation in lattice QCD

The Numerical simulation in lattice QCD is the most rigorous method to study QCD at finite temperature. The simulations show that the restoration of chiral symmetry takes place at $T_c \sim 150$ MeV. In the case of massless two flavors, the phase transition has been shown to be of second order. The detailed analysis in two light flavors and one medium-heavy quark, which corresponds to the real world, is still under way [9].

At present, there are several problems in lattice QCD. Among others, there are two difficulties which are related to this thesis:

1. The $SU(N) \times SU(N)$ chiral symmetry cannot be defined on the lattice in four-dimension.
2. It is rather difficult to treat real-time modes in a straight forward way.

From the reason 1, the pion, which is the Nambe-Goldstone boson, obtains a finite mass in lattice QCD [10]. The second problem is related to Euclidean space-time. Since lattice QCD is defined in Euclidean space-time, one must translate Green's functions from imaginary-time to real-time by analytic continuation to study real-time modes. Although this analytic continuation requires information of infinite number of points, the numerical simulations produce only finite number of data points [11].

Hard thermal loops resummation scheme

Hard thermal loops resummation scheme (HTLRS) [8] has been known as a method for resumming higher order terms of the QCD perturbation at finite T. Generally, it is known that the naive perturbation theory break down at the high temperature

[12, 13], even if the coupling constant is small. Since number of excited particles increases as T increases, particles properties are effectively modified at high T. One of such phenomena is the Debye screening. In the naive perturbation theory, such effect appears in a manner that higher order terms have larger contributions than lower order terms. This large contributions are called hard thermal loops (HTLs). HTLRS resums the higher order terms at high temperature up to $O(gT)$, where g is the coupling constant in QCD, when the external momenta are "soft". The "soft" means that the scale is of $O(gT)$. By this method, soft gluon damping rate, dilepton production rate and so on were calculated in the QGP phase [14] .

However, several difficulties appear in HTLRS.

- It is difficult, in practice, to calculate the next-to-leading order term, namely $O(g^2T)$ contributions. No one has tried the calculation.
- Since it is an effective resummation which works only at high temperature, it cannot be applied to the system at low temperature.
- When one studies theories with spontaneously symmetry breaking (SSB), loop-expansion is relevant. However, HTLRS is the weak coupling expansion.

Thus, lattice QCD and HTLRS have some limitations. Apart from these methods, effective theories have been studied so far instead of QCD at finite T [15]. We will explain this approach in the following section.

1.3 Difficulties in self-consistent methods at finite T

It is difficult to treat non-perturbative QCD effects at low energies by analytic methods. Therefore, use of the effective models sometimes helps to understand essential physics at low energies (see the reviews [16, 17] and reference cited therein). The linear and non-linear σ models, and the Nambu-Jona-Lasinio model are the typical examples of such effective theories in QCD. However, a serious problem of tachyonic pole may appear [12], when one studies the restoration of symmetries using effective models such as the linear σ-model. This problem shows up even below T_c, and it causes the breakdown of the thermal perturbation theory. Therefore, a resummation method applicable for wide range of temperature from low T to high T is required when effective models are used at finite T

So far, several methods have been proposed for this resummation [15], and the self-consistent method among others is considered to be a promising one. However, there are two major problems in such method [18].

- T-dependent ultraviolet divergences appear, and the renormalization becomes non-trivial at finite T.
- The Nambe-Goldstone (NG) theorem at finite T is not trivially satisfied when spontaneously symmetry breaking (SSB) occurs.

In finite temperature field theories, T-dependent divergences should not appear due to the Boltzmann distribution function $e^{-E/T}$ (E is an energy of the particle) [19]. Since finite T loop integrals contain always the factor $e^{-E/T}$, the integrals at finite T always converge at large momentum. However, in self-consistent methods, divergences which depend on T appear, because mass terms, which are determined by self-consistent conditions, receive T-dependence.

Another difficulty is the NG-theorem. The symmetry of the Lagrangian may have been broken explicitly by self-consistent conditions, and the NG-theorem may not be fulfilled. In other words, self-consistent conditions should, in principle, preserve the symmetry, and some constraint on the self-consistent conditions from the original symmetry should appear. However, in the methods proposed so far, such condition was not clear.

1.4 Optimized perturbation theory at finite T

Optimized perturbation theory (OPT) at finite T has been developed by us in ref.[20] as a resummation method for solving the above problems. It has the following advantages.

1. It is possible to correctly resum hard thermal loops at high temperature.
2. Renormalization can be carried out at each order of OPT.
3. The Nambu-Goldstone theorem is satisfied in any given order of OPT.

There are three major purposes of this thesis and the organization of this thesis is as follows.

First of all, in chapter 2, we formulate OPT as a generalized mean-field theory [21]. Similar idea is sometimes called the delta-expansion, the variational perturbation theory and so on, and has been applied for the field theory at finite T in [22, 23] and for the quantum mechanics in [24].

Secondary, in chapter 3, we examine whether our method can correctly describe the phase transition using $\lambda\phi^4$ theory as an example. The principle of minimal sensitivity (PMS) condition and the criterion of the fastest apparent convergence (FAC) condition [25] (see, Sec.2.2.2) in one-loop and two-loop order are investigated.

Thirdly, in chapter 4, OPT is applied to a physical system, the $O(4)$ linear σ model which is considered as an effective theory of QCD with two flavors. We investigate the soft mode which is a characteristic mode in second order or weakly first order phase transition. One can see that OPT plays the crucial role for the discussion in this chapter. Detectability of the soft mode through $\sigma \to 2\gamma$ process at finite T in experiments is also discussed.

In chapter 5, we give summary and remarks.

Chapter 2

Optimized perturbation theory at finite temperature

In this chapter, we introduce the optimized perturbation theory (OPT) at finite temperature. Firstly, we illustrate the necessity of resummation at finite T using $\lambda\phi^4$ theory. Secondly, we give our definition of OPT. The proofs of the renormalizability and Nambu-Goldstone theorem in OPT are also shown.

2.1 Necessity of resummation at finite T

It is known that naive perturbation theories break down at finite T, especially at high T [12]. This is because large T compensate the powers of the coupling constant. To illustrate this, let us consider $\lambda\phi^4$ theory,

$$\mathcal{L} = \frac{1}{2}[(\partial\phi)^2 - \mu^2\phi^2] - \frac{\lambda}{4!}\phi^4. \tag{2.1}$$

Firstly, we consider the case $\mu^2 > 0$ (λ is always taken to be positive for the stability of the system). At finite T, the lowest order self-energy correction, which is shown in Fig.2.1 (A), reads

$$-i\frac{\lambda\kappa^{2\varepsilon}}{2}\int\frac{d^np}{(2\pi)^n}\left[\frac{i\hbar}{p^2-\mu^2+i\epsilon} + 2\pi n_B(|p_0|)\delta(p^2-\mu^2)\right]. \tag{2.2}$$

Here, we take the dimensional regularization scheme [26]: κ is the renormalization point which compensates the dimension of λ, and $\varepsilon = (4-n)/2$. n_B is the Bose-Einstein distribution function:

$$n_B(|p_0|) = \frac{1}{e^{\beta|p_0|}-1}, \tag{2.3}$$

where $\beta = 1/T$. The $\hbar$ is explicitly written for later use.

The order of eq.(2.2) is λT^2 at high T. However, Fig.2.1 (B) is of $O(\lambda T^2 \times \frac{\lambda T}{\mu})$ and n-loop diagram in (C) is of $O(\lambda^n T^{2n-1}/\mu^{2n-3})$. The power of T/μ increases by one by attaching the tadpole diagram. Namely, the higher order diagrams are larger than the lower ones at high T. Thus, higher order terms must be resummed to get sensible results at high T [27].

The loop-expansion [28], which is another perturbation theory (not an expansion of the coupling constant), also breaks down at finite T. This can be also illustrated by using eq.(2.1). At $T = 0$, the loop-expansion corresponds to the expansion by $\hbar$. Therefore, it can treat the quantum effects systematically. Thus, the loop-expansion is often used for theories with spontaneous symmetry breaking (SSB). However, at finite T, the equation (2.2) shows that the vacuum part (first term) is of $O(\hbar)$, but thermal part (second term) is of $O(\hbar^0)$. Therefore, the loop expansion does not coincide with the expansion of $\hbar$ at finite T. When the thermal corrections become large at high T, one should resum this classical effects first. The Debye screening is one of such classical effects. Therefore, naive loop-expansion does not work.

When $\mu^2 < 0$, the difficulty of the loop-expansion appears in another way. In this case, the tree-level mass becomes

$$m_0^2 = \mu^2 + \frac{\lambda}{2}\varphi^2(T), \tag{2.4}$$

where φ is the thermal expectation value of the field ϕ;

$$\varphi(T) = \langle\phi\rangle_T. \tag{2.5}$$

Usually, as the temperature increases, $\varphi(T)$ decreases. Therefore, m_0^2 becomes tachyonic even below the critical temperature T_c where $\varphi(T)$ becomes zero. This tachyonic pole destroys the perturbation theory, and makes studies of the phase transition impossible in effective theories at finite T. Thus, one should resum the higher order terms at finite temperature even at low T.

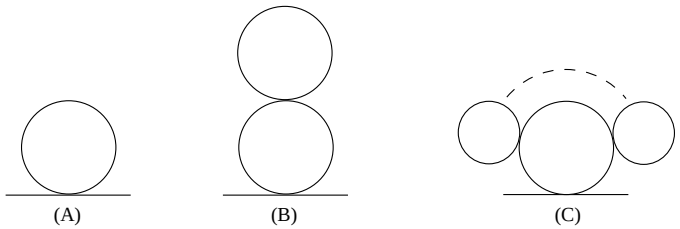

Figure 2.1: Bubble and cactus diagrams in $\lambda\phi^4$-theory.

2.2 Optimized perturbation theory

2.2.1 Motivations of OPT

The hard thermal loops resummation scheme (HTLRS) [8, 29] is one of the most successful resummation method at high temperature, and have been applied to gauge theory and $\lambda\phi^4$ theory [30]. Its concept is a "weak coupling expansion" and a hierarchy of scales, namely $O(T)$ is called hard, $O(gT)$ and $O(g^2T)$ are called soft and super soft respectively. The advantage of it is to preserve the gauge symmetry in contrast with the bare perturbation theory. The latter leads to gauge dependent results for physical quantities at finite T [31].

The effective Lagrangian for Euclidean $SU(N)$ gauge theory is constructed by adding and subtracting the following term to the Lagrangian:

$$\delta\mathcal{L} = \mathcal{L}_f + \mathcal{L}_\gamma, \tag{2.6}$$

$$\mathcal{L}_f = im_f^2\bar{\psi}(x)\int\frac{d\Omega}{4\pi}\frac{\hat{K}\!\!\!/}{\hat{K}\cdot D}\psi(x), \tag{2.7}$$

$$\mathcal{L}_\gamma = -m^2\mathrm{Tr}\int\frac{d\Omega}{4\pi}F_{\mu\alpha}\frac{\hat{K}_\alpha\hat{K}_\beta}{(\hat{K}\cdot D)^2}F_{\beta\mu}, \tag{2.8}$$

where $D_\mu = \partial_\mu + igA_\mu$, $F^a_{\mu\nu} = \partial_\mu A^a_\nu - \partial_\nu A^a_\mu + gf_{abc}A^b_\mu A^c_\nu$ and $\hat{K} = (-i, \vec{k}/|k|)$. In QCD ($SU(3)$ gauge theory), $m_f^2 = g^2T^2/6$, $m^2 = g^2T^2(3 + N_F/2)/6$ and N_F is number of fermions. One of the notable features is the existence of infinite number of vertices to preserve the gauge symmetry. Now, the effective Lagrangian is written as

$$\mathcal{L} = (\mathcal{L} + \delta\mathcal{L}) - \delta\mathcal{L} = \mathcal{L}_{eff} - \delta\mathcal{L}, \tag{2.9}$$

where $\mathcal{L}$ is the original ($SU(N)$ gauge theory) Lagrangian. The propagators and vertices contain $O(gT)$ effects arising from the $\mathcal{L}_{eff}$ term and the last term $-\delta\mathcal{L}$ is treated as a counter term to avoid any double counting. Many physical quantities, for example, the gluon damping rate, the production rate of soft dileptons in a quark-gluon plasma, have been calculated using this method [8, 29, 14].

On the other hand, for theories with SSB, loop-expansion is relevant rather than the weak-coupling expansion. This is because we need to calculate the effective potential [32] to search the ground state of a system.

In the following, we will develop an optimized perturbation theory (OPT), which is an improved loop expansion, to finite T systems [20]. Similar idea have been studied by Okopińska [22] and Banerjee and Mallik [23]. In ref.[22], they study the $O(N)$ ϕ^4 theory with the principle of minimal sensitivity (PMS) condition (see Step 3 in Sec.2.2.2). Since their formulation is not based on the loop-expansion (see

Step 1 in Sec.2.2.2), they could not prove renormalizability. Also, the NG-theorem appears in rather complicated way. In ref.[23], they study $\lambda\phi^4$ theory with the fastest apparent convergence (FAC) condition (see Step 3 in Sec.2.2.2) at high T. They carry out the renormalization up to two-loop order in the symmetric phase. However, the rigorous definition of their method in higher orders and a proof of the renormalizability in higher orders are not given. Also, numerical studies of the gap-equation (see Step 3 in Sec.2.2.2) are not performed. In this chapter, we will give our definition of OPT (Sec.2.2.2), and prove the renormalizability (Sec.2.3) and the NG-theorem in the $O(N)$ ϕ^4 theory (Sec.2.4). These are proved at any given order of δ (an expansion parameter in OPT).

2.2.2 OPT

We will explain our method by dividing it into three steps. $\lambda\phi^4$ theory is used for illustration:

$$\begin{aligned}
\mathcal{L}(\phi_0;\mu_0^2,\lambda_0) &= \frac{1}{2}[(\partial\phi_0)^2-\mu_0^2\phi_0^2]-\frac{\lambda_0}{4!}\phi_0^4 \\
&= \frac{1}{2}[(\partial\phi)^2-\mu^2\phi^2]-\frac{\lambda}{4!}\phi^4 \\
&\quad +\frac{1}{2}(Z-1)(\partial\phi)^2-\frac{1}{2}(Z_\mu Z-1)\mu^2\phi^2-\frac{\lambda}{4!}(Z_\lambda Z^2-1)\phi^4+D\mu^4 \\
&= \frac{1}{2}[(\partial\phi)^2-\mu^2\phi^2]-\frac{\lambda}{4!}\phi^4 \\
&\quad +\frac{1}{2}A(\lambda)(\partial\phi)^2-\frac{1}{2}B(\lambda)\mu^2\phi^2-\frac{1}{4!}C(\lambda)\phi^4+D(\lambda)\mu^4 \\
&= \mathcal{L}(\phi;\mu^2,\lambda).
\end{aligned} \tag{2.10}$$

Here we have explicitly written the arguments μ^2 and λ in $\mathcal{L}$ for later use. The suffix 0 indicates unrenormalized quantities. The terms A, B, C and D to the standard notation of the counter terms are $A=Z-1$, $B=Z_\mu Z-1$ and $C=\lambda(Z_\lambda Z^2-1)$, where Z's are defined by $\phi_0=\sqrt{Z}\phi$, $\lambda_0=Z_\lambda\lambda$ and $\mu_0^2=Z_\mu\mu^2$. Since we adopt the mass independent renormalization scheme, namely $\overline{MS}$ scheme [33], with the dimensional regularization, the argument of A, B, C and D is only λ. For simplicity, we omit the dimension-full factor κ^{4-n} to be multiplied to λ. Here, κ is the renormalization point and n is the number of dimensions. The $O(N)$ case will be discussed in Section 2.4 and we show the NG theorem is fulfilled.

Step 1 (Definition of the δ expansion)

The loop-wise δ expansion for the effective action is defined as

$$\Gamma[\varphi^2]=\delta\ln\int[d\phi]\exp\left[\frac{1}{\delta}\int_0^{1/T}d^4x\left[\mathcal{L}(\phi+\varphi;\mu^2,\lambda)+J\phi\right]\right], \tag{2.11}$$

where $J \equiv -\partial\Gamma[\varphi]/\partial\varphi$ and $\int_0^{1/T} d^4x \equiv \int_0^{1/T} d\tau \int d^3x$. At zero temperature, it corresponds to the naive $\hbar$ expansion [32]. However, it dose not coincident with the $\hbar$ expansion at finite temperature, because $\hbar$ is also contained in the upper limit of the integral.

The counter terms are also expanded in δ. Because the renormalization is performed at zero temperature, these are same with counter terms in the naive loop expansion. Since we use the $\overline{MS}$ scheme, the UV divergences in the symmetry broken phase ($\mu^2 < 0$) can be removed by the same counter terms in the symmetric phase ($\mu^2 > 0$) [34, 35].

In ref.[22], they introduce the "δ" as

$$\mathcal{L}_\delta \equiv \frac{1}{2}\phi i D^{-1}\phi + \delta(\mathcal{L} - \frac{1}{2}\phi i D^{-1}\phi). \tag{2.12}$$

Here, iD^{-1} is determined by $\mathcal{D}\Gamma/\mathcal{D}D = 0$ (see Step 3), where Γ is the effective action which is calculated by the δ-expansion. Thus, this δ-expansion does not correspond to the loop-expansion in contrast with our approach.

Step 2 (Splitting the mass and coupling)

The mass and the coupling constant are split as

$$\begin{array}{rclcl} \mu^2 & = & m^2 - (m^2 - \mu^2) & = & m^2 - \chi, \\ \lambda & = & g - (g - \lambda) & = & g - \eta. \end{array} \tag{2.13}$$

Namely, we add and subtract the mass term m^2 and the coupling constant g, and define $\chi \equiv m^2 - \mu^2$ and $\eta \equiv g - \lambda$. Then, eq.(2.13) is substituted in the Lagrangian (2.10):

$$\begin{aligned} \mathcal{L}(\phi; m^2, \chi, g, \eta) &\equiv \mathcal{L}(\phi; m^2 - \chi, g - \eta) \\ &= \frac{1}{2}[(\partial\phi)^2 - m^2\phi^2] - \frac{g}{4!}\phi^4 + \frac{1}{2}\chi\phi^2 + \frac{\eta}{4!}\phi^4 \\ &\quad + \frac{1}{2}A(g-\eta)(\partial\phi)^2 - \frac{1}{2}B(g-\eta)(m^2-\chi)\phi^2 \\ &\quad - \frac{1}{4!}C(g-\eta)\phi^4 + D(g-\eta)(m^2-\chi^2)^2. \end{aligned} \tag{2.14}$$

It is important that the identities (2.13) are used not only in the standard mass and coupling terms but also in counter terms [36] to show the order by order renormalization in OPT.

To get a non-trivial loop expansion, we need to assign δ as

$$m^2 = O(1), \quad \lambda = O(1), \quad \chi = O(\delta), \quad \eta = O(\delta). \tag{2.15}$$

Thus, the tree-level mass becomes $m^2+g\varphi^2/2$ instead of $\mu^2+\lambda\varphi^2/2$ in the symmetry broken phase. The order of δ is increased by inserting the new vertex $\chi\phi^2/2$ or $\eta\phi^4/4!$. The physical reason behind this assignment (2.15) is the fact that χ and η reflects the effect of interactions.

Since (2.14) is only a rearrangement of the parameters, the effective action should not depend on the arbitrary parameters m^2 and g. If they are calculated in all orders, it must not depend on these. However, since we cannot calculate all orders in actual calculations, the physical quantities depend on artificial parameters in practice. Methods for determination of these parameters are given in the next step.

Step 3 (Determination of m^2 and g)

One can determine the optimal parameters m^2 and g by the methods proposed by Stevenson [25].

(a) The principle of minimal sensitivity (PMS) :

$$\frac{\partial \mathcal{O}_L}{\partial m} = 0, \quad \frac{\partial \mathcal{O}'_{L'}}{\partial g} = 0. \tag{2.16}$$

The $\mathcal{O}_L$ ($\mathcal{O}'_{L'}$) is the physical quantity calculated up to L-th (L'-th) order. Since m^2 and g are artificial parameters added by hand, the physical quantities should not depend on these.

(b) The criterion of the fastest apparent convergence (FAC):

$$\mathcal{O}_L - \mathcal{O}_{L-n} = 0, \quad \mathcal{O}'_{L'} - \mathcal{O}'_{L'-n'} = 0, \tag{2.17}$$

where n (n') is chosen in the range, $1 \leq n \leq L$ ($1 \leq n \leq L'$). This condition requires that the perturbative corrections in $\mathcal{O}'_L$ ($\mathcal{O}'_{L'}$) should be as small as possible for a suitable value of m (g).

These conditions reduce to self-consistent gap equations. Therefore, OPT corresponds to a generalization of the mean field approximation.

When one studies a theory with spontaneously symmetry broken (SSB), the ground state of the system must be searched. The vacuum is determined by the stationary point of the effective potential $V(\varphi^2)$ with respect to φ which is defined as

$$V(\varphi^2) = -\frac{\Gamma[\varphi^2 = \text{const.}]}{\int_0^{1/T} d^4x}. \tag{2.18}$$

However, as mentioned before, the perturbation theory at finite order has explicit m^2 and g dependence. So, V calculated up to the L-th order, which is denoted

by $V_L(\varphi^2, m^2, g)$, depends on m^2 and g, and one must determine not only vacuum expectation value φ_0 but also these parameters. The condition for the stationary point reads

$$\left.\frac{\partial V_L(\varphi^2, m^2, g)}{\partial \varphi}\right|_{\varphi=\varphi_0} = 0 \tag{2.19}$$

The derivative with respect to φ does not act on m^2 and g by definition even if $m^2(\varphi)$ and $g(\varphi)$ depend on φ after solving the equation (2.16) or (2.17). However, if we choose $V_L(\varphi, m^2, g)$ as O_L and $O'_{L'}$ in (2.16), which is most relevant quantity to study the static nature of the phase transition, following relation holds:

$$\begin{aligned}\frac{dV_L(\varphi^2, m^2(\varphi), g(\varphi))}{d\varphi} &= \frac{\partial V_L(\varphi^2, m^2, g)}{\partial \varphi} + \frac{\partial V_L(\varphi^2, m^2, g)}{\partial m^2}\frac{\partial m^2}{\partial \varphi} + \frac{\partial V_L(\varphi^2, m^2, g)}{\partial g}\frac{\partial g}{\partial \varphi} \\ &= \frac{\partial V_L(\varphi^2, m^2, g)}{\partial \varphi}\end{aligned} \tag{2.20}$$

This is an advantage of the PMS condition for theories with SSB.

2.3 Renormalization in OPT

We mention here why the renormalization in self-consistent methods is not a trivial issue. In the naive perturbation theory, there is no new UV divergences at $T \neq 0$ because of the natural cutoff from the Boltzmann distribution function. Therefore, all the UV divergences at finite T are removed by the $T = 0$ counter terms. This statement has been proved in imaginary-time and real-time formalisms [19].

On the other hand, in self-consistent methods, the naive renormalization procedure does not work, because the tree-level mass terms get T-dependence (for example, $M^2(T) = m^2 + g(T)\varphi^2/2$) which is determined by the self-consistent gap-equation [18]. Therefore, T-dependent divergences arise.

In ref.[23], however, the renormalization happened to be successful at least up to the two-loop order. The main difference of ref.[23] and ref.[18] is whether the renormalization is performed before of after imposing the gap-equation.

In the method of ref.[18], one imposes the unrenormalized gap-equation first, and then the divergences are tried to be removed. However, in this procedure, it is hard to carry out the renormalization in higher orders. Since the optimized parameters such as $m^2(T)$ and $g(T)$ contain higher loop contributions through the self-consistent gap-equation, the divergences also contain higher loops. Thus, the counter terms should be also resummed to higher order terms.

On the other hand, in our method explained in the previous section, the finite gap-equations are obtained initially, because the renormalization is performed at first

(in Step 2). This means that the resummations of counter terms are automatically performed as well as physical parameters. (It is essential to use the resummed parameters $m^2(T)$ and $g(T)$ in the counter terms.) In ref.[23], similar idea appears but was pursued only for weak coupling expansion at high T up to two-loop.

2.3.1 Proof of the renormalizability in OPT

Consider a naive m-th loop order renormalized correction to the effective action: $\Gamma_R^{(m)}$. Then, the effective action up to n-th order can be written as

$$\Gamma_R^n = \sum_{m=0}^{n} \Gamma_R^{(m)}. \tag{2.21}$$

Here, each $\Gamma_R^{(m)}$ is written by the sum of $\Gamma^{(m)}$ which does not contain any counter terms and $C^{(m)}$ which contains at least more than one counter terms:

$$\Gamma_R^{(m)} = \Gamma^{(m)} + C^{(m)}. \tag{2.22}$$

Also, $\Gamma_R^{(m)}$ can be expanded by the renormalized mass μ^2 and the renormalized coupling λ around $\mu^2 = 0$ and $\lambda = 0$:

$$\Gamma_R^{(m)} = \sum_{i=0}^{\infty}\sum_{j=0}^{l} (\mu^2)^i \lambda^j (\Gamma_{ij}^{(m)} + C_{ij}^{(m)}), \tag{2.23}$$

where,

$$\Gamma_{ij}^{(m)} = \frac{1}{i!j!}\frac{\partial^i}{\partial(\mu^2)^i}\frac{\partial^j}{\partial\lambda^j}\Gamma^{(m)}\Big|_{\mu^2=0,\lambda=0}, \tag{2.24}$$

$$C_{ij}^{(m)} = \frac{1}{i!j!}\frac{\partial^i}{\partial(\mu^2)^i}\frac{\partial^j}{\partial\lambda^j}C^{(m)}\Big|_{\mu^2=0,\lambda=0}. \tag{2.25}$$

Since $\Gamma_R^{(m)}$ is finite, $\Gamma_{ij}^{(m)} + C_{ij}^{(m)}$ must be finite.

Next, we consider OPT. In this method, μ^2, λ are re-shuffled as eq.(2.13). Then, eq.(2.13) is substituted in (2.23),

$$\Gamma_R^{(m)} = \sum_{i=0}^{\infty}\sum_{j=0}^{l} (m^2 - \chi)^i (g - \eta)^j (\Gamma_{ij}^{(m)} + C_{ij}^{(m)}). \tag{2.26}$$

Since $m^2 = O(1)$, $\lambda = O(1)$, $\chi = O(\delta)$ and $\eta = O(\delta)$, the order of δ increases by including $\chi = O(\delta)$ and/or $\eta = O(\delta)$. Thus, by expanding the parameters $(m^2 - \chi)^i$ and $(g - \eta)^j$ in eq.(2.26) higher order terms in δ are generated:

$$\begin{aligned}\Gamma_R^{(m)} &= \Gamma_R^{(m)}(\delta^m) + \Gamma_R^{(m)}(\delta^{(m+1)}) + \cdots \\ &= \sum_{i=0}^{\infty}\sum_{j=0}^{l}[(m^2)^i g^j - \{i\chi(m^2)^{i-1}g^j + j\eta(m^2)^i g^{j-1}\} + \cdots](\Gamma_{ij}^{(m)} + C_{ij}^{(m)}),\end{aligned} \tag{2.27}$$

where,

$$\Gamma_R^{(m)}(\delta^{m+a+b}) \equiv {}_iC_a(-\chi)^a(m^2)^{i-a}{}_jC_b(-\eta)^b g^{j-b}(\Gamma_{ij}^{(m)} + C_{ij}^{(m)}). \tag{2.28}$$

After all, up to m-th δ order correction, $\Gamma_R^{\delta^m}$ reads

$$\Gamma_R^{\delta^m} = \sum_{s=0}^{m} \Gamma_R^{(m-s)}(\delta^m). \tag{2.29}$$

Since the renormalization is carried out up to m-th order, each $\Gamma_R^{(l)}$ $(0 \leq l \leq m)$ is finite. Thus, $\Gamma_R^{\delta^m}$ is also finite.

If theory does not have a mass term, the renormalization of OPT is defined as a limit $\mu^2 \to 0$ of eq.(2.29). By doing this, one can obtain Debye mass even when the original Lagrangian does not have a mass term.

2.4 Nambu-Goldstone theorem

Application of OPT to the Lagrangian with $O(N)$ symmetry is straightforward. ϕ^2 is just replaced by $\vec{\phi}^2$ in (2.14):

$$\begin{aligned}\mathcal{L}(\vec{\phi}; m^2, \chi, g, \eta) &= \frac{1}{2}[(\partial\vec{\phi})^2 - m^2\vec{\phi}^2] - \frac{g}{4!}(\vec{\phi}^2)^2 + \frac{1}{2}\chi\vec{\phi}^2 + \frac{\eta}{4!}(\vec{\phi}^2)^2 \\ &\quad + \frac{1}{2}A(g-\eta)(\partial\vec{\phi})^2 - \frac{1}{2}B(g-\eta)(m^2-\chi)\vec{\phi}^2 \\ &\quad - \frac{1}{4!}C(g-\eta)(\vec{\phi}^2)^2 + D(g-\eta)(m^2-\chi^2)^2,\end{aligned} \tag{2.30}$$

where $\vec{\phi} = (\phi_1, \cdots, \phi_N)$. The equation (2.30) has the manifest $O(N)$ invariance. Since our δ-expansion is a modified loop expansion, the effective action $\Gamma[\vec{\varphi}^2]$ and effective potential $V(\vec{\varphi}^2)$ have invariance order by order under $O(N)$ transformation:

$$\varphi_i = \varphi_i + i\theta^a T_{ij}^a \varphi_j, \tag{2.31}$$

where $\vec{\varphi}$ is the thermal expectational value of $\vec{\phi}$ and $\mathbf{T}^a$ is the generator of $O(N)$ symmetry. This fact leads to the infinitesimal invariant condition for the L-th order effective potential:

$$\frac{\partial V_L(\vec{\varphi}^2, m^2, g)}{\partial\varphi_j} T_{jk}^a \varphi_k = 0. \tag{2.32}$$

The derivative with respect to φ_i reads

$$\frac{\partial V_L(\vec{\varphi}^2, m^2, g)}{\partial\varphi_j} T_{ji}^a = -\frac{\partial^2 V_L(\vec{\varphi}^2, m^2, g)}{\partial\varphi_i\partial\varphi_j} T_{jk}^a \varphi_k. \tag{2.33}$$

At the stationary point, the l.h.s. of (2.33) vanishes, and the r.h.s. of (2.33) satisfies the following equation:

$$\frac{\partial^2 V_L(\vec{\varphi}^2, m^2, g)}{\partial\varphi_i \partial\varphi_j} T^a_{jk}\varphi_k = D^{-1}_{ij}(0) T^a_{jk}\varphi_k = 0, \tag{2.34}$$

where we use the fact that the second derivative with respect to φ for the L-th order effective potential is equivalent to the Matsubara propagator at zero frequency and momentum calculated up to L-th order. Since the symmetry is spontaneously broken, $T^a_{jk}\varphi_k \neq 0$ for at least one direction. Thus, the NG theorem is proved.

There is a remark on the NG-theorem. The equation (2.30) is essential for proving the NG-theorem. In general, the decomposition (2.13) may be replaced by

$$\mu^2\vec{\phi}^2 = m^2_{ij}\phi_i\phi_j - (m^2_{ij} - \mu^2\delta_{ij})\phi_i\phi_j, \tag{2.35}$$

where δ_{ij} is the Kronecker delta. If one takes $m^2_{ij} \neq m^2\delta_{ij}$, the Lagrangian is not $O(N)$ invariant. This leads to non $O(N)$ invariant effective potential, and (2.32) is not satisfied. Thus, the NG-theorem is not fulfilled in any finite orders of the δ-expansion. For example, when $O(N)$ symmetry spontaneously breaks down to $O(N-1)$ symmetry, one may be tempted to make a decomposition

$$\mu^2\vec{\phi}^2 = m^2_r\phi^2_1 + \sum_{i=2}^{N} m^2_c\phi^2_i - (m^2_r - \mu^2)\phi^2_1 - \sum_{i=2}^{N}(m^2_c - \mu^2)\phi^2_i \tag{2.36}$$

to impose the self-consistent conditions for the radial mode and the rotational modes independently. In this case, the effective potential $V(\varphi^2_1, \sum_{i=2}^{N}\varphi^2_i)$ has only $O(N-1)$ symmetry and we cannot have constraints for $D^{-1}_{ij}(0)$ such as eq.(2.34).

2.5 Summary of OPT

The optimized perturbation theory is explained in 3 steps:

1. Counter terms in the δ-expansion is prepared.
2. The mass and coupling constant in the Lagrangian are split by introducing artificial parameters.
3. The parameters are optimized.

OPT has several advantages from other self-consistent resummation methods. The renormalization at finite temperature is trivially performed in OPT. This method can resum the counter terms systematically and the renormalization is carried out before imposing the gap-equation. Since our approach preserves the symmetry,

NG-theorem is also trivially satisfied. Contrary to our method, many of the self-consistent methods proposed so far suffer from these problems [18, 37].

Our solutions to the long standing problems in the self-consistent resummation methods can be summarized as the following.

- One should resum the counter terms.
- Keep the original symmetry of the Lagrangian.

Our method naturally satisfies the above conditions.

Chapter 3

Phase transition in $\lambda\phi^4$ theory

In this chapter, we demonstrate an application of OPT to $\lambda\phi^4$ theory. We calculate the effective potential up to 2-loop level using the real time formalism [38, 39]. Only a mass term is optimized in this chapter. The PMS condition for the effective potential and the FAC condition for the two point self-energy at zero momentum are examined. We also discuss the extension to the shift of the coupling term.

3.1 Calculation of the effective potential in the real time formalism

We briefly explain how to calculate the effective potential in the real time formalism [39].

In the real time formalism, the Lagrangian of (2.1) becomes

$$\mathcal{L}[\phi_1\phi_2] = \frac{1}{2}\phi_a D_\beta^{-1ab}\phi_b - U[\phi_1] + U[\phi_2], \tag{3.1}$$

where D_β^{ab} is 2×2 propagator and $U[\phi] = \lambda\phi^4/4!$. In momentum space, the propagator D_β^{ab} reads

$$iD_\beta^{ab}(k) = \begin{pmatrix} \cosh\theta & \sinh\theta \\ \sinh\theta & \cosh\theta \end{pmatrix} \begin{pmatrix} \frac{i}{k^2-\mu^2+i\varepsilon} & 0 \\ 0 & \frac{-i}{k^2-\mu^2-i\varepsilon} \end{pmatrix} \begin{pmatrix} \cosh\theta & \sinh\theta \\ \sinh\theta & \cosh\theta \end{pmatrix}, \tag{3.2}$$

where

$$\cosh^2\theta = \frac{1}{1-e^{-\beta|k_0|}}, \tag{3.3}$$

and $\beta = 1/T$. Using the equation

$$\delta(x) = \frac{1}{\pi}\lim_{\varepsilon\to 0}\frac{\varepsilon}{x^2+\varepsilon^2}, \tag{3.4}$$

we find an useful expression:

$$iD_\beta^{ab}(k) = \begin{pmatrix} \frac{i}{k^2-\mu^2+i\varepsilon} & 0 \\ 0 & \frac{-i}{k^2-\mu^2-i\varepsilon} \end{pmatrix} + 2\pi\delta(k^2-\mu^2) \begin{pmatrix} \frac{1}{e^{\beta|k_0|}-1} & \frac{-e^{-\beta|k_0|/2}}{1-e^{-\beta|k_0|}} \\ \frac{-e^{-\beta|k_0|/2}}{1-e^{-\beta|k_0|}} & \frac{1}{e^{\beta|k_0|}-1} \end{pmatrix}. \quad (3.5)$$

The first term corresponds to the zero temperature propagator and the second term is an additional temperature dependent term through the Bose-Einstein distribution function.

The generating functional $Z[j_1 j_2]$ is defined as

$$Z[j_1 j_2] = \int [d\phi_a] \exp[i \int d^4x d^4y \frac{1}{2}\phi_a D_\beta^{-1ab} \phi_b + i \int d^4x - U[\phi_1] + U[\phi_2] + j_a \phi_a], \quad (3.6)$$

where $a, b = 1, 2$. This leads the connected generating functional $W[j_1 j_2]$:

$$W[j_1 j_2] = \frac{1}{i} \ln Z[j_1 j_2]. \quad (3.7)$$

The classical fields $\varphi_1[j_1 j_2]$ and $\varphi_2[j_1 j_2]$ are defined as

$$\varphi_1[j_1 j_2] = \frac{\delta W[j_1 j_2]}{\delta j_1}, \quad (3.8)$$

$$\varphi_2[j_1 j_2] = \frac{\delta W[j_1 j_2]}{\delta j_2}. \quad (3.9)$$

The finite temperature effective action $\Gamma[\varphi_1 \varphi_2]$ in real time formalism is given as the Legendre transformation of $W[j_1 j_2]$,

$$\Gamma[\varphi_1 \varphi_2] = W[j_1 j_2] - \int d^4x j_a \varphi_a, \quad (3.10)$$

with

$$\frac{\delta \Gamma[\varphi_1 \varphi_2]}{\delta \varphi_a} = -j_a. \quad (3.11)$$

For the constant fields φ_1, φ_2, we get the effective potential $V[\varphi_1 \varphi_2]$,

$$\Gamma[\varphi_1 \varphi_2] = -V[\varphi_1 \varphi_2] \int d^4x. \quad (3.12)$$

The ground state where the external sources should vanish can be found by

$$\frac{\delta \Gamma[\varphi_1 \varphi_2]}{\delta \varphi_a} = 0, \quad (3.13)$$

or alternatively,

$$\frac{\partial V[\varphi_1 \varphi_2]}{\partial \varphi_a} = 0. \quad (3.14)$$

It is proved [39] that the relationship between the effective potential calculated by the imaginary time formalism V_β^E and the real time formalism is as follow,

$$\left.\frac{\partial V[\varphi_1\varphi_2]}{\partial\varphi_1}\right|_{\varphi_1=\varphi_2=\varphi} = \frac{\partial V_\beta^E[\varphi]}{\partial\varphi}. \tag{3.15}$$

Thus, the procedure to calculate the physical effective potential in the real time formalism can be summarized as:

1. Calculate the 1-point φ_1 (tadpole) function.
2. Set $\varphi_1 = \varphi_2 = \varphi$.
3. Integrate over φ.

This method corresponds to a generalized Weinberg's tadpole method [40] for the evaluation of effective potentials in the finite temperature field theory.

Here, let us calculate the effective potential in the two-loop order at finite temperature for (2.10):

$$\begin{aligned}\mathcal{L}(\phi;\mu^2,\lambda) &= \frac{1}{2}[(\partial\phi)^2-\mu^2\phi^2]-\frac{\lambda}{4!}\phi^4 \\ &\quad +\frac{1}{2}A(\lambda)(\partial\phi)^2-\frac{1}{2}B(\lambda)\mu^2\phi^2-\frac{1}{4!}C(\lambda)\phi^4+D(\lambda)\mu^4.\end{aligned} \tag{3.16}$$

The coefficients of counter terms in 2-loop level [41] are

$$\begin{aligned}A(\lambda) &= -\frac{\lambda^2}{(4\pi)^4}\frac{1}{24\bar{\varepsilon}}, \\ B(\lambda) &= \frac{\lambda}{(4\pi)^2}\frac{1}{2\bar{\varepsilon}}+\frac{\lambda^2}{(4\pi)^4}\left(\frac{1}{2\bar{\varepsilon}^2}-\frac{1}{4\bar{\varepsilon}}\right), \\ C(\lambda) &= \frac{\lambda^2}{(4\pi)^2}\frac{3}{2\bar{\varepsilon}}+\frac{\lambda^3}{(4\pi)^4}\left(\frac{9}{4\bar{\varepsilon}^2}-\frac{3}{2\bar{\varepsilon}}\right), \\ D(\lambda) &= -\frac{1}{(4\pi)^2}\frac{1}{4\bar{\varepsilon}}-\frac{\lambda}{(4\pi)^4}\frac{1}{8\bar{\varepsilon}^2},\end{aligned} \tag{3.17}$$

where we adopt the modified minimal subtraction ($\overline{MS}$) scheme. (The multiple factor $\kappa^{(4-n)}$ to λ has been dropped as before.) The Feynman rules in real time formalism are given in Fig.A.1 in Appendix A. The effective potential for (3.16) has been calculated in [42] at zero temperature and in [30, 39, 43] at $T \neq 0$. The resalt is (see, Appendix C)

$$V = V^0 + V^1 + V^2, \tag{3.18}$$

$$V^0 = \frac{1}{2}\mu^2\varphi^2+\frac{\lambda}{4!}\varphi^4, \tag{3.19}$$

$$V^1 = -\frac{1}{(4\pi)^2}\frac{M^4}{4}(\frac{3}{2} - \ln\frac{M^2}{\kappa^2}) + \int_0^\infty \frac{dk}{(2\pi)^2}\frac{2}{\beta}k^2\ln(1-e^{-\beta E}), \tag{3.20}$$

$$V^2 = \frac{\lambda}{2}K_t^2 + \frac{\lambda^2\varphi^2}{4}S_s + \frac{\lambda^2\varphi^2}{4}C_f, \tag{3.21}$$

where $M = \mu^2 + \lambda\varphi^2/2$, $\beta = 1/T$ and $E = \sqrt{k^2+M^2}$. The definitions of K_t, S_s and C_f are found in Appendix C (eq.(C.7), eq.(C.14) and eq.(C.8), respectively).

3.2 Application of OPT to $\lambda\phi^4$ theory

Let us apply OPT to eq.(3.16). This leads to

$$\begin{aligned}\mathcal{L}(\phi; m^2, \chi, g, \eta) &= \frac{1}{2}[(\partial\phi)^2 - m^2\phi^2] - \frac{g}{4!}\phi^4 + \frac{1}{2}\chi\phi^2 + \frac{\eta}{4!}\phi^4 \\ &\quad + \frac{1}{2}A(g-\eta)(\partial\phi)^2 - \frac{1}{2}B(g-\eta)(m^2-\chi)\phi^2 \\ &\quad - \frac{1}{4!}C(g-\eta)\phi^4 + D(g-\eta)(m^2-\chi^2)^2,\end{aligned} \tag{3.22}$$

where we used eq.(2.13). The additional Feynman rules are shown in Fig.A.2 in Appendix A. New diagrams for the one-point function and the vacuum energy are shown in Fig.D.1 and Fig.D.2, respectively.

Up to $O(\delta)$, the effective potential (3.18) becomes

$$V = V^0 + V^\delta + V^{\delta^2}, \tag{3.23}$$

$$V^0 = \frac{1}{2}m^2\varphi^2 + \frac{g}{4!}\varphi^4, \tag{3.24}$$

$$\begin{aligned}V^\delta &= -\frac{1}{2}\chi\varphi^2 - \frac{\eta}{4!}\varphi^4 - \frac{1}{(4\pi)^2}\frac{M^4}{4}(\frac{3}{2} - \ln\frac{M^2}{\kappa^2}) \\ &\quad + \int_0^\infty \frac{dk}{(2\pi)^2}\frac{2}{\beta}k^2\ln(1-e^{-\beta E}),\end{aligned} \tag{3.25}$$

$$V^{\delta^2} = (\chi + \frac{\eta\varphi^2}{2} + \frac{g}{2}K_t)K_t + \frac{g^2\varphi^2}{4}(S_s + C_f). \tag{3.26}$$

In $\lambda\phi^4$ theory at high T, the tadpole diagram Fig.2.1 (A) is the only hard thermal loop (HTL), and we must resum these cactus type diagram (Fig.2.1). Since they do not depend on external momentum, only the mass term is modified. Thus, HTLs resummation is performed by shifting the mass term. This happens only when one considers the theory such as $\lambda\phi^4$ model. If we consider the quantum chromodynamics, all vertices with N external gluons and vertices with $N-2$ external gluons and two external quarks become HTLs which must be summed up. In $\lambda\phi^4$ theory, on the other hand, by optimizing the mass term is enough in order to resum the HTLs.

In the following, we adopt an optimization only for the mass term in $\lambda\phi^4$ theory for simplicity. Namely, we set $\eta = 0$ in (3.22) and (3.23). We consider the case $\mu^2 < 0$, and the restoration of the symmetry is discussed under various conditions (PMS and FAC, see Sec.2.2.2). The full OPT case (optimization of the mass and coupling terms) is discussed in Sec.3.5.

3.3 The PMS condition

In this section, we investigate PMS conditions. Since we study the static nature of the phase transition, the thermal effective potential $V(\varphi, m^2)$ is chosen as the relevant physical quantity O_L in Step 3 in section 2.2.2. As we will show in Sec.3.3.1, $O(\delta)$ effective potential with PMS condition cannot resum the HTLs. Thus, $O(\delta^2)$ is the lowest order when one uses PMS condition.

3.3.1 1-loop analysis

When studying the phase transition, the most reasonable quantity to be optimized is the effective potential. Therefore, in the $O(\delta)$-level, we adopt a condition

$$\frac{\partial V^{0+\delta}(\varphi, m^2)}{\partial m^2} = 0, \tag{3.27}$$

where $V^{0+\delta}(\varphi, m^2) = V^0 + V^\delta$ (see, eq.(D.1) in Appendix.D). However, this condition does not lead to the appropriate gap-equation.

The differentiation with respect to m^2 corresponds to cutting one of the internal lines of $V(\varphi, m^2)$ because the power of the propagator is raised by one. As one can easily see from Fig.C.4, cutting the internal line of $V(\varphi, m^2)$ cannot produce the HTLs (like Fig.2.1 (a)). Therefore, eq.(3.27) cannot sum the tadpole type diagrams, and it is not meaningful to adopt the PMS condition in the $O(\delta)$-level. Thus, we need to go to the next order which is two-loop.

3.3.2 2-loop analysis

The PMS condition for the 2-loop effective potential reads

$$\frac{\partial V^{0+\delta+\delta^2}(\varphi, m^2)}{\partial m^2} = 0, \tag{3.28}$$

where $V^{0+\delta+\delta^2}(\varphi, m^2) = V^0 + V^\delta + V^{\delta^2}$. Cutting one of the internal lines of Fig.C.5 (a) leads to HTLs in scalar theory. The explicit form of (3.28) is shown in Appendix

D [1]. At high T (in the symmetric phase), eq.(3.28) reduces to

$$\left.\frac{\partial V^{0+\delta+\delta^2}(\varphi,m^2)}{\partial m^2}\right|_{\varphi=0} \stackrel{\beta m^2\to 0}{\longrightarrow} (\chi-\frac{\lambda T^2}{24})\frac{T}{16\pi m}. \tag{3.29}$$

This equation gives the following solution:

$$m^2(T)=\mu^2+\frac{\lambda T^2}{24}, \tag{3.30}$$

which corresponds to the Debye screening mass at high T. Thus, the condition (3.28) correctly resums higher order terms and recovers the reliability of the perturbation theory at finite T.

To determine the vacuum, we must also solve [2]

$$\left.\frac{\partial V(\varphi,m^2)}{\partial\varphi}\right|_{\varphi=\varphi_0}=0. \tag{3.31}$$

As we noted in section 2.2.2, the differentiation with respect to φ does not act on m^2. However, the gap-equation eq.(3.28) leads to

$$\begin{aligned}\frac{dV(\varphi,m^2(\varphi))}{d\varphi} &= \frac{\partial V(\varphi,m^2)}{\partial\varphi}+\frac{\partial V(\varphi,m^2)}{\partial m^2}\frac{\partial m^2}{\partial\varphi}\\ &= \frac{\partial V(\varphi,m^2)}{\partial\varphi}.\end{aligned} \tag{3.32}$$

Thus, in this case, the total derivative with respect to φ is equal to the partial one. This is one of the reasons why we adopt eq.(3.28) to study the phase transition.

Initial condition

We will solve eq.(3.28) and eq.(3.31) numerically. There are three parameters; μ^2, λ and κ. (m^2 is determined by eq.(3.28).) Since we assume that the loop expansion at $T=0$ is an valid approximation, the renormalization point κ is chosen so that $\mu^2=m^2$ is satisfied. This means that there is no effect from optimization at $T=0$. In other worlds, we use the OPT only for the resummation at finite T, (Note that $\mu^2=m^2$ at $T=0$ should be obtained from the result of solving eq.(3.28) and eq.(3.31) simultaneously.) Although the explicit values of the parameters are not important for our qualitative study (in fact, these parameters will be normalized by their initial values), following initial values are used, $\lambda=10.0$ and $\varphi_0=10.0$, for simplicity. As the result of solving eq.(3.28) and eq.(3.31) simultaneously, we obtain $\mu^2=m^2=-170$, $\kappa^2=87.6$ and $M^2=m^2+\frac{\lambda}{2}\varphi_0^2=330$.

[1] Here, $\frac{\partial V^{0+\delta+\delta^2}(\varphi,m^2)}{\partial m^2}$ means $\frac{dV^{0+\delta+\delta^2}(\varphi,M^2,m^2,g=\lambda,\chi,\eta=0)}{dm^2}$ as shown in Appendix D.

[2] Here, $\frac{\partial V^{0+\delta+\delta^2}(\varphi,m^2)}{\partial\varphi}$ means $\frac{dV^{0+\delta+\delta^2}(\varphi,M^2(\varphi),m^2,g=\lambda,\chi,\eta=0)}{d\varphi}$.

Results of numerical calculation

The results of numerical calculations in the PMS condition are shown in Fig.3.1. Fig.3.1 (A) shows the tree-level mass $M^2(T) = m^2(T) + \lambda\varphi_0/2$ with the left vertical scale and the optimized parameter $m^2(T)$ with the right vertical scale. $M^2(T)$ is clearly not tachyonic for all T. This result and eq.(3.30) confirm that OPT with two-loop PMS condition for $V(\varphi, m^2)$ is successful for the resummation of HTLs.

Fig.3.1 (B) shows the temperature dependence of the thermal expectation value ($\varphi_0(T) \equiv \langle\phi\rangle_T$) divided by φ_0 at zero temperature. From this result, the phase transition can be shown to be the second order. Fig.3.2 (A) shows the second derivative of $V(\varphi, m^2)$ with respect to φ, which also shows the second order nature of the transition. Since the transition is of second order, the effective potential becomes flat at $\varphi_0 = 0$ at the critical temperature T_c, which is expressed by the following equation:

$$\frac{\partial^2 V(\varphi = 0, m^2)}{\partial \varphi^2} = 0. \tag{3.33}$$

We can confirm this feature also from Fig.3.2 (A). The effective potentials at $T = 0$ and T_c are shown in Fig.3.2 (B). We note here that the second order transition for $\lambda\phi^4$-theory is expected from the renormalization group analysis [44] and lattice simulation at finite T [45].

We found that the critical exponent β which is defined by

$$\varphi_0(T) \propto \left|\frac{T - T_c}{T_c}\right|^{\beta} \tag{3.34}$$

becomes 0.5 in the two-loop analysis. This is the value expected from the Landau mean-field theory, which implies that our approximation is still within the level of the mean-field theory. Since OPT corresponds to a generalized mean field theory, it is in fact anticipated. A possibility of going beyond the mean-field exponents is discussed in Sec.3.5.

In Fig.3.2 (C), the minimum value of the thermal effective potential $V(\varphi_0, m^2)$, which is equivalent to the Gibbs free energy, is shown. Its value decreases monotonously as T increases.

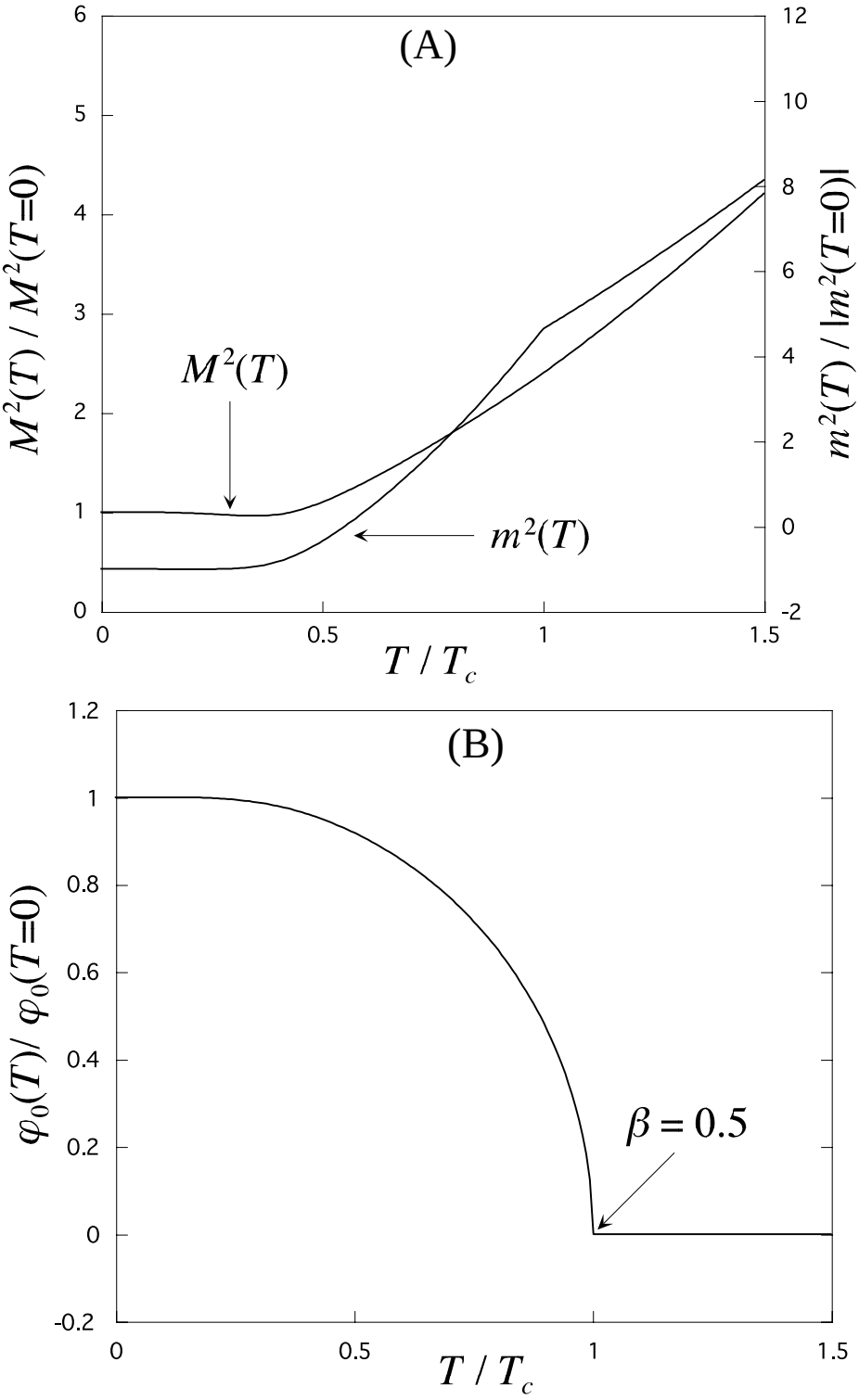

Figure 3.1: (A): The tree level mass $M^2(T) = m^2 + \lambda\varphi_0/2$ with the left vertical scale and the mass parameter $m^2(T)$ with the right vertical scale obtained from the PMS condition. They are normalized by their vales at $T = 0$. (B): Vacuum expectation value φ_0 normalized by $\varphi_0(T = 0)$.

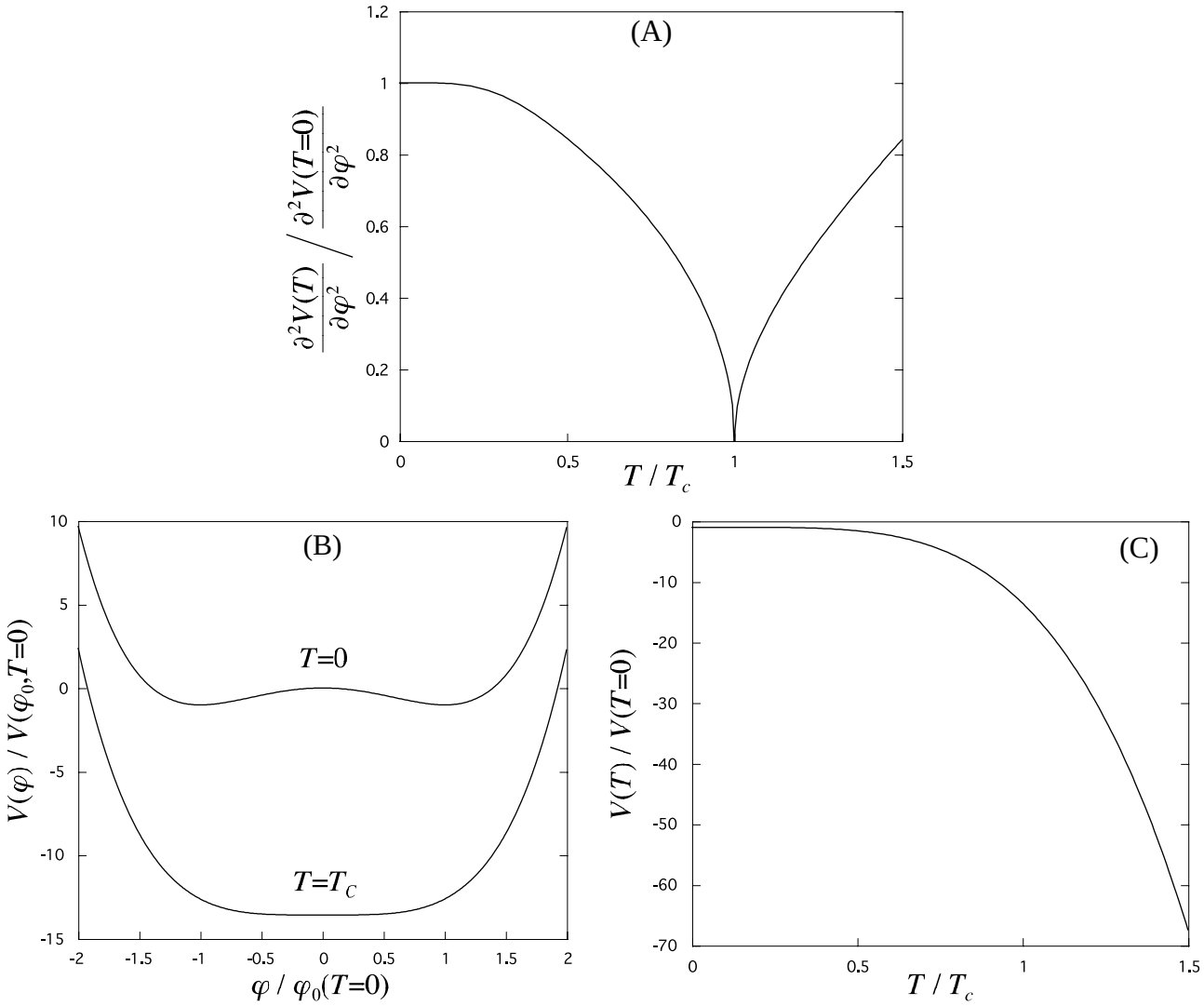

Figure 3.2: (A): Second derivative of $V(T)$ with respect to φ in the PMS condition. (B): Effective potentials at $T = 0$ and T_c. (C): Minimum values of the effective potential as a function of T.

3.4 The FAC condition

In this subsection, we apply the FAC condition. The simplest condition to resum the HTLs in this case is

$$\Sigma_R(\omega = 0, |\vec{k}| = 0; T) = 0, \tag{3.35}$$

where Σ_R is a retarded two-point self-energy which is defined as

$$\Sigma_R(\omega, \vec{k}; T) = \left. \frac{\partial^2 V(\varphi, m^2)}{\partial \varphi^2} \right|_{\varphi=\varphi_0}. \tag{3.36}$$

In the following, we will investigate the above condition in one-loop and two-loop orders.

3.4.1 1-loop analysis

The HTLs can be resummed even in the one-loop FAC condition of eq.(3.35). Therefore, many studies before [18] have adopted this condition for simplicity, and it could solve the tachyon problem at low T. However, the phase transition becomes first order in this condition [18]. Here, we don't recapitulate these results because they have been much discussed in the literature. Instead, we examine the two-loop condition of eq.(3.35) in Sec.3.4.2 to compare the result with that in PMS condition discussed in the Sec.3.3.2.

3.4.2 2-loop analysis

Since physics should not depend on artificial parameter m^2, one expects that the result should not depend on the choice of optimized conditions. However, the 2-loop PMS condition eq.(3.28) leads to the second order phase transition, and 1-loop FAC condition is known to lead to the first order transition. Therefore, it is necessary to study whether the FAC condition in the two-loop level gives the second order phase transition or not.

For the FAC condition in $O(\delta^2)$, we adopt

$$\Sigma_R^{\delta^2}(\omega, \vec{k}; T) = \left.\frac{\partial^2 V^{\delta^2}(\varphi, m^2)}{\partial \varphi^2}\right|_{\varphi=\varphi_0} = 0. \tag{3.37}$$

Explicit formula for V^{δ^2} is given in Appendix.D. At high T, eq.(3.37) is reduced to

$$\begin{aligned}\left.\frac{\partial^2 V^{\delta^2}}{\partial \varphi^2}\right|_{\varphi=0} \overset{\beta m^2 \to 0}{\longrightarrow} \quad & \frac{\lambda T}{16\pi m}(\chi - \frac{\lambda T^2}{24}) + \frac{\lambda^2 m^2}{2(4\pi)^4}\{c + (-2 + \frac{1}{2}\ln\frac{m^2}{\kappa^2})\ln\frac{m^2}{\kappa^2}\} \\ & + \frac{\lambda^2 T^2}{24(4\pi)^2}(3.30 - \ln\frac{T^2}{\kappa^2}).\end{aligned} \tag{3.38}$$

The first term of r.h.s. produces the resummation of the HTLs.

Initial condition

The initial parameters (at $T = 0$) are chosen as $\mu^2 = m^2$, $\lambda = 10.0$ and $\varphi_0 = 10.0$ as well as pervious section. $\mu^2 = m^2$ means our perturbation corresponds to the naive loop-expansion at $T = 0$. The resultant other values, which are determined by solving eq.(3.31) and eq.(3.37) simultaneously, are $\mu^2 = m^2 = -166$, $\kappa^2 = 137$ and $M^2 = m^2 + \frac{\lambda}{2}\varphi_0^2 = 334$.

Results of numerical calculation

The results are shown in Fig.3.3 and Fig.3.4. One can see that qualitative features of the figures are the same with the PMS results in Fig.3.1 and Fig.3.2 [3]. From Fig.3.3 (A), one can see that the tachyon problem is cured also in this case. Fig.3.3 (B), Fig.3.4 (A) and Fig.3.4 (B) show the second order phase transition with $\beta = 0.5$. The Gibbs free energy decreases uniformly (Fig.3.4 (C)). Thus, the 2-loop condition in both PMS and FAC give qualitatively the same results. This is a desired property and shows the validity of OPT.

[3]The physical reason for the shoulder structure around $T/T_c \simeq 0.7$ in Fig.3.3 (B) and Fig.3.4 (A) is not understood yet.

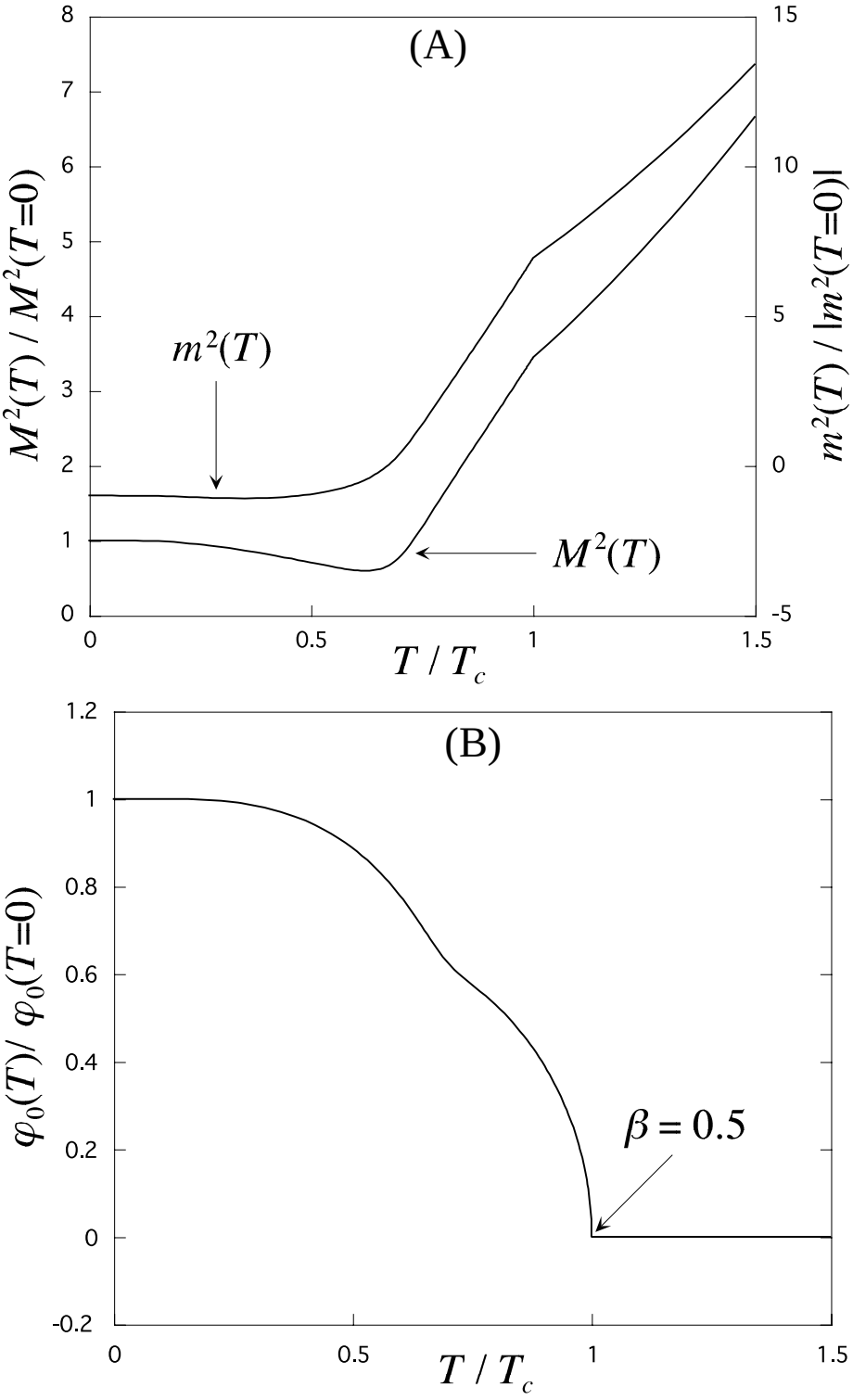

Figure 3.3: (A): The tree level mass $M^2(T) = m^2 + \lambda\varphi_0/2$ with the left vertical scale, and the mass parameter $m^2(T)$ with the right vertical scale in the case of the FAC condition. They are normalized by their values at $T = 0$. (B): Vacuum expectation value φ_0 normalized by $\varphi_0(T = 0)$.

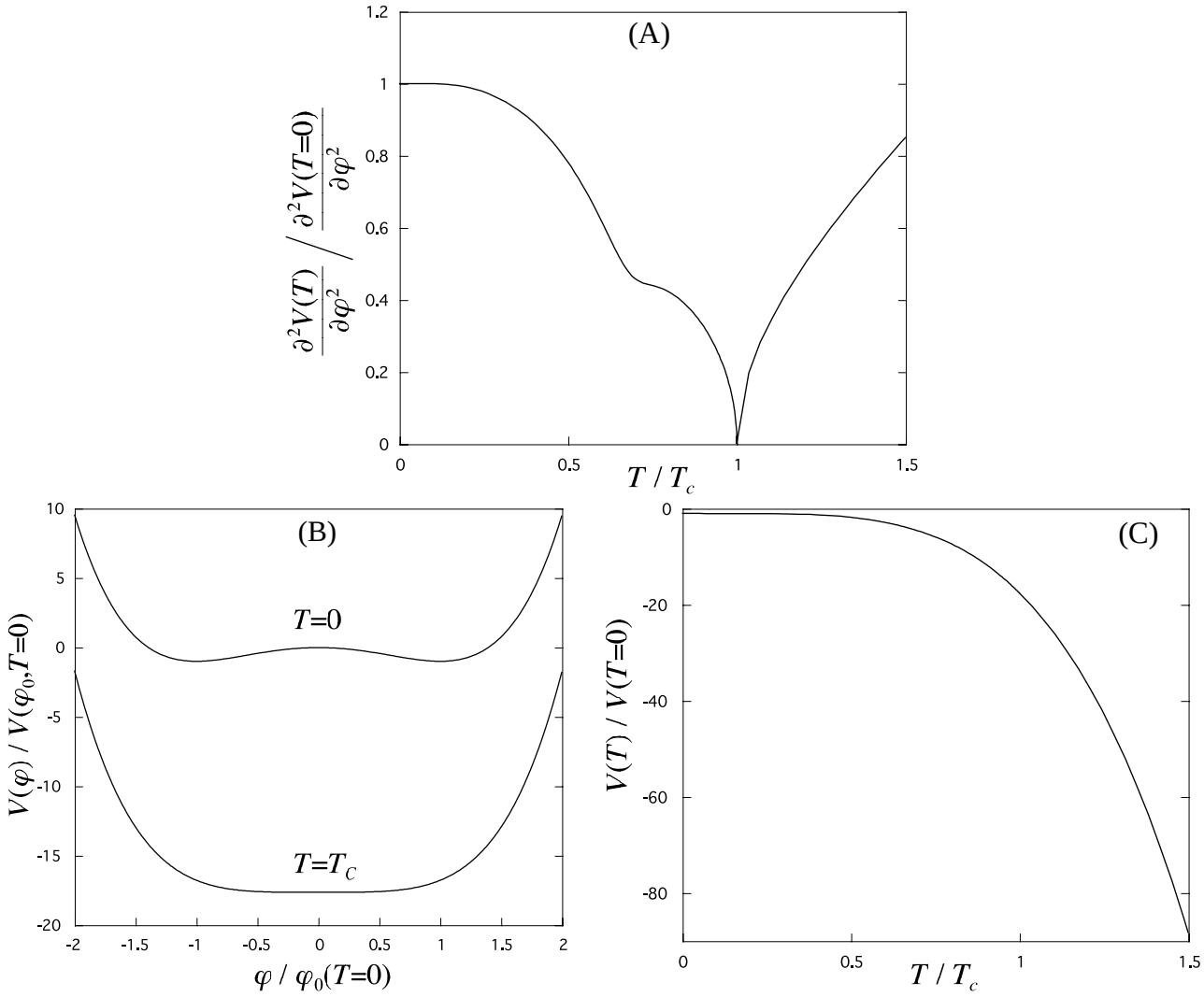

Figure 3.4: (A): Second derivative of $V(T)$ with respect to φ in the FAC condition. (B): Effective potential at $T = 0$ and T_c. (C): Minimum values of the effective potential as a function of T.

3.5 Some remarks

We tested the two conditions (3.28) and (3.37) in OPT to study the phase transition for $\lambda\phi^4$ theory. Both conditions give qualitatively the same results and show that the resummations are successfully done. However, there are three remarks in order.

FAC with $O(\delta)+O(\delta^2)$

One may try a two-loop FAC condition:

$$\Sigma_R^{\delta+\delta^2}(\omega,\vec{k};T)=\left.\frac{\partial^2 V^{\delta+\delta^2}(\varphi,m^2)}{\partial\varphi^2}\right|_{\varphi=\varphi_0}=0. \tag{3.39}$$

instead of (3.37). This condition implies that all the loop corrections vanish at zero external momentum. In other words, m^2 contains all contributions up to two-loop order. From eq.(3.39), the following equation follows:

$$\frac{\partial^2 V^{0+\delta+\delta^2}}{\partial\varphi^2}=M^2=m^2+\frac{\lambda}{2}\varphi^2. \tag{3.40}$$

At $T=T_c$, if one assumes a second order phase transition, eq.(3.40) must be zero, namely $m^2(=M^2)=0$. However, vanishing tree-level mass causes infrared divergence in the loop integrals. Actually, the left hand side (l.h.s) of eq.(3.31) diverges as $M^2\to 0$. Thus, $M^2=0$ is never satisfied at $T=T_c$. From this argument, one can see the second order phase transition cannot be achieved in the condition eq.(3.40). [4]

Full OPT

The full OPT, which includes an optimization of the coupling constant, has a possibility not only of avoiding the above infrared problem but also of going beyond the mean field approximation near T_c. Therefore, it will be very interesting to explore this direction. The PMS condition for $V(\varphi,m^2,g)$ in such an approach requires tree-loop calculation, which can be understood as follows. Suppose one chooses PMS condition in two-loop level as

$$\frac{\partial V^{0+\delta+\delta^2}(\varphi,m^2,g)}{\partial m^2}=0,\quad \frac{\partial V^{0+\delta+\delta^2}(\varphi,m^2,g)}{\partial g}=0. \tag{3.41}$$

(As shown in Appendix D, eq.(3.41) implies that eq.(D.19) and eq.(D.23) are equal to zero.) In the symmetric phase ($\varphi=0$), eq.(3.41) can be reduced to eq.(D.26) and eq.(D.27). From eq.(D.27), $K_t=0$ is obtained, which gives a solution for $m^2(\varphi)$. (Note that K_t depends on g only through $M^2=m^2+g\varphi^2/2$.) Then, it is substituted in eq.(D.26) as;

$$\left.\frac{\partial V(\varphi,m^2,g)}{\partial m^2}\right|_{\varphi=0}=\frac{\partial K_t}{\partial M^2}\chi=0. \tag{3.42}$$

[4] In ref.[23], they use eq.(3.39) as the FAC condition. Thus, their calculation leads to a first order phase transition. See also, ref.[46].

Since it also does not depend on g, we can't determine g. Thus, eq.(3.41) cannot give a solution for m^2 and g, simultaneously.

On the other hand, in the three-loop calculation, $V(\varphi, m^2, g)$ has a following term:

$$-g\frac{\partial K_t}{\partial M^2}(\chi + \frac{g}{2}K_t). \tag{3.43}$$

This leads to the HTLs (tadpole diagram) in $\partial V/\partial g$ in eq.(3.41), and eq.(3.41) obtains g-dependence even in the symmetric phase. Thus, the full OPT with PMS condition for tree-loop effective potential has a possibility to give a solution for m^2 and g simultaneously.

What about FAC condition in full OPT ? Suppose we take the following FAC condition:

$$\frac{\partial^2 V^{\delta^2}(\varphi, m^2, g)}{\partial \varphi^2} = 0, \quad \frac{\partial^4 V^{\delta^2}(\varphi, m^2, g)}{\partial \varphi^4} = 0. \tag{3.44}$$

Unfortunately, we could not find a solution which improves the previous results near T_c in the two-loop level. We have tried all possible variations ($V^{\delta^2}(\varphi, m^2, g)$ in eq.(3.44) is replaced by $V^{\delta+\delta^2}(\varphi, m^2, g)$, $V^{\delta}(\varphi, m^2, g)$ and so on), but improved solutions were not obtained for the critical exponent. Thus, in the two-loop order, it seems that it is not possible to improve the previous analysis near $T = T_c$ in the full OPT with FAC condition. In any case, further study along this line is necessary.

Limiting temperature

For sufficiently high T, there are no solutions in (3.28) and (3.37) for $m^2(T)$, because the logarithmic terms of the form $\ln(T/\kappa)$ dominate. This means the renormalization point κ, which is removed at $T = 0$, becomes a bad choice as T increases. To avoid this situation, one may try the renormalization group improvement. Since the typical "scale" of this system is temperature T, one may choose κ as $\kappa = T$. In this case, the logarithmic terms are fixed, and no large $\ln(T/\kappa)$ appears. This renormalization group improvement extends the applicability of OPT. However, in non-asymptotically free theories such as $\lambda\phi^4$ and $O(N)$ ϕ^4-theories, there eventually appears the Landau pole where the running coupling constant $\lambda(\kappa) = \lambda(T)$ diverges at a certain T [47, 48]. Thus, beyond this temperature, the theory is not applicable any more.

Chapter 4

The $O(4)$ linear σ model

In this chapter, we consider the $O(4)$ linear σ model to study the soft mode in QCD. Applying OPT is shown to be essential for this purpose. The soft mode has been widely studied in condensed matter physics as a signal of second order phase transition. From the results of lattice simulations [9] and renormalization group analysis [44], it is believed that the chiral transition in QCD with massless two flavors is of second order. Then, it is important to study such soft mode in QCD. Unfortunately, the lattice QCD simulations cannot treat the real-time modes in a straight forward way [11]. Therefore, we have studied the soft mode using an effective theory of QCD [16, 17], which is the $O(4)$ linear σ model.

The spectral function of the mesic mode in QCD is defined as

$$\rho_\phi(\omega, \vec{k}; T) \equiv -\frac{1}{\pi}\mathrm{Im}D^R_\phi(\omega, \vec{k}; T), \tag{4.1}$$

where $D^R_\phi(\omega, \vec{k}; T)$ is the retarded correlation function

$$D^R_\phi(\omega, \vec{k}; T) = -i\int d^4x e^{ikx}\theta(t)\langle[\phi(t, \vec{x}), \phi(0, \vec{0})]\rangle_T. \tag{4.2}$$

$\phi(t, \vec{x})$ is quark bilinears such as $\bar{q}q(t, \vec{x})$ or $\bar{q}i\gamma_5 q(t, \vec{x})$ in QCD, and $\langle\cdots\rangle_T$ denotes the thermal expectation value. This spectral functions of mesons at finite T were first studied in [49] using the Nambu-Jona-Lasinio model as an effective theory of QCD in the large N_c limit. This analysis shows that the mass and the width of the scalar meson σ, which has a large width due to the strong decay $\sigma \to 2\pi$ at $T = 0$, decreases as T increases. Eventually, σ shows up as a sharp resonance near the critical point of the chiral transition. Also, the detectability of such resonance was studied in the context of the ultra-relativistic heavy ion collisions [50]. Also, the spectral integrals in QCD at finite T were studied using the operator product expansion [51].

In the following, we adopt a toy model "the $O(4)$ linear σ model" in the 1-loop level at finite T to study ρ_ϕ. This model is written in terms of the pseudo scalar

meson π and the scalar meson σ, and has the common $O(4)$ symmetry with the two flavor QCD. Therefore, we can regard this model as a low energy effective theory of QCD, and it has been used to study the real-time dynamics and critical phenomena [52, 53] from its tractableness.

4.1 Determination of the parameters at $T = 0$

The Lagrangian of the $O(4)$ linear σ model [1] is

$$\begin{aligned}\mathcal{L} &= \frac{1}{2}[(\partial\vec{\phi})^2 - \mu^2\vec{\phi}^2] - \frac{\lambda}{4!}(\vec{\phi}^2)^2 + h\sigma \\ &\quad + \frac{1}{2}A(\partial\vec{\phi})^2 - \frac{1}{2}B\mu^2\vec{\phi}^2 - \frac{1}{4!}C(\vec{\phi}^2)^2 + D\mu^4, \end{aligned} \tag{4.3}$$

with $\vec{\phi} = (\sigma, \vec{\pi})$. $\kappa^{2\varepsilon}$ in which should appear front of λ in the dimensional regularization is dropped for simplicity. (κ is the renormalization point and $\varepsilon = (4-n)/2$.) $h\sigma$ is an explicit symmetry breaking term which plays a role of the small finite quark masses in QCD. The π meson obtains a mass by this term in the symmetry broken phase. The second line of eq.(4.3) shows counter terms, and their one-loop values are

$$A = 0, \quad B = \frac{\lambda}{(4\pi)^2}\frac{1}{\bar{\varepsilon}}, \quad C = \frac{\lambda^2}{(4\pi)^2}\frac{2}{\bar{\varepsilon}}, \quad D = -\frac{1}{(4\pi)^2}\frac{1}{\bar{\varepsilon}}, \tag{4.4}$$

where $\bar{\varepsilon} \equiv \frac{2}{4-n} - \gamma + \ln(4\pi)$ with γ being the Euler constant.

When $\mu^2 < 0$, this model breaks the symmetry as $O(4) \to O(3)$. The replacement $\sigma \to \sigma + \xi$ leads to the Lagrangian

$$\begin{aligned}\mathcal{L} &= \frac{1}{2}[(\partial\sigma)^2 - m_{0\sigma}^2\sigma^2] + \frac{1}{2}[(\partial\vec{\pi})^2 - m_{0\pi}^2\vec{\pi}^2] \\ &\quad + \frac{\lambda\xi}{3!}\sigma\vec{\phi}^2 + \frac{\lambda}{4!}(\vec{\phi}^2)^2 + (-m_{0\pi}^2\xi + h)\sigma \\ &\quad + \frac{1}{2}A(\partial\vec{\phi})^2 - \frac{1}{2}B\mu^2\{(\sigma+\xi)^2 + \vec{\pi}^2\} - \frac{1}{4!}C\{(\sigma+\xi)^2 + \vec{\pi}^2\}^2 + D\mu^4, \end{aligned} \tag{4.5}$$

where $\xi \equiv \langle\sigma\rangle_T$ and

$$m_{0\sigma}^2 = \mu^2 + \frac{\lambda}{2}\xi^2, \quad m_{0\pi}^2 = \mu^2 + \frac{\lambda}{6}\xi^2. \tag{4.6}$$

[1] This is also called the $SU_L(2) \times SU_R(2)$ linear σ model. It is invariant under the $SU(2)$ and axial $SU(2)$ transformations

$$\left\{\begin{array}{lcl}\sigma & \to & \sigma \\ \vec{\pi} & \to & \vec{\pi} + \vec{\alpha}\times\vec{\pi}\end{array}\right., \quad \left\{\begin{array}{lcl}\sigma & \to & \sigma + \vec{\beta}\cdot\vec{\pi} \\ \vec{\pi} & \to & \vec{\pi} + \vec{\beta}\sigma\end{array}\right. .$$

This is consistent with the chiral transformation in eq.(1.1), if one assume $\sigma \sim \bar{q}q$ and $\vec{\pi} \sim \bar{q}\frac{\vec{\tau}}{2}i\gamma_5 q$, where $\vec{\tau}$ is the Pauli matrix.

$m_{\sigma peak}$ (MeV)	μ^2 (MeV^2)	λ	h (MeV^3)	κ (MeV)	Γ (MeV)
550	-284^2	73.0	123^3	255	260
750	-375^2	122	124^3	325	657
1000	-469^2	194	125^3	401	995

Table 4.1: Vacuum parameters corresponding to $m_{\sigma peak} = 550$, 750, 1000 MeV

ξ is determined by the stationary condition of the effective potential;

$$\left.\frac{\partial V(\vec{\varphi}^2)}{\partial \sigma}\right|_{\sigma=\xi,\vec{\pi}=0} = 0. \tag{4.7}$$

To determine the renormalized couplings μ^2, λ, h and the renormalization point κ at $T = 0$, we adopt the following physical conditions:

1. Physical mass condition for the pion;

$$D_\pi^{-1}(k^2 = m_\pi^2) = 0. \tag{4.8}$$

   Here, we take $m_\pi = 140$ MeV, and D_π is the Feynman propagator for the pion in the one-loop order.

2. Partially conserved axial-vector current (PCAC) relation in one-loop;

$$f_\pi m_\pi^2 = h\sqrt{Z_\pi}. \tag{4.9}$$

   Here $f_\pi = 93$ MeV and Z_π is the finite wave function renormalization constant for the pion on its mass-shell.

3. The peak position of the spectral function in the σ channel

$$\left.\frac{\partial \rho_\sigma(k^2)}{\partial k^2}\right|_{k^2=m^2_{\sigma peak}} = 0. \tag{4.10}$$

   The $m_{\sigma peak}$ is taken to be 550 MeV, 750 MeV or 1000 MeV (see below).

4. On-shell condition for the pion:

$$m_{0\pi} = m_\pi = 140\text{MeV}, \tag{4.11}$$

   where $m_{0\pi}$ is the tree-level mass defined in (4.6) and m_π is the physical pion mass.

Recently, the σ meson was reported in the Particle Data Table [54] as

$$\sqrt{s_{pole}} = (400 - 1200) - i(300 - 500),$$
$$m_{BW} = 400 - 1200, \quad \Gamma_{BW} = 600 - 1000, \tag{4.12}$$

where s_{pole} is the pole position in the complex s-plane and m_{BW} (Γ_{BW}) is Breit-Wigner mass (width). Since the σ meson has a large width, we define the physical mass as its peak position of the spectral function. The mass of the σ meson determined from eq.(4.10) is chosen so that the value covers the range of experimental ambiguity. Instead of eq.(4.10), one may take the π-π scattering phase shift [52] to determine the parameters. Recently, the π-π scattering phase shift has been re-analyzed in [55] and we can use these results, and our choice (4.10) is consistent with these results. However, our main conclusions do not receive qualitative change by the different choice of the σ meson mass.

The condition $m_{0\pi} = m_\pi$ in (4.11) is crucial for our purpose. Generally speaking, the condition to determine the renormalization point κ is optional [56]. However, since we are interesting in the spectral function, $m_{0\pi} = m_\pi$ is the most relevant condition. This is because the spectral function in the σ channel starts from a continuum threshold which is determined by the tree-level pion mass $m_{0\pi}$. Therefore, we obtain the physical threshold at $\sqrt{s_{th}} = 2m_\pi = 280$ MeV by the condition of (4.11) even in the one-loop level.

Resultant parameters are summarized in Table 4.1. In Fig.4.1 shown is the spectral functions ρ_σ and ρ_π defined in (4.1) at $T = 0$ with $s \equiv \omega^2 - \mathbf{k}^2$. ρ_π has a one particle peak at 140 MeV and a continuum. This continuum spectrum is made by multi-particles states ($\pi + \sigma$ state) which starts from $\sqrt{s_{th}} = m_{0\pi} + m_{0\sigma}$ in the one-loop approximation [2]. In the σ channel, ρ_σ does not have one particle pole, and shows a broad peak starting from the threshold $2m_{0\pi} = 280$ MeV. We define the peak position of this spectrum as the physical σ-meson mass. Since the σ meson has a large phase space for decaying into two pions due to the strong $\sigma - 2\pi$ coupling, the width becomes very large at $T = 0$. The half width of the peak is 260 MeV, 657 MeV and 995 MeV for $m_{\sigma peak} = 550$ MeV, 750 MeV and 1000 MeV, respectively. This indicates that the σ pole is located far from the real axis on the complex s plane.

[2] In the two-loop level, the lowest threshold becomes $\sqrt{s_{th}} = 3m_{0\pi}$ ($< m_{0\sigma}$)

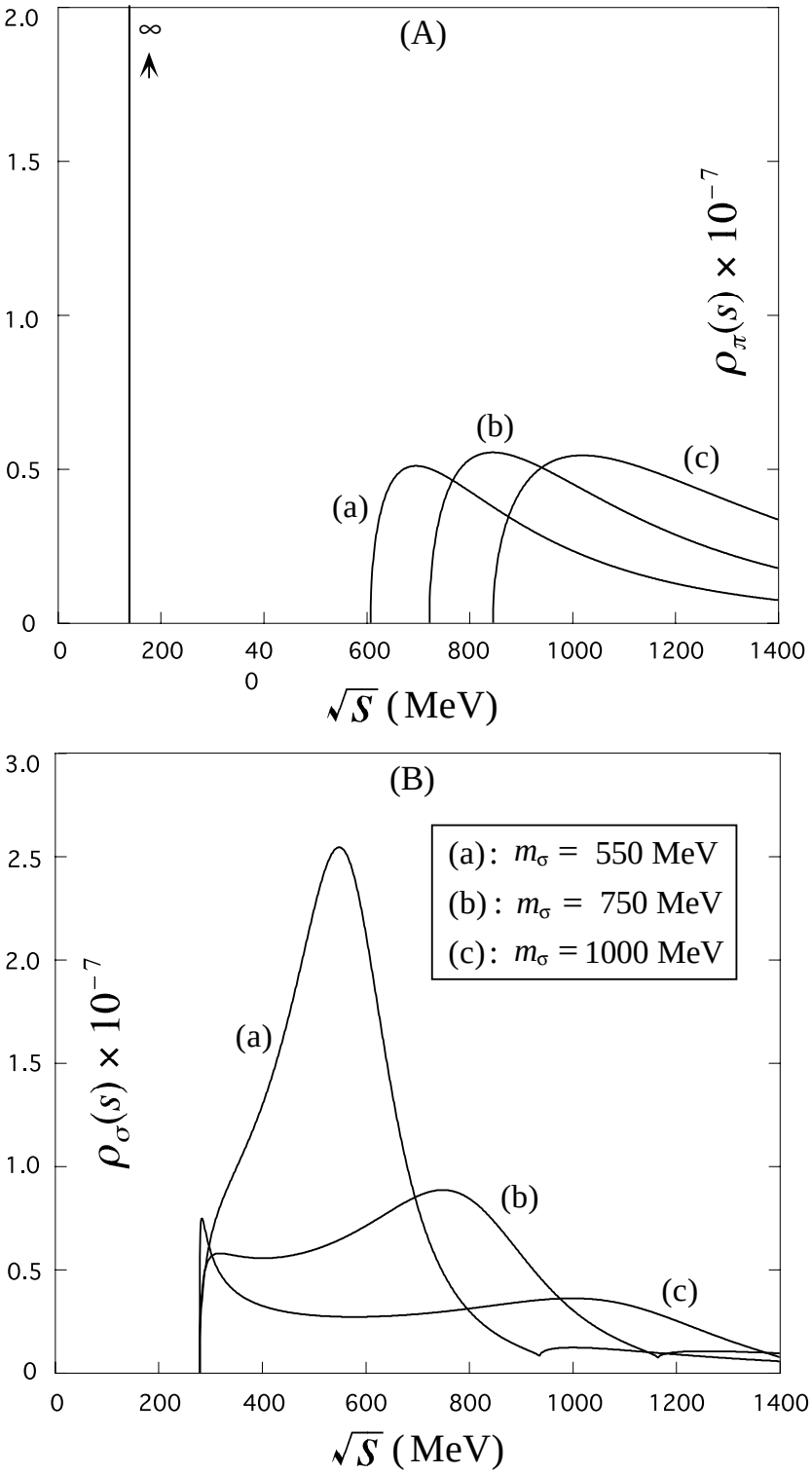

Figure 4.1: Spectral functions at $T = 0$ in the π channel (A) and in the σ channel (B) for $m_{\sigma peak} = 550$ MeV, 750 MeV and 1000 MeV.

4.2 Application of OPT

Now, let us apply OPT to the $O(4)$ linear σ model. In this application, we consider only a mass optimization for simplicity. Similar to the case of $\lambda\phi^4$ theory, HTLs are only tadpole type diagrams in this model. Therefore, a resummation to cure the various problems in the finite T perturbation theory can be carried out in the one-loop FAC condition for the self-energy of the pion.

According to Step 2 in Sec. 2.2.2, we rewrite eq.(4.3) in $O(\delta)$ as

$$\begin{aligned}\mathcal{L} &= \frac{1}{2}[(\partial\vec{\phi})^2 - m^2\vec{\phi}^2] - \frac{\lambda}{4!}(\vec{\phi}^2)^2 + \frac{1}{2}\chi\vec{\phi}^2 + h\sigma \\ &\quad -\frac{1}{2}Bm^2\vec{\phi}^2 - \frac{1}{4!}C(\vec{\phi}^2)^2 + Dm^4. \end{aligned} \tag{4.13}$$

Since χ is already $O(\delta)$, $B\chi$ and $2Dm^2\chi$ starts from $O(\delta^2)$, and $D\chi^2$ start from $O(\delta^3)$. Therefore, these terms can be neglected in the one loop approximation.

The thermal effective potential $V(\vec{\varphi}, m^2)$ is obtained by the similar calculation with that in $\lambda\phi^4$ theory in the previous chapter;

$$\begin{aligned}V(\vec{\varphi},m^2) &= \frac{1}{2}\mu^2\varphi^2 + \frac{\lambda}{4!}(\vec{\varphi}^2)^2 - h\sigma \\ &\quad +\frac{1}{64\pi^2}\left[m_{0r}^4 \ln\left|\frac{m_{0r}^2}{\kappa^2 e^{3/2}}\right| + 3m_{0c}^4 \ln\left|\frac{m_{0c}^4}{\kappa^2 e^{3/2}}\right|\right] \\ &\quad +T\int\frac{d^3k}{(2\pi)^2}\left[\ln(1-e^{-E_r/T}) + 3\ln(1-e^{-E_c/T})\right], \end{aligned} \tag{4.14}$$

where,

$$m_{0r}^2 = m^2 + \frac{\lambda}{2}(\vec{\varphi}^2)^2, \quad m_{0c}^2 = m^2 + \frac{\lambda}{6}(\vec{\varphi}^2)^2, \tag{4.15}$$

and $E_i \equiv \sqrt{\vec{k}^2 + m_{0i}^2}$ for $i = r, c$. The first term $\frac{1}{2}\mu^2\varphi^2$ of the r.h.s in eq.(4.14) is the sum of $\frac{1}{2}m^2\varphi^2$ (which is $O(\delta^0)$) and $-\frac{1}{2}\chi\varphi^2 = -\frac{1}{2}(m^2-\mu^2)\varphi^2$ (which is $O(\delta)$). The stationary point ξ is determined by

$$\left.\frac{\partial V(\vec{\varphi}^2, m^2)}{\partial\sigma}\right|_{\sigma=\xi,\vec{\pi}=0} = 0 \tag{4.16}$$

as well as eq.(4.7). As we have mentioned before, the derivative with respect to σ does not act on m^2. When $\xi \neq 0$, the tree-level masses become

$$m_{0\pi}^2 = m^2 + \frac{\lambda}{6}\xi^2, \quad m_{0\sigma}^2 = m^2 + \frac{\lambda}{2}\xi^2. \tag{4.17}$$

μ^2 is replaced by m^2 which has extra temperature dependence through the gap-equation obtained in Sec.4.2.1.

In the finite T perturbation theory, a general form of the retarded propagator can be written as

$$iD_\phi^R(\omega,\vec{k};T) = \frac{i}{k^2 - m_{0\phi}^2 - \Sigma_\phi^R(\omega,\vec{k};T)}, \tag{4.18}$$

where $k^2 = \omega^2 - \mathbf{k}^2$. From eq.(4.1), the spectral function is written as

$$\rho_\phi(\omega,\vec{k};T) = -\frac{1}{\pi}\frac{\mathrm{Im}\Sigma_\phi^R}{(k^2 - m_{0\phi}^2 - \mathrm{Re}\Sigma_\phi^R)^2 + (\mathrm{Im}\Sigma_\phi^R)^2}. \tag{4.19}$$

In the real time formalism, the retarded self-energy Σ_ϕ^R is calculated as follows [38].

1. Calculate the 11-component of the 2×2 self-energy: $\Sigma_\phi^{ab}(\omega,\vec{k})$ $(a,b = 1,2)$.

2. The 11-component of the self-energy is related to the retarded self-energy through the following equations:

$$\begin{aligned} \mathrm{Re}\Sigma_\phi^R(\omega,\vec{k};T) &= \mathrm{Re}\{\Sigma_\phi^{11}(\omega,\vec{k}) + \Sigma_\phi^{11}(\omega,\vec{k};T)\}, \\ \mathrm{Im}\Sigma_\phi^R(\omega,\vec{k};T) &= \tanh(\frac{\omega}{2T})\mathrm{Im}\{\Sigma_\phi^{11}(\omega,\vec{k}) + \Sigma_\phi^{11}(\omega,\vec{k};T)\}. \end{aligned} \tag{4.20}$$

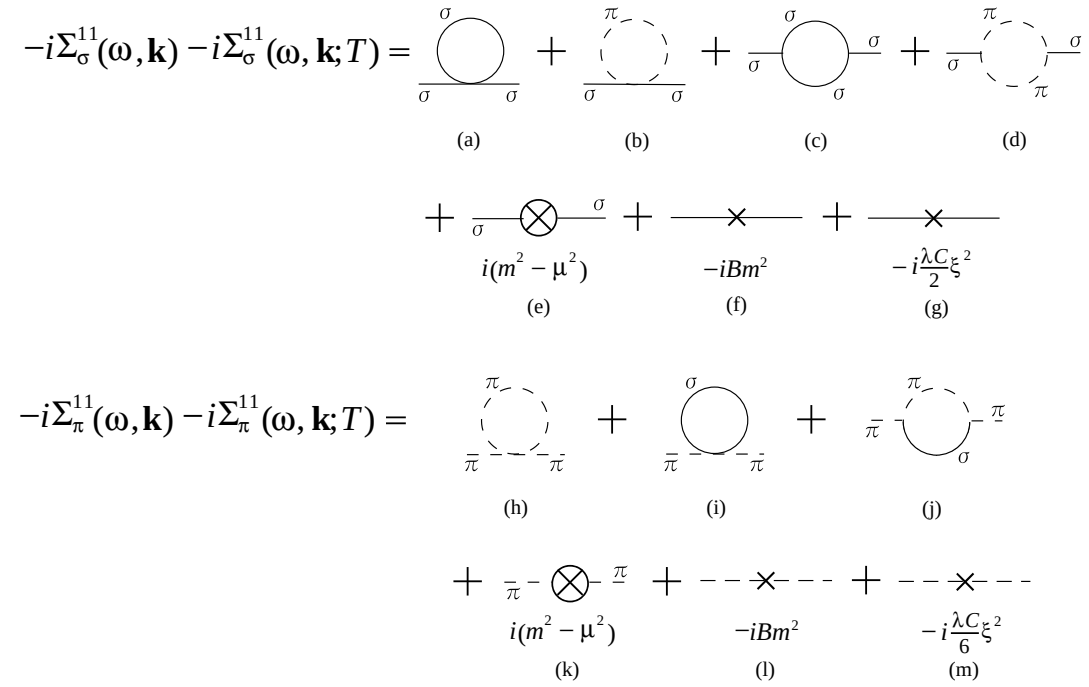

Figure 4.2: One-loop self-energy Σ^{11} for σ and π in OPT at finite T.

Here we defined a T-independent 11-component self-energy $\Sigma_\phi^{11}(\omega,\vec{k})$ and an explicit T-dependent 11 self-energy $\Sigma_\phi^{11}(\omega,\vec{k};T)$. The term "explicit" means that it has the

Bose-Einstein distribution functions. Note that $\Sigma_\phi^{11}(\omega, \vec{k})$ depends implicitly on T through $m^2(T)$ and $\xi(T)$.

Fig.4.2 shows one-loop diagrams in OPT for Σ_ϕ^{11}. Their explicit calculations are given in Appendix E. One can easily check that the NG theorem discussed in Sec.2.4 is satisfied by comparing eq.(4.16) and the inverse pion propagator at zero momentum $[D_\pi^R(0, \vec{0}; T)]^{-1}$.

4.2.1 FAC condition

As a condition for optimization, we take a FAC condition for the self-energy of the pion in the one-loop level. Since the PMS condition for the thermal effective potential requires two-loop calculations to resum the HTLs as explained in the previous chapter, an economical way to resum the HTLs is the FAC condition. However, it must be noted that the calculation in two-loop order is necessary in order to obtain the right second order phase transition in the chiral limit. As will be shown in Sec.4.2.2, the phase transition does not occur, namely cross over, when the pion mass takes the realistic value: $m_\pi = 140$ MeV. Therefore, in the real world case, the FAC condition in the one-loop order may still be valid. (See, Sec.4.2.3.)

Since we are interested in the spectral functions, a possible FAC condition is

$$\Sigma_\pi^R(\omega = m_\pi, \vec{0}; T) = 0. \tag{4.21}$$

This condition gives the correct threshold for the σ channel because it is determined by the tree-level mass $m_{0\pi}$. However, eq.(4.21) does not always have a real solution for m^2. At finite T, the pion obtains a width due to the Landau damping process;

$$\pi + \pi^{thermal} \to \sigma. \tag{4.22}$$

Here, $\pi^{thermal}$ is a background thermal π meson. Therefore, when the kinematics are satisfied in the above process, eq.(4.21) has an imaginary part. For static pion, the energy-momentum conservation law reads

$$\begin{aligned} \pi(\omega, \vec{0}) + \pi^{thermal}(E_\pi, \vec{k}) &\to \sigma(E_\sigma, \vec{k}), \\ \omega + \sqrt{\vec{k}^2 + m_{0\pi}^2} &= \sqrt{\vec{k}^2 + m_{0\sigma}^2}. \end{aligned} \tag{4.23}$$

From eq.(4.23) and $k^2 \geq 0$ constraint, we obtain the following region where Landau damping occurs;

$$0 \leq \omega^2 \leq (m_{0\sigma} - m_{0\pi})^2, \quad (m_{0\sigma} + m_{0\pi})^2 \leq \omega^2. \tag{4.24}$$

Therefore, the lowest pion pole has an imaginary part when $m_\pi(= \omega) + m_{0\pi} \leq m_{0\sigma}$. Note that it is purely the thermal background effect.

To avoid the problem of imaginary m^2, one may try another condition,

$$\Sigma_\pi^R(\omega = 0, \vec{0}; T) = 0. \tag{4.25}$$

This condition is investigated in [23] in the two-loop level ($L = n = 2$) for $\lambda\phi^4$ theory above T_c. Since $\mathrm{Im}\Sigma_\pi^R(\omega = 0, \vec{0}; T)$ vanishes identically, a real solution for m^2 exists. Unfortunately, eq.(4.25) is incompatible with the condition eq.(4.11) at $T = 0$ for finding the optimal renormalization point κ:

$$\Sigma_\pi^R(\omega = m_{0\pi}, \vec{0}; T = 0) = 0. \tag{4.26}$$

Thus, we adopt a hybrid condition

$$\Sigma_\pi^{11}(\omega = m_{0\pi}, \vec{0}) + \Sigma_\pi^{11}(\omega = 0, \vec{0}; T) = 0. \tag{4.27}$$

This condition is consistent with eq.(4.26). Also, there is no imaginary part from the Landau damping.

From Appendix E, the explicit form of the self-energy for pion can be obtained as

$$\Sigma_\pi^{11}(\omega = m_{0\pi}, \vec{0}) = \frac{\lambda}{6}\left[5\tilde{I}_\pi^{(1)} + \tilde{I}_\sigma^{(1)} - i\frac{2}{3}\lambda\xi^2\tilde{I}^{(3)}\right]_{\omega=m_{0\pi}} - (m^2 - \mu^2), \tag{4.28}$$

$$\Sigma_\pi^{11}(\omega = 0, \vec{0}; T) = \frac{\lambda}{6}\left[5F_\pi^{(1)} + F_\sigma^{(1)} - i\frac{2}{3}\lambda\xi^2\ (F^{(4)} + F^{(5)})\right]_{\omega=0} \tag{4.29}$$

The function $\tilde{I}$ is defined as the finite part of I, and the definitions of I and F are found in Appendix E.

Since eq.(4.29) vanishes by definition at $T = 0$, eq.(4.27) must reduce to eq.(4.26). There is only one solution which satisfies this condition:

$$m^2(T = 0) = \mu^2. \tag{4.30}$$

Thus, at $T = 0$, OPT with the FAC condition (4.27) is equivalent to the ordinary loop expansion.

At high T, the approximate $O(4)$ symmetry of eq.(4.13) is restored, and $\xi(T)$ approaches zero. In that phase, the gap-equation eq.(4.27) reduces to

$$m^2 = \mu^2 + \lambda\left[\int\frac{d^3k}{(2\pi)^3}\frac{n_B(E(m))}{E(m)} + \frac{m^2}{16\pi^2}\ln\frac{m^2}{e\kappa^2}\right], \tag{4.31}$$

with $E(m) = \sqrt{m^2 + \vec{k}^2}$. When $\beta M^2 \simeq \beta m^2 \ll 1$, the thermal part (the first term in the large parenthesis) dominates and eq.(4.31) reduces to

$$m^2(T) = \mu^2 + \frac{\lambda}{12}T^2. \tag{4.32}$$

This is nothing but the Debye screening mass in the $O(4)$ scalar model, and is thus desired at high T. Note also that eq.(4.21) and eq.(4.25) have the same solution at high T. However, in this model, the coupling λ is not so small (see, Table 4.1), and the condition $\beta m^2 \ll 1$ is not realized as a solution of eq.(4.27) at high T. Thus, we needs to solve eq.(4.27) numerically which will be shown in Sec.4.2.2.

For intermediate values of T, namely $\xi \sim T$, there is no reason that the cactus diagrams Fig.4.2 (h,i) dominate. Fig.4.2 (h,i) are roughly of $O(\lambda T^2)$ and Fig.4.2 (j) is of $O(\lambda^2\xi^2 T/M)$. In order for $\xi \sim M$, Fig.4.2 (j) may be larger than Fig.4.2 (h,i). Thus, we should not neglect the contribution like Fig.4.2 (j) for the gap-equation. OPT with the FAC condition (4.27) can sum not only the cactus diagrams Fig.4.2 (h,i) but also the diagram Fig.4.2 (j).

Similar to the results in the previous chapter, there is no solution of eq.(4.27) at sufficiently high T with a fixed κ. The limiting temperature is $T_l = 500, 430, 420$ MeV for $m_{\sigma peak}(T=0) = 500, 750, 1000$ MeV, respectively. Also, it can be show that this difficulty is cured by the renormalization group improvement. However, the Landau pole exists in any case, and the running coupling $\lambda(\kappa = T)$ diverges at $T = 440, 450, 490$ MeV for $m_{\sigma peak}(T=0) = 500, 750, 1000$ MeV, respectively. Thus, one again encounters an upper bound of T which limits the validity of the one loop analysis in OPT.

4.2.2 Numerical Results

Temperature dependence of the mass parameters and the condensate are shown in Fig.4.3 and Fig.4.4. Fig.4.3 (A) shows the tree-level masses eq.(4.17) and the artificial mass parameter $m^2(T)$ for $m_{\sigma peak}(T=0) = 550$ MeV. The tree-level masses $m^2_{0\phi}(T)$ don't show tachyonic behavior and approaches to $m^2(T)$ (because $\xi(T) \to 0$). Therefore, tachyon problem is cured by OPT with the FAC condition eq.(4.27).

Fig.4.3 (B) shows the chiral condensate $\xi(T)$, which is defined by eq.(4.16), for $m_\pi(T=0) = 140$ MeV and $m_\pi(T=0) = 30$ MeV with $m_{\sigma peak} = 550$ MeV. $\xi(T)$ decreases uniformly as T increases, which is a behavior expected for the chiral condensate away from the chiral limit. As $h \to 0$, namely approaching the chiral limit, $\xi(T)$ starts to have sudden change at a certain temperature. Below a critical value of h, $\xi(T)$ develops multiple solutions for given T, which could be an indication of a first order phase transition. This will be discussed in the next subsection.

$m_\pi(T=0) = 30$ MeV corresponds to the case just below the critical value of h which is shown by the dashed line in Fig.4.3 (B) for comparison. By using the Gell-Mann-Oakes-Renner relation [57], we can translate the pion mass to the quark

mass. The critical mass of the quark $m_q^{\rm crit.}$ corresponding to the critical h reads

$$\frac{m_q^{\rm crit.}}{m_q^{\rm phys.}} = \left(\frac{m_\pi^{\rm crit.}}{m_\pi^{\rm phys.}}\right)^2 = 0.08, \tag{4.33}$$

where $m_q^{\rm phys.}$ is the physical light-quark mass to $m_\pi^{\rm phys.} = 140$ MeV. The critical temperature T_c, which is defined as a point in which the derivative of $\xi(T)$ with respect to T diverges, is $T_c \simeq 170$ MeV for $m_q^{\rm crit.}/m_q^{\rm phys.} = 0.08$.

Fig.4.4 (A) shows $m_{0\phi}^2(T)$ for $m_{\sigma peak}(T=0) = 750, 1000$ MeV with $m_\pi = 140$ MeV. The qualitative behaviors are similar to Fig.4.3 (A). Also, Fig.4.4 (B) shows the chiral condensate $\xi(T)$ for $m_\sigma(T=0) = 750, 1000$ MeV. A qualitative difference from Fig.4.4 (A) and (B) is not observed. Therefore, our results are insensitive to the choice of the σ meson mass as far as $m_\pi(T=0) = 140$ MeV is imposed.

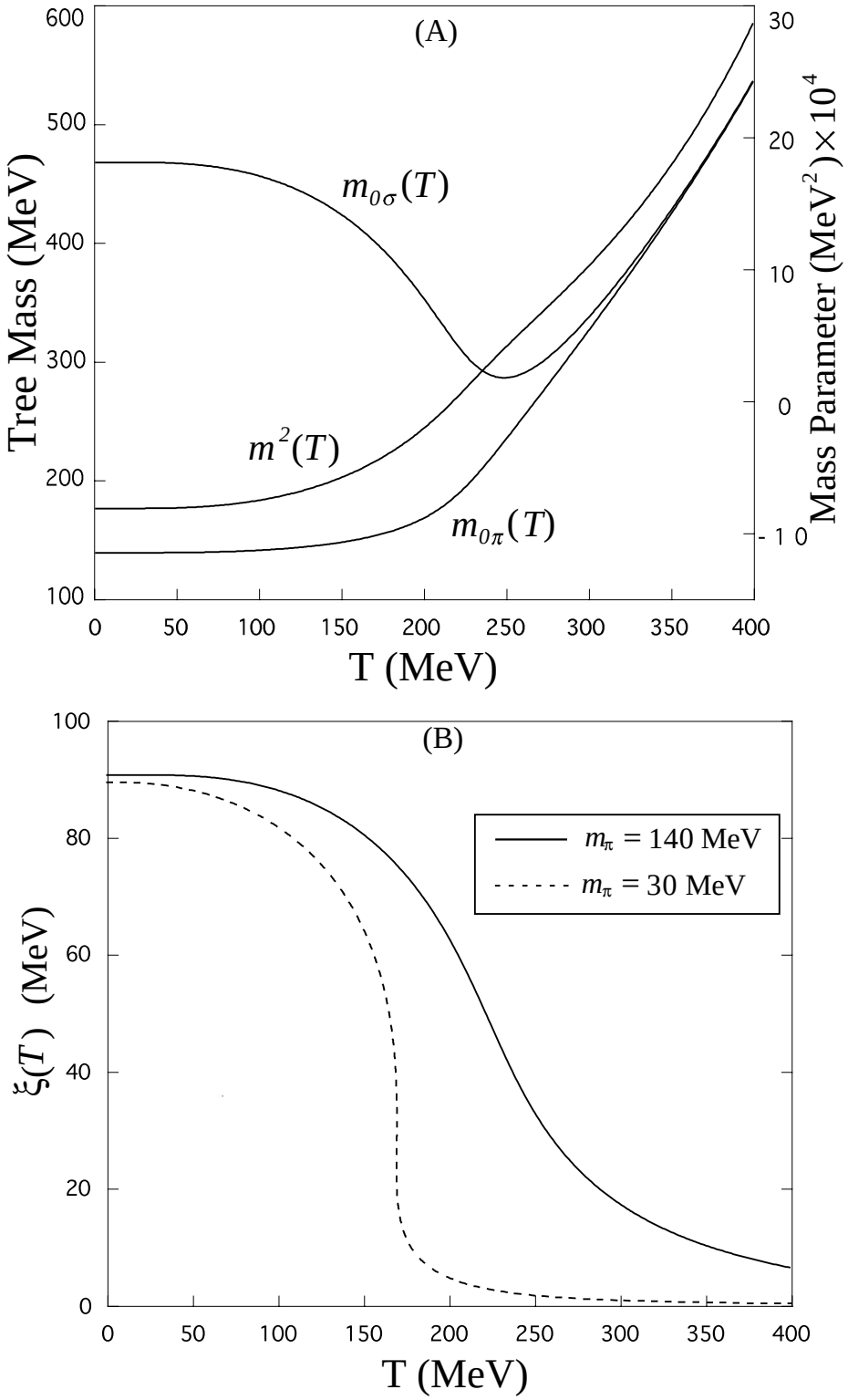

Figure 4.3: (A) Masses in the tree-level $m_{0\pi}(T)$ and $m_{0\sigma}(T)$ shown with left vertical scale, and the mass parameter $m^2(T)$ with the right vertical scale. (B) $\xi(T)$ for $m_\pi(T=0) = 140$ MeV and 30 MeV with $m_{\sigma peak}(T=0) = 550$ MeV.

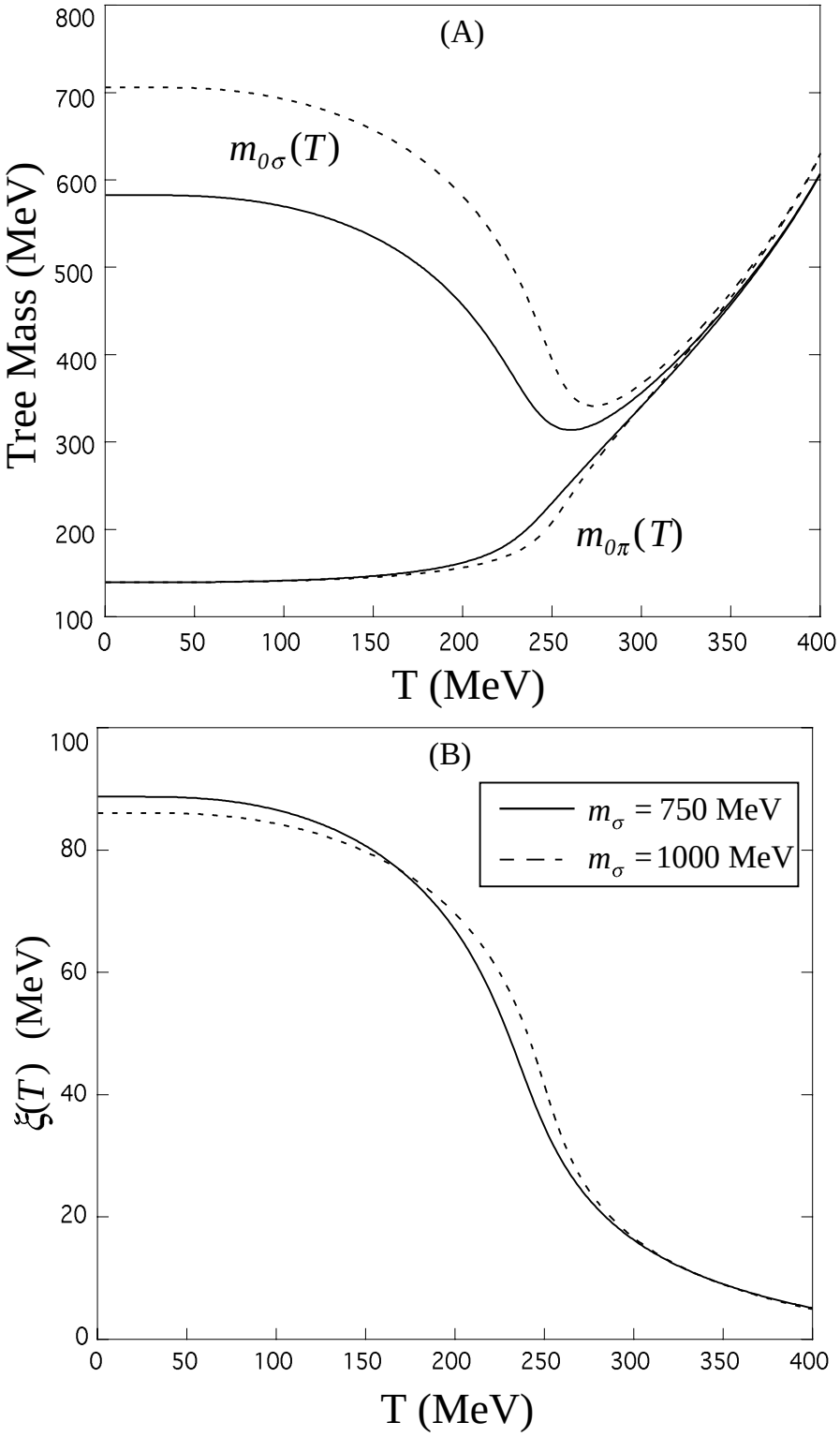

Figure 4.4: (A) Masses in the tree-level $m_{0\pi}(T)$ and $m_{0\sigma}(T)$. (B) $\xi(T)$ for $m_{\sigma peak}(T=0) = 750$MeV and 1000 MeV with $m_\pi = 140$ MeV.

4.2.3 Chiral limit

As we mentioned before, FAC conditions in the one-loop level lead to incorrect result for the order of the phase transition in $O(N)$ scalar model, which has been known for a long time [18]. As is shown in the first reference of [18], the first order nature is an artifact of the mean-field analysis in the one-loop level. In this section, we will give further analysis on this point.

In the chiral limit ($h = 0$), the FAC condition (4.27) for $m^2(T)$ can be solved analytically in the broken phase. From the NG-theorem, the pion channel must have zero-mass pole ($\omega = 0, \vec{k} = 0; T$). Therefore,

$$m_{0\pi}^2 + \Sigma_\pi^R(\omega = 0, \vec{0}; T) = 0. \tag{4.34}$$

This equation can be also obtained by the stationary condition for $\xi(T)$:

$$\left.\frac{\partial V^{chiral\ limit}(\vec{\varphi}^2)}{\partial \sigma}\right|_{\sigma=\xi,\vec{\pi}=0} = \xi[m_{0\pi}^2 + \Sigma_\pi^R(0, \vec{0}; T)] = 0. \tag{4.35}$$

For $\xi(T) \neq 0$, a simultaneous solution of eq.(4.27) and eq.(4.35) reads

$$m_{0\pi}^2 = \Sigma_\pi^R(0, \vec{0}; T) = 0. \tag{4.36}$$

Thus, we obtain the following solution:

$$m^2 = -\frac{\lambda}{6}\xi^2, \quad m_{0\pi}^2 = 0 \quad \text{and} \quad m_{0\sigma}^2 = \frac{\lambda}{3}\xi^2. \tag{4.37}$$

By substituting this into eq.(4.35), one obtains

$$\xi\left[\mu^2 + \frac{\lambda}{6}\xi^2 + \frac{\lambda^2}{96\pi^2}\xi^2 \ln\left|\frac{\lambda\xi^2}{3\kappa^2 e}\right| + \frac{\lambda}{2}\int \frac{d^3k}{(2\pi)^3}\left(\frac{n_B(E_\sigma)}{E_\sigma} + \frac{n_B(E_\pi)}{E_\pi}\right)\right] = 0, \tag{4.38}$$

where $E_\sigma = \sqrt{\vec{k}^2 + \lambda\xi^2/3}$ and $E_\pi = |\vec{k}|$.

The solid line in Fig.4.5 shows the chiral condensate in the chiral limit (the numerical solution of eq.(4.38)), and the dashed line indicates the case for $m_\pi = 10$ MeV. For $T_1 = 126\text{MeV} < T < T_2 = 153\text{MeV}$, $\xi(T)$ has multiple solutions for given T, which is usually understand as a signal of the first order phase transition. T_1 and the behavior of $\xi(T)$ for $T \sim T_1$ can be solved analytically by expanding (4.38) in terms of ξ near $\xi = 0$, which leads to

$$T_1 = \sqrt{\frac{12}{\lambda}}|\mu|, \quad \xi(T > T_1) \simeq \frac{4\pi}{\sqrt{3\lambda}}(T - T_1). \tag{4.39}$$

One can, however, show that this is not a real first order phase transition. In fact, the Gibbes free energy $V(\varphi = \xi, m^2; T)$ near the chiral limit, which is a thermodynamic quantity, has a discontinuity at $T = T_2$ (see, Fig.4.6). Since the free

energy must be a continuous function of T, this fact can be taken as a signal that OPT with the FAC condition in the one-loop level breaks down near the chiral limit. The real world with $m_\pi(T=0) = 140$ MeV does not suffer from this difficulty, thus we can use the FAC condition in the one-loop level for calculating physical processes as far as the gap-equation has only one solution for given T.

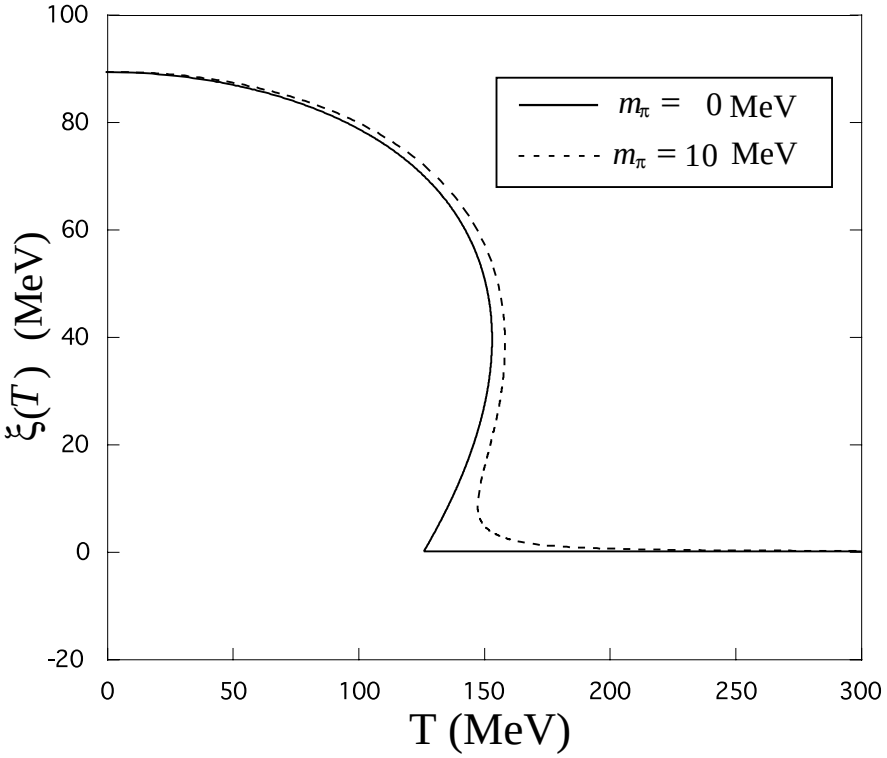

Figure 4.5: $\xi(T)$ for $m_{\sigma peak}(T=0) = 550$MeV with $m_\pi = 0$ MeV and $m_\pi = 10$ MeV.

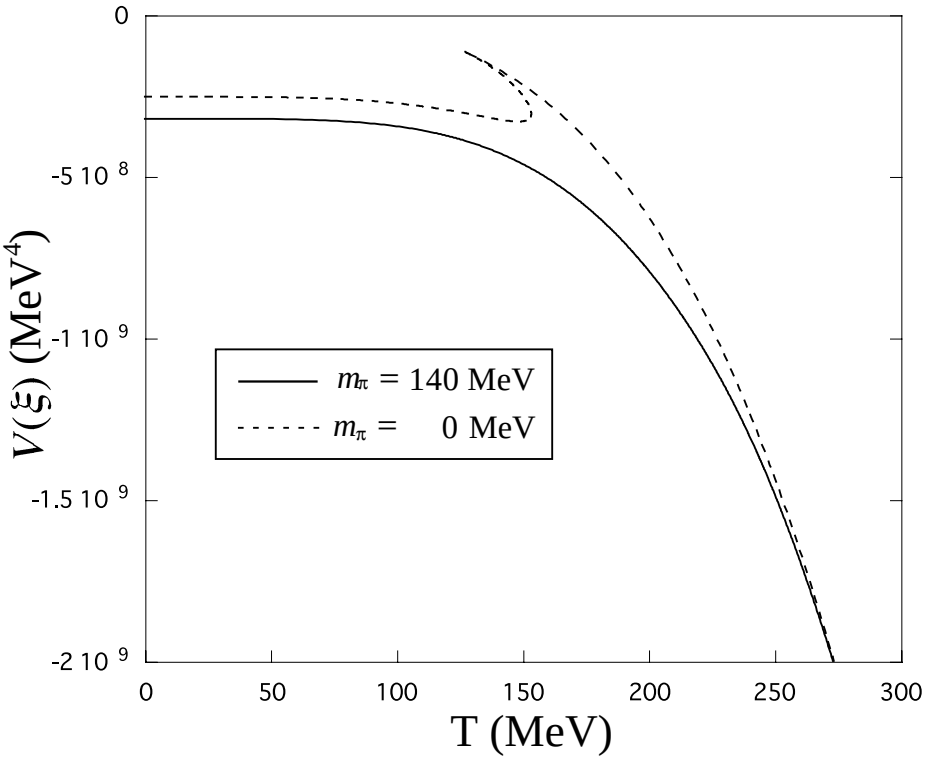

Figure 4.6: Minimum value of the effective potential as a function of T for $m_\pi(T = 0) = 140$ MeV and 0 MeV (chiral limit) with $m_{\sigma peak}(T = 0) = 550$ MeV.

4.3 Spectral functions

The spectral functions $\rho_{\pi,\sigma}(\omega, \vec{0}; T)$ for $T = 50, 120, 145$ MeV with $m_{\sigma peak}(T = 0) = 550$ MeV are shown in Fig.4.7 (A) and (B).

As we have mentioned before, a continuum develops for $0 < \omega < m_{0\sigma} - m_{0\pi}$ in the π-channel. Although the pion obtains a width due to the induced decay $\pi + \pi^{\rm thermal} \to \sigma$, the pole structure is still distinct. The width is about 50 MeV at $T = 145$ MeV. It is the property of the NG-boson that the peak position does not change so much, and this is consistent with other calculations based on the low T expansion [58].

In the σ-channel, the peak position moves to the lower mass direction as T increases. This is because the partial restoration of chiral symmetry occurs and the σ-meson mass begins to be degenerate with the pion mass. When $T \simeq 145$ MeV, the σ-spectral function just above the continuum threshold becomes very sharp. This can be understood as follows. Let us define ω_{real} as solutions of

$$\mathrm{Re}[D^R_\sigma(\omega_{real}, \vec{0})]^{-1} = \omega^2_{real} - m^2_{0\pi} - \mathrm{Re}\Sigma^R_\sigma(\omega_{real}, \vec{0}; T) = 0. \tag{4.40}$$

ω_{real} controls the peak position of ρ_σ, because l.h.s. of eq.(4.40) appears in the denominator of (4.19). Note that the imaginary part of $[D^R_\sigma(\omega,\vec{0})]^{-1}$ is proportional to the phase space factor:

$$\mathrm{Im}\Sigma^R_\sigma(\omega,\vec{0};T) \propto \theta(\omega - 2m_{0\pi})\sqrt{1-\frac{4m^2_{0\pi}}{\omega^2}}, \tag{4.41}$$

and it is a smooth function of ω. In Fig.4.7 (C), $\mathrm{Re}[D^R_\sigma(\omega,\vec{0})]^{-1}$ for $T = 50, 120, 145$ is shown. For $T < 145$ MeV, $\mathrm{Re}[D^R_\sigma(\omega,\vec{0})]^{-1}$ has only one zero for given T, which roughly corresponds to the position of the broad peak in Fig.4.7 (B). On the other hand, when $T = 145$ MeV, eq.(4.40) has two solutions. Higher one is from the original "effective" mass and lower one is from the cusp in lower ω region. This cusp is located accurately at $\omega = 2m_{0\pi}$ which is the continuum threshold of the σ-spectral function. The cusp originates from the fourth diagram of the σ self-energy in Fig.4.2. This cusp makes the threshold spike in the spectral function.

For $T > 145$ MeV, this cusp creates a pole without an imaginary part, which is understood as an one-particle pole (see, Fig.4.8). Thus, since the threshold enhancement occurs just before creating the one-particle peak, it is understood as the state in which the threshold coincides with the one-particle peak. However, it occurs at relatively low T. In fact, this one-particle pole is created not from the larger ω_{real} which creates the broad peak at $T = 0$ but from the cusp structure. This is because this phenomena is caused by a combined effect of the partial restoration of chiral symmetry (decreasing $m_{0\sigma}$) and the strong coupling of $\sigma - 2\pi$ (cusp structure).

In the π-channel, similar threshold enhancement occurs just below $\omega = m_{0\sigma} - m_{0\pi}$ for $T \simeq 165$ MeV. Since pion obtains a width at finite T, the same mechanism is applied. For $T > 165$ MeV, the pion becomes again an one-particle pole in this approximation.

Fig.4.8 (A) shows the spectral functions of π and σ at $T = 180$ MeV. π and σ have simple one-particle poles, which is expected in previous analyses [49, 51]. This is because the decay $\sigma \to 2\pi$ and induced decay $\pi + \pi^{thermal} \to \sigma$ are kinematically forbidden. These poles gradually merge as T increases. The real parts of π and σ propagators are given in Fig.4.8 (B) for the comparison with Fig.4.7 (C).

For sufficiently high T, the system is expected to be a deconfinement phase in QCD. In this phase, the decay $(\sigma,\pi) \to q\bar{q}$ should occur. However, in the linear σ model presented in the section, this sort of decay is not included. In the Nambu-Jona-Lasinio model where such coupling is allowed above T_c, σ and π generally obtain large with for $T \gg T_c$. Nevertheless, it has been shown that such decays are not important near $T \sim T_c$ and stable collective modes exist for $T \geq T_c$ [16].

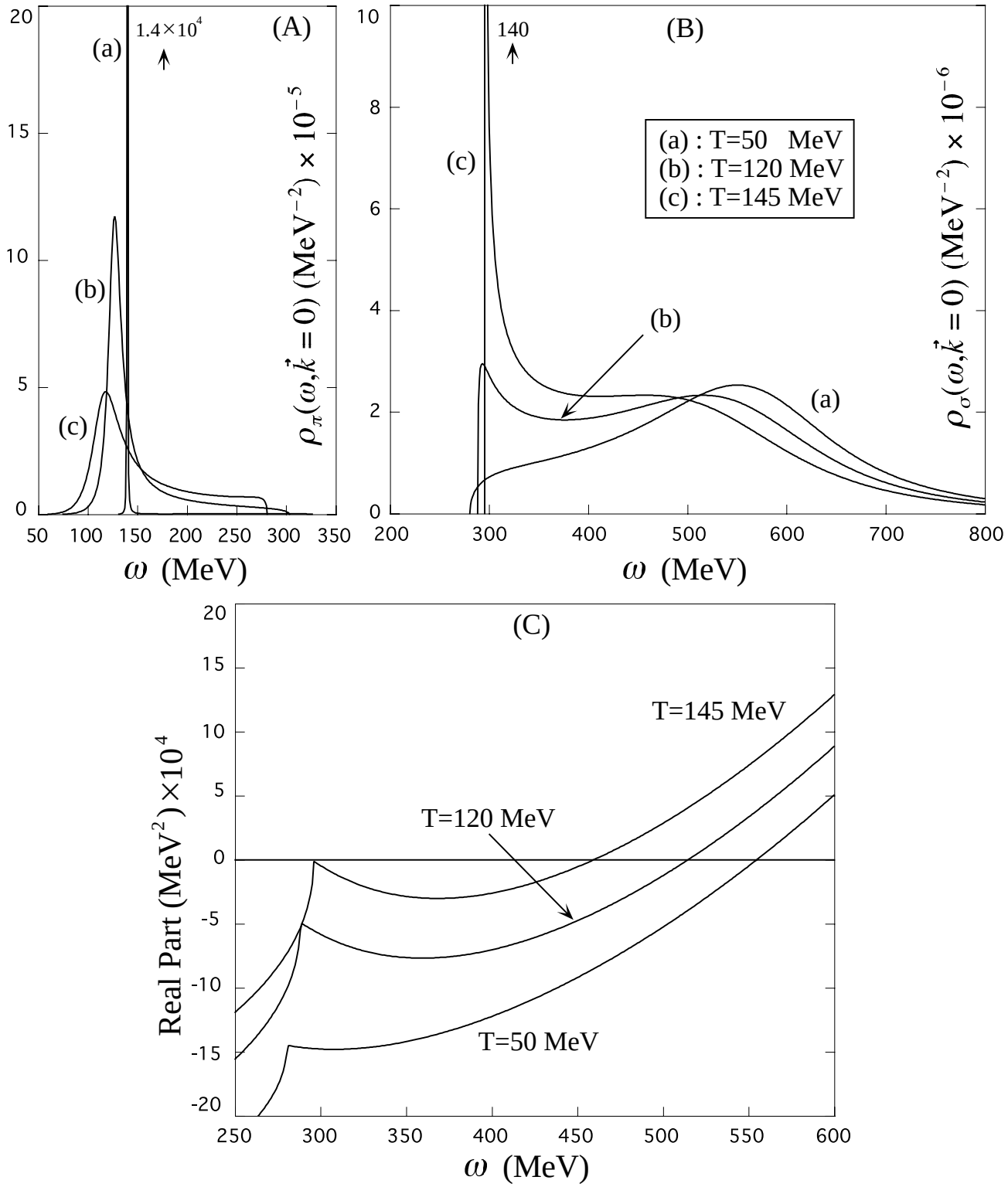

Figure 4.7: Spectral functions in the π channel (A) and in the σ channel (B) for $T = 50, 120, 145$ MeV with $m_{\sigma peak}(T = 0) = 550$ MeV. The real part of $(D^R_\sigma(\omega, \vec{0}; T))^{-1}$ as a function of ω is shown in (C).

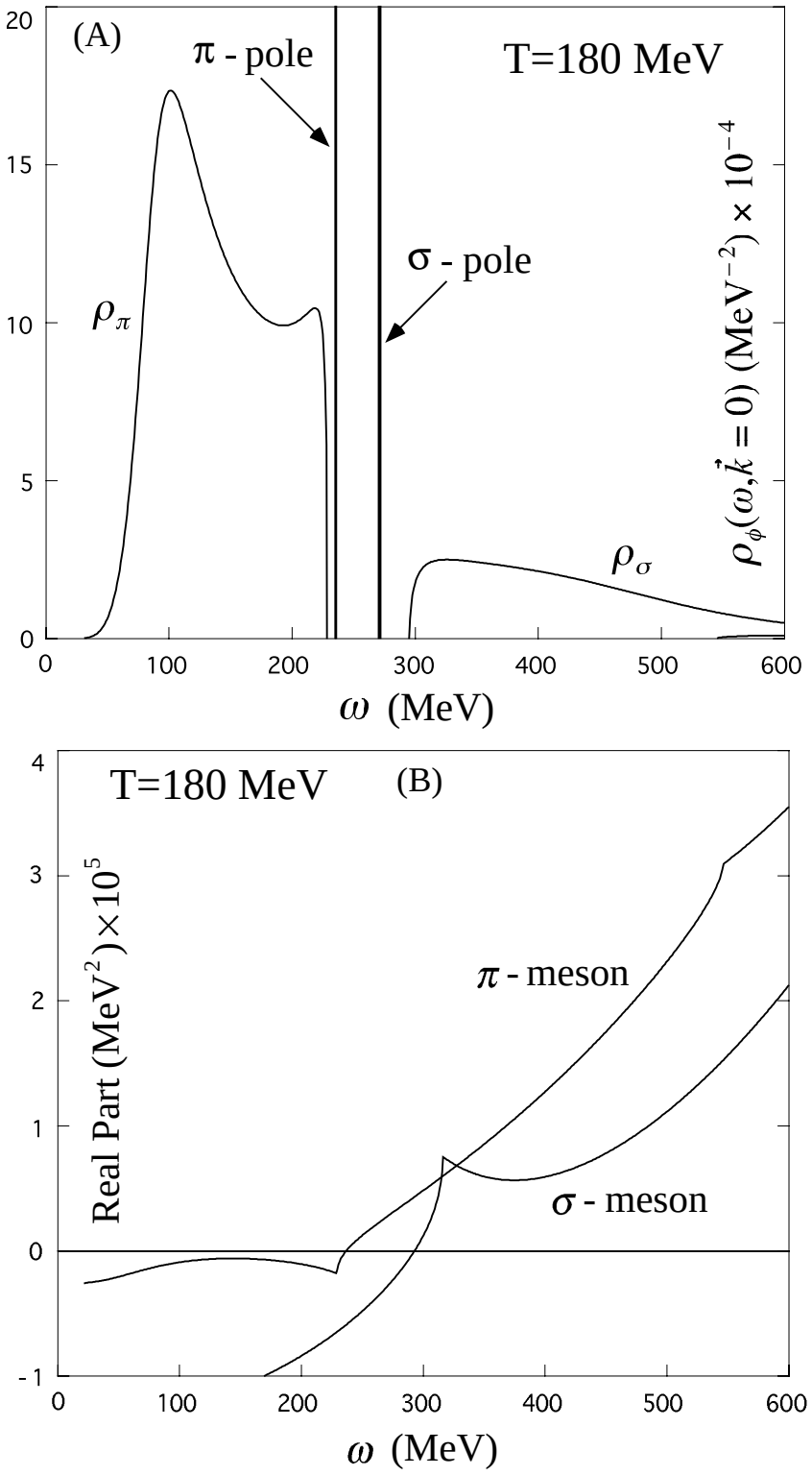

Figure 4.8: (A) Spectral functions in the π and σ channels at $T = 180$ MeV. (B) The real part of $[D^R_\pi(\omega,\vec{0};T]^{-1}$ and $[D^R_\sigma(\omega,\vec{0};T)]^{-1}$ as a function of ω at $T = 180$ MeV with $m_{\sigma peak}(T = 0) = 550$ MeV.

4.4 Diphoton emission rate through $\sigma \to 2\gamma$

One of the main purposes of RHIC and LHC [3] is to observe deconfinement and the restoration of chiral symmetry. Many signatures have been proposed to look for the experimental evidence of this phenomena [59]. One of the candidates of such signature is the emission of leptons and photons from hot plasma [60]. Since leptons and photons interact only weakly with matter, it is possible to carry information of the hot plasma. In this section, we propose a signature of the chiral restoration in the diphoton emission from the decay $\sigma \to 2\gamma$ [61].

4.4.1 Formulation of diphoton emission rate

We first derive a formula of diphoton emission rate.

A S-matrix element of the $\sigma \to 2\gamma$ process can be written as

$$S_{fi} = ig_{\sigma\gamma\gamma}\langle f + 2\gamma | \int d^4x \hat{F}_{\mu\nu}(x)\hat{F}^{\mu\nu}(x)\hat{\sigma}(x)|i\rangle, \tag{4.42}$$

where $g_{\sigma\gamma\gamma}$ is the $\sigma\gamma\gamma$ coupling which will be given later. $|f\rangle$ ($|i\rangle$) is the finial (initial) state of a hot hadronic plasma, and

$$\hat{F}_{\mu\nu} = \partial_\mu \hat{A}_\nu - \partial_\nu \hat{A}_\mu, \tag{4.43}$$

$$\hat{A}_\mu = \int \frac{d^3k}{\sqrt{2\omega(2\pi)^3}} \varepsilon_\mu [\hat{a}(\vec{k})e^{-ikx} + \hat{a}^\dagger(\vec{k})e^{ikx}]. \tag{4.44}$$

Here, ε_μ is polarization vector, $\hat{a}(\vec{k})$ and $\hat{a}^\dagger(\vec{k})$ are the annihilation and creation operators for the photon, which satisfy

$$\begin{aligned} [\hat{a}(\vec{k}), \hat{a}^\dagger(\vec{k'})] &= \delta^3(\vec{k} - \vec{k'}), \\ [\hat{a}(\vec{k}), \hat{a}(\vec{k'})] &= [\hat{a}^\dagger(\vec{k}), \hat{a}^\dagger(\vec{k'})] = 0, \end{aligned} \tag{4.45}$$

with $k = (\omega = |\vec{k}|, \vec{k})$. Using $\hat{\sigma}(x) = e^{ipx}\hat{\sigma}(0)e^{-ipx}$ and $|\gamma(k)>= \sqrt{2\omega(2\pi)^3}\hat{a}^\dagger(\vec{k})|0>$, S_{fi} reads

$$\begin{aligned} S_{fi} &= -4ig_{\sigma\gamma\gamma}(2\pi)^4\delta^4(k_1 + k_2 + P_f - P_i) \\ &\quad \times \{(k_1 \cdot k_2)(\varepsilon_1 \cdot \varepsilon_2) - (k_1 \cdot \varepsilon_2)(k_2 \cdot \varepsilon_1)\}\langle f|\hat{\sigma}(0)|i\rangle, \end{aligned} \tag{4.46}$$

where, k_1 and k_2 are the four-momenta of photons and P_i (P_f) is a total four-momentum of the initial (finial) system. The diphoton emission rate N_σ from the σ-meson in the hot plasma is given by [3]

$$\frac{dN_\sigma}{d^4x} = \sum_{i,f} e^{-\beta E_i} \frac{|S_{fi}|^2}{TV} \frac{d^3k_1}{2\omega_1(2\pi)^3} \frac{d^3k_2}{2\omega_2(2\pi)^3}$$

[3]Since we use the invariant normalization, $dN_\sigma = Fd\Gamma(\sigma \to 2\gamma; T)$, where $F = 2m_\sigma$ is the flux and $d\Gamma$ is the decay rate for a σ into 2γ at finite T.

$$= \sum_{i,f} e^{-\beta E_i} \frac{16|g_{\sigma\gamma\gamma}|^2}{4\omega_1\omega_2} \{(k_1\cdot k_2)(\varepsilon_1\cdot\varepsilon_2) - (k_1\cdot\varepsilon_2)(k_2\cdot\varepsilon_1)\}^2$$
$$\times(2\pi)^4\delta^4(k_1+k_2+P_f-P_i)|\langle f|\hat{\sigma}(0)|i\rangle|^2 \frac{d^3k_1}{(2\pi)^3}\frac{d^3k_2}{(2\pi)^3}, \qquad (4.47)$$

where TV is the space-time volume. Using the definition of the spectral at finite T, we obtain

$$\rho_\sigma = (2\pi)^3 \sum_{n,m} \frac{e^{-\beta E_n}}{Z} |\langle n|\hat{\sigma}|m\rangle|^2 (e^{-\beta E_{mn}}-1)\delta^4(P+P_{mn}) \qquad (4.48)$$
$$= -\frac{1}{\pi}\mathrm{Im}D^R_\sigma \qquad (4.49)$$

After summing up the polarization ($\sum \varepsilon_1^\mu \varepsilon_1^\nu = -g^{\mu\nu}$), we get

$$\omega_1\omega_2 \left.\frac{dN_\sigma}{d^3k_1 d^3k_2 d^4x}\right|_{k_1+k_2=0} = \frac{2|g_{\sigma\gamma\gamma}|^2}{(2\pi)^5}\omega^4 \frac{\rho_\sigma(\omega,\vec{q}=0;T)}{e^{\beta\omega}-1}, \qquad (4.50)$$

where $Q=(\omega=\omega_1+\omega_2, \vec{q}=\vec{k_1}+\vec{k_2})$ is diphoton total four-momentum. To translate the variables from k_1 and k_2 into Q, we integrate eq.(4.50) in terms of k_1 and k_2:

$$\frac{dN_\sigma}{d^4x} = \int \frac{d^3k_1 d^3k_2}{\omega_1\omega_2}\omega_1\omega_2 \frac{dN_\sigma}{d^3k_1 d^3k_2}$$
$$= \int d^4q \delta^4(q-k_1-k_2) \int \frac{d^3k_1 d^3k_2}{\omega_1\omega_2}\omega_1\omega_2 \frac{dN_\sigma}{d^3k_1 d^3k_2}$$
$$= \int d^4q \frac{2}{(2\pi)^4}|g_{\sigma\gamma\gamma}|^2\omega^4 \frac{\rho_\sigma(\omega,\vec{q}=0;T)}{e^{\omega/T}-1}. \qquad (4.51)$$

Dividing this by 2 originating from the bose statistics, we get a final expression of the kinematics diphoton yield per unit space-time volume in back to back kinematics:

$$\frac{dN_\sigma}{d^4x d^4q} = \frac{1}{(2\pi)^4}|g_{\sigma\gamma\gamma}|^2\omega^4 \frac{\rho_\sigma(\omega,\vec{q}=0;T)}{e^{\omega/T}-1}. \qquad (4.52)$$

Diphoton rate from $\pi^0(\omega,\vec{q}) \to \gamma(k_1)+\gamma(k_2)$ is obtained by replacing "σ" of eq.(4.52) with "π". The S-matrix element of this process is given by

$$S_{fi} = i g_{\pi^0\gamma\gamma}\langle f+2\gamma| \int d^4x F_{\mu\nu}\tilde{F}^{\mu\nu}\pi^0|i\rangle, \qquad (4.53)$$

where $g_{\pi^0\gamma\gamma}$ is the coupling constant of $\pi^0\gamma\gamma$ vertex including form factor and $\tilde{F}^{\mu\nu} = \varepsilon^{\mu\nu\lambda\rho}F_{\lambda\rho}/2$ ($\varepsilon^{\mu\nu\lambda\rho}$ is totally antisymmetric tensor). The following calculations are similarly done.

4.4.2 Estimation of $g_{\sigma\gamma\gamma}$ and $g_{\pi^0\gamma\gamma}$

In order to estimate $g_{\sigma\gamma\gamma}$, we consider the interaction of charged pions with $U(1)$ gauge field,

$$\tfrac{1}{2}(\partial_\mu \pi^a)^2 \to \tfrac{1}{2}(D_\mu \pi^a)^2, \tag{4.54}$$

$$D_\mu = \partial_\mu + ie_3 A_\mu, \quad \text{with} \quad e_3 = e \begin{pmatrix} 1 & & \\ & 0 & \\ & & -1 \end{pmatrix}. \tag{4.55}$$

In this extension, the σ meson can decay into diphoton through the pion-loop. Here, another contributions, which come from constituent-quark loops, are also included in our calculation. The former corresponds to a long distant contribution, and the later is a short distant contribution [62]. Thus, we define the $g_{\sigma\gamma\gamma}$ as

$$g_{\sigma\gamma\gamma} \equiv g_{\sigma\to 2\pi\to\gamma\gamma} + g_{\sigma\to q\bar{q}\to\gamma\gamma}. \tag{4.56}$$

In order to consider $\pi^0 \to \gamma\gamma$ process simultaneously in a consistent way, we use the chiral quark model with $U(1)$ gauge interaction [16] to estimate it:

$$\mathcal{L}_{\mathcal{CQM}} = \bar{q} i \not{D} q - g\bar{q}(\sigma + i\gamma_5 \vec{\tau}\cdot\vec{\pi})q - V(\vec{\phi}), \tag{4.57}$$

where $iD_\mu = i\partial_\mu - e_\tau A_\mu$ with $e_\tau = \frac{1}{2}e(\tau_3 + \frac{1}{3})$, $\bar{q}q = \bar{u}u + \bar{d}d$, $V(\vec{\phi}) = \frac{1}{2}\mu^2\vec{\phi}^2 + \frac{\lambda}{4!}(\vec{\phi}^2)^2$ ($\vec{\phi} = (\sigma, \vec{\pi})$). After the dynamical breaking of chiral symmetry, σ is replaced as $\sigma \to \sigma + f_\pi$:

$$\mathcal{L}_{\mathcal{CQM}} = \bar{q}(i\not{\partial} - m_q)q - g\bar{q}(\sigma + i\gamma_5\vec{\tau}\cdot\vec{\pi})q - V(\sigma + f_\pi, \vec{\pi}), \tag{4.58}$$

with $m_q = gf_\pi$. Here, we use $m_q = 300$ MeV, which is a consistent-quark mass, and $f_\pi = 93$ MeV which is pion decay constant. The contribution to $g_{\sigma\to 2\pi\to\gamma\gamma}$ and $g_{\sigma\to q\bar{q}\to\gamma\gamma}$ are shown in Fig.4.9 [4].

The result of the calculation of Fig.4.9 (a), (b) and (c) is

$$g_{\sigma\to 2\pi\to\gamma\gamma} = \frac{\alpha\lambda\xi}{12\pi}\left\{\frac{1}{q^2} - \frac{4m_{0\pi}^2}{(q^2)^2}\left(\sin^{-1}\frac{\sqrt{q^2}}{2m_{0\pi}}\right)^2\right\}, \tag{4.59}$$

where $q^\mu = (\omega, \vec{q})$ is the total four-momentum of diphoton and α is the fine structure constant $1/137$. Detail calculations are given in Appendix F. Fig.4.9 (d) and (e) show the consistent-quark-loop contribution, and it reads

$$g_{\sigma\to q\bar{q}\to\gamma\gamma} = -\frac{5m_q^2\alpha}{3\pi f_\pi}\left\{\frac{1}{q^2} + \frac{q^2 - 4m_q^2}{(q^2)^2}\left(\sin^{-1}\frac{\sqrt{q^2}}{2m_q}\right)^2\right\}. \tag{4.60}$$

[4] Our calculation for the coupling constants is performed at $T = 0$.

The contribution to $g_{\pi^0\gamma\gamma}$ is only from quark-loops [63], which is shown in Fig.4.9 (d) and (e), and the result is

$$g_{\pi^0\gamma\gamma} = -\frac{\alpha m_q^2}{\pi q^2 f_\pi}\left(\sin^{-1}\frac{\sqrt{q^2}}{2m_q}\right)^2 . \tag{4.61}$$

Detail calculations are also summarized in Appendix F. Note that $g_{\sigma\to 2\pi\to\gamma\gamma}$ becomes complex when $\sqrt{q^2} > 2m_{0\pi}$, and $g_{\sigma\to q\bar{q}\to\gamma\gamma}$ and $g_{\pi^0\gamma\gamma}$ are complex when $\sqrt{q^2} > 2m_q$. Thus, the following replacement should be done in those cases;

$$\sin^{-1}\frac{\sqrt{q^2}}{2m} \to \frac{\pi}{2} + i\cosh^{-1}\frac{\sqrt{q^2}}{2m} \quad \text{for} \quad \sqrt{q^2} > 2m. \tag{4.62}$$

Results of $g_{\sigma\gamma\gamma}$ and $g_{\pi^0\gamma\gamma}$ are shown in Fig.4.10. Peaks of $g_{\sigma\gamma\gamma}$ and $g_{\pi^0\gamma\gamma}$ are located at $2m_{0\pi}$ and $2m_q$, respectively.

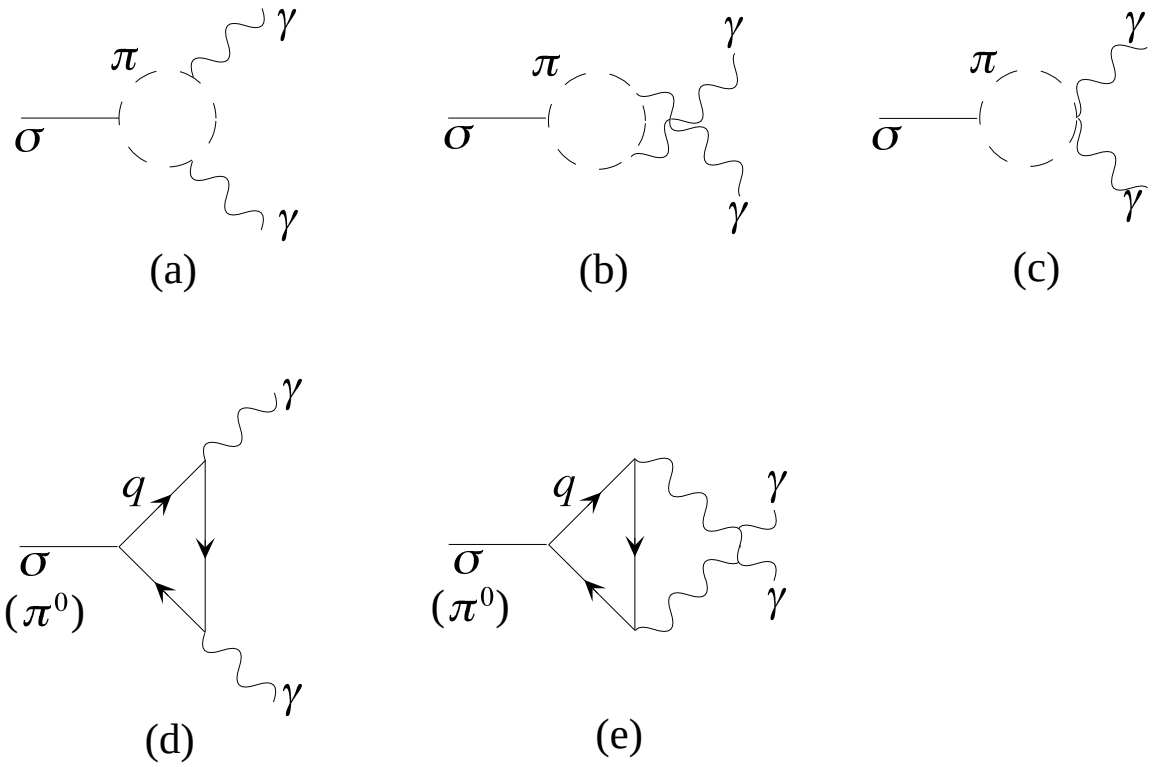

Figure 4.9: Various contribution to $g_{\sigma\gamma\gamma}$. (a), (b) and (c) are the effects from pion-loop, and (d) and (e) are from the quark-loop. $g_{\pi\gamma\gamma}$ has only quark-loop contributions from (d) and (e).

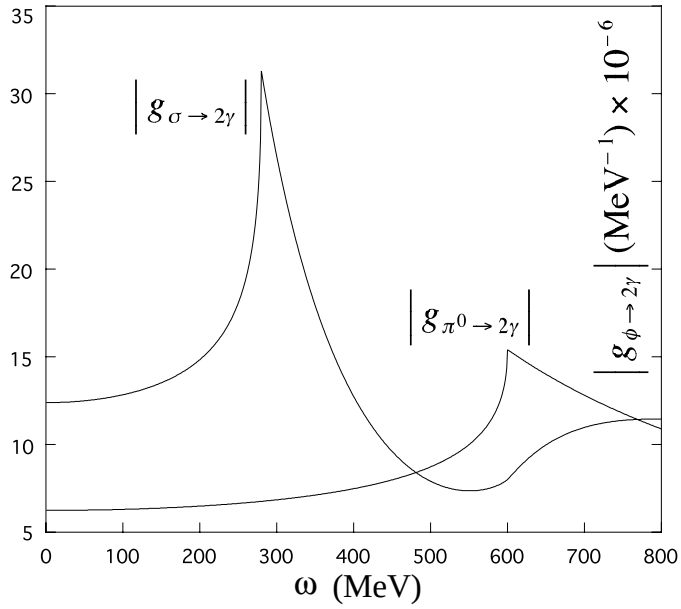

Figure 4.10: The effective coupling $g_{\sigma\gamma\gamma}$ and $g_{\pi\gamma\gamma}$ as a function of ω.

4.4.3 Main background for diphoton

The main background to the $\sigma \to 2\gamma$ process is the pair annihilation of the thermal pions;

$$\pi^+_{thermal}(p_1) + \pi^-_{thermal}(p_2) \to \gamma(k_1) + \gamma(k_2). \tag{4.63}$$

This contributions are sketched in Fig.4.11.

The $\pi^+\pi^-$ coss-section $d\sigma$ can be written as

$$d\sigma = \frac{|\mathcal{M}|^2}{F} dQ, \tag{4.64}$$

where $\mathcal{M}$ is an invariant amplitude, F is the flax and

$$dQ = (2\pi)^4 \delta^4(p_1 + p_2 - k_1 - k_2) \frac{d^3k_1}{(2\pi)^3 2k_1^0} \frac{d^3k_2}{(2\pi)^3 2k_2^0}. \tag{4.65}$$

Here, ps denote the thermal pion momenta and ks are the photon momenta. The diphoton emission rate reads

$$\frac{dN}{d^4x} = \int \frac{n_B(E_1)}{(2\pi)^3 2E_1} d^3p_1 \frac{n_B(E_2)}{(2\pi)^3 2E_2} d^3p_2 F \frac{d\sigma}{d^4x}. \tag{4.66}$$

The final form of the background diphoton rate with back to back kinematics is given by

$$\frac{dN}{d^4x d^4q} = \frac{2\alpha^2}{(2\pi)^4} n_B^2(\frac{\omega}{2}) D \left\{ 1 + \frac{2m_\pi^2}{\omega^2} + \frac{2m_\pi^2(\omega^2 - 2m_\pi^2)}{\omega^4 D} \ln \frac{1-D}{1+D} \right\}, \tag{4.67}$$

with

$$D = \sqrt{1 - \frac{4m_\pi^2}{\omega^2}}. \tag{4.68}$$

Derivation of eq.(4.67) is given in Appendix F.

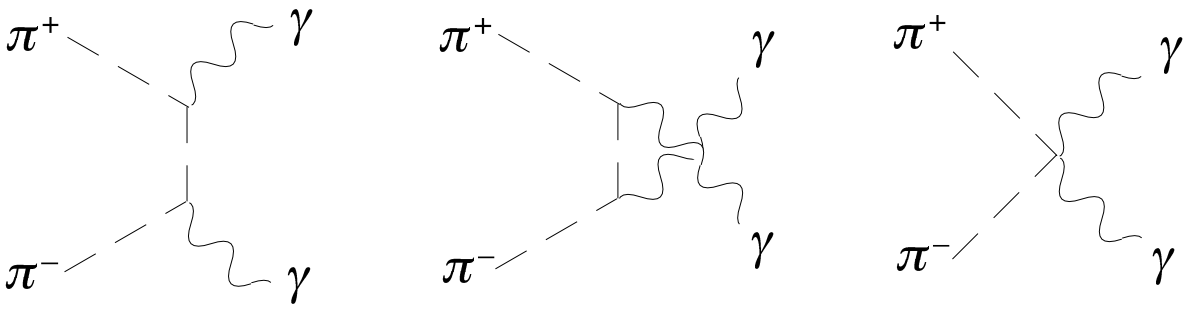

Figure 4.11: The main background to the $\sigma \to 2\gamma$ process. π^+ and π^- are the thermal pions which obey the Bose-Einstein distribution.

4.4.4 Result

All of the above contributions to the diphoton emission rate at $T = 145$ MeV are shown in Fig.4.12. The threshold enhancement through $\sigma \to 2\gamma$ process occurs in a narrow region of the diphoton invariant mass and in a narrow region of T. Independent analysis of this phenomena using NJL-model shows a similar enhancement from $\sigma \to 2\gamma$ [64]. It is an open problem whether this enhancement can be seen in the future RHIC experiment. Also, similar enhancement may be seen at finite density [65]. This is closely related to the recent CHAOS data on $\pi^+\pi^-$ detection in the pion-nucleus reactions.

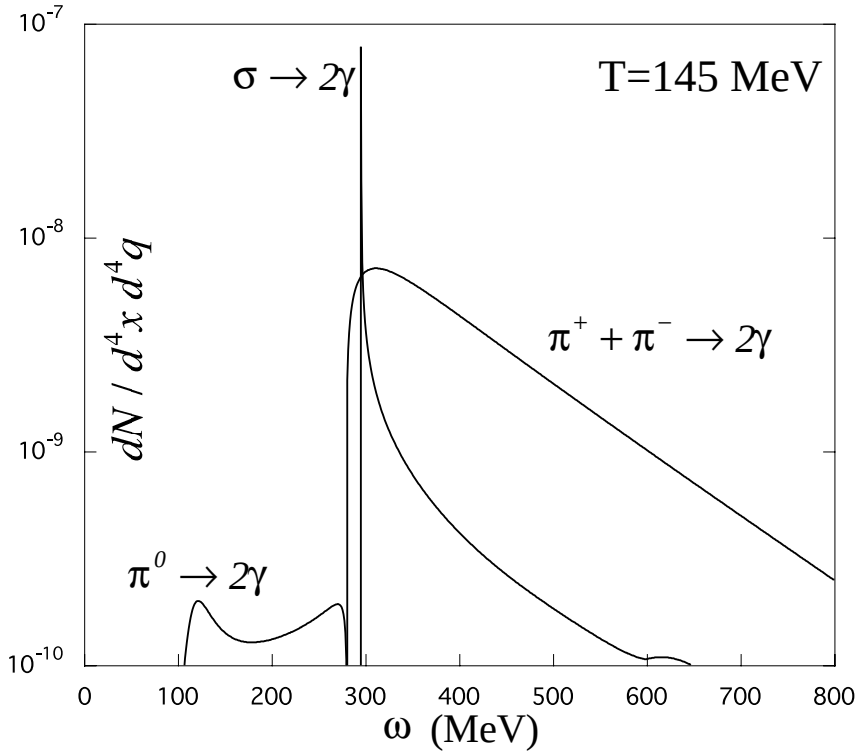

Figure 4.12: Diphoton yield per unit space-time volume in the back to back kinematics at T=145 MeV for $m_{\sigma peak}(T=0) = 550$ MeV.

Chapter 5

Summary

In this thesis, we have developed an optimized perturbation theory (OPT) at finite temperature (T) in the $O(N)$ $\lambda\phi^4$ theory. The naive loop expansion for theories with spontaneous symmetry breaking is known to breakdown at low T (tachyon pole problem) and high T (hard thermal loops (HTLs) problem). On the other hand, we have shown that OPT does not suffer from such difficulties. This is because that OPT can resum the higher order terms of the naive perturbation in a consistent way by imposing appropriate conditions such as the principle of minimal sensitivity (PMS) or the fastest apparent convergence (FAC).

In chapter 2, we have explicitly shown that OPT has two advantages over other self-consistent resummation methods.

The first advantage is that one can carry out the renormalization of ultraviolet divergences systematically in any given order of OPT. Because the renormalization is performed before imposing the gap-equation, the finite gap-equation is obtained. Thus, the renormalization and the resummation can be done separately in OPT, while they are mixed in other self-consistent approaches.

The second advantage is that the Nambe-Goldstone (NG) theorem at finite T is automatically satisfied in OPT. Since OPT preserves the symmetry of the effective potential in each orders of the expansion, the NG theorem follows automatically. This is in contrast to the other self-consistent methods in which the symmetry of the effective potential is not manifest in their approximation.

In chapter 3, we applied OPT to $\lambda\phi^4$ theory to examine whether it can be describe the finite T phase transition correctly. Carrying out the two-loop computation of the effective potential in OPT, we have found that both PMS and FAC give the correct second order transition. The critical exponent β, however, is found to take the mean-field value at this level. The full OPT, where both the mass and the coupling constant are shifted, may or may not improve the result. This remains as an open problem.

In chapter 4, we have applied OPT to the $O(4)$ linear σ model which is supposed to be an effective theory of QCD. The spectral functions of the pion (NG-boson) and the σ-meson (fluctuations of the chiral order parameter) are studied using the FAC condition for the pion self-energy in the one-loop order. Thanks to OPT, problems related to the naive loop-expansion at finite T are cured. Also, the spectral function in the σ-channel obtains correct threshold at the twice of the pion mass. We found that the spectral function of σ-channel has a strong enhancement near the two-pion threshold at certain T, although the σ-spectrum has only a broad structure at $T = 0$. This is due to a combined effect of the partial restoration of the chiral symmetry and the strong coupling of $\sigma\pi\pi$.

To study its phenomenological consequence, we examine the diphoton decay $\sigma \to 2\gamma$ in the hot plasma. The threshold enhancement over the $\pi^+_{thermal} + \pi^-_{thermal} \to 2\gamma$ background can be seen in a relatively small region of T and the invariant mass distribution of the diphoton. Observation of such peak structure in future RHIC experiment is an interesting but challenging problem. Similar threshold enhancement with the same physical origin at finite baryon density has been recently studied both theoretically and experimentally.

Application of the idea of OPT to the gauge theories at finite T will be also an interesting future problem. However, to go beyond the hard thermal loops (HTLs) resummation scheme, one must solve two problems.

- Since infinite number of N-point vertex functions (N-gauge boson vertices and (N-2)-gauge boson 2-fermion vertices) become HTLs in gauge theories and a naive mass term breaks the gauge symmetry, one must take into account infinite number of effective vertices like HTLs resummation scheme. However, this infinite number vertices may cause a difficulty of the renormalization.

- It is known that HTLs resummation scheme breaks down at high T due to the so called magnetic mass problem [66].

Therefore, one may need further generalization of OPT in gauge theories.

Acknowledgments

I am greatly indebted to Prof. T. Hatsuda for his helpful discussions and encouragements. Without his guidances, this thesis would not be completed.

This thesis owes much to the helpful comments of Prof. T. Kunihiro. He introduced me to the idea of OPT. Also, I gratefully acknowledge useful discussions with Dr. M. Asakawa. He provided me many advice from the experimental point of view. I wish to express my gratitude to Prof. T. Matsui for giving me on an opportunity to stay in the Yukawa Institute for Theoretical Physics and for his useful comments on this work. I also acknowledge Prof. K. Kanaya who gives me very useful comments about the triviality of $\lambda\phi^4$ theory.

I would like to thank Prof. T. Kohmura, Dr. T. Une and Dr. Y. Hashimoto for their supports and encouragements. I feel very grateful to members of the theoretical nuclear physics group in university of Tsukuba. Especially, I wish to acknowledge useful advice from Dr. H. Shiomi. In addition, various physics relating this thesis was studied together with Mr. K. Takahashi to whom I thank.

I also wish to thank all members of the Yukawa Institute for Theoretical Physics and the nuclear theory group at Kyoto university.

Appendix A

Feynman rules for $\lambda\phi^4$ theory in real time formalism

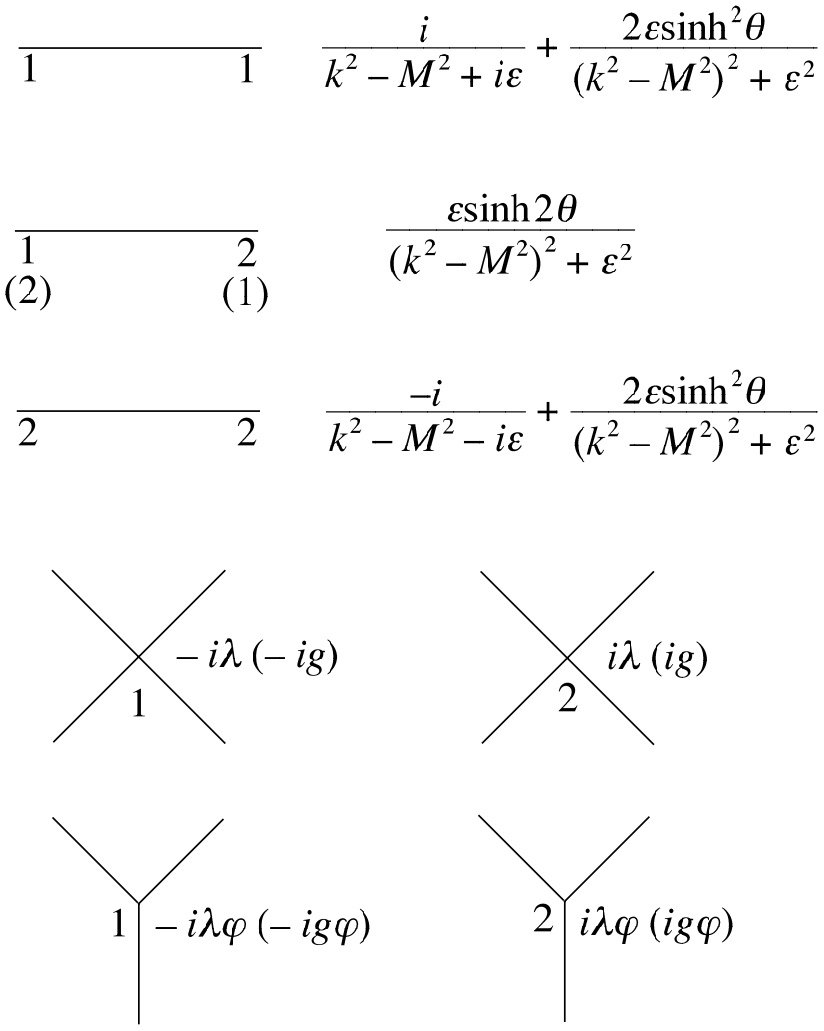

Figure A.1: Feynman rules for $\lambda\phi^4$ theory. The index 1 (2) corresponds to the type 1 (2) vertex.

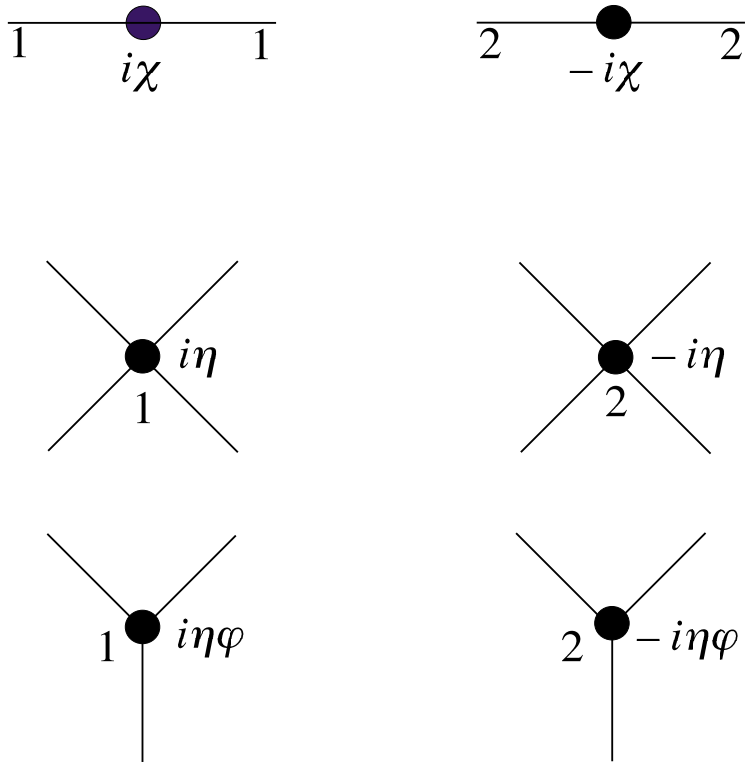

Figure A.2: Additional Feynman rules for $\lambda\phi^4$ theory in OPT. The index 1 (2) corresponds to the type 1 (2) vertex.

Appendix B

Useful formulas

In this appendix, we summarize formulas which are used in this thesis. Notations for dimensional regularization are the following:

$$\varepsilon = \frac{4-n}{2}, \quad g_{\mu\nu}g^{\mu\nu} = n, \tag{B.1}$$

where n is a space-time dimension. Formulas of momentum integrals are

$$\int \frac{d^nk}{(2\pi)^n} \ln(k^2 - 2kp - m^2) = -i\frac{\Gamma(\varepsilon-2)}{(4\pi)^{2-\varepsilon}}(p^2+m^2)^{2-\varepsilon}, \tag{B.2}$$

$$\int \frac{d^nk}{(2\pi)^n} \frac{1}{(k^2-2kp-m^2)^\alpha} = i\frac{\Gamma(\varepsilon+\alpha-2)}{(4\pi)^{2-\varepsilon}}\frac{(-1)^\alpha}{(p^2+m^2)^{\varepsilon+\alpha-2}}, \tag{B.3}$$

$$\int \frac{d^nk}{(2\pi)^n} \frac{k^\mu}{(k^2-2kp-m^2)^\alpha} = i\frac{\Gamma(\varepsilon+\alpha-2)}{(4\pi)^{2-\varepsilon}}\frac{(-1)^\alpha p^\mu}{(p^2+m^2)^{\varepsilon+\alpha-2}}, \tag{B.4}$$

$$\int \frac{d^nk}{(2\pi)^n} \frac{k^\mu k^\nu}{(k^2-2kp-m^2)^\alpha} = i\frac{\Gamma(\varepsilon+\alpha-2)}{(4\pi)^{2-\varepsilon}}\frac{(-1)^\alpha p^\mu p^\nu}{(p^2+m^2)^{\varepsilon+\alpha-2}} \tag{B.5}$$

$$- i\frac{\Gamma(\varepsilon+\alpha-3)}{(4\pi)^{2-\varepsilon}}\frac{(-1)^\alpha g^{\mu\nu}/2}{(p^2+m^2)^{\varepsilon+\alpha-3}}, \tag{B.6}$$

where Γ is Γ function which is defined as

$$\Gamma(\alpha) = \frac{1}{s^{-\alpha}}\int_0^\infty e^{-st}t^{\alpha-1}dt. \tag{B.7}$$

When $\varepsilon \simeq 0$, Γ functions are expanded as

$$\Gamma(\varepsilon) = \frac{1}{\varepsilon} - \gamma + \frac{\varepsilon}{2}\left(\gamma^2 + \frac{\pi^2}{6}\right) + O(\varepsilon^2), \tag{B.8}$$

$$\Gamma(\varepsilon-1) = -\frac{1}{\varepsilon} + (\gamma-1) - \frac{\varepsilon}{2}\left(\gamma^2 - 2\gamma + \frac{\pi^2}{6} + 2\right) + O(\varepsilon^2), \tag{B.9}$$

$$\Gamma(\varepsilon-2) = \frac{1}{2\varepsilon} + (\frac{3}{2} - \gamma) + \frac{\varepsilon}{4}\left(\gamma^2 - 3\gamma + \frac{\pi^2}{6} + \frac{7}{2}\right) + O(\varepsilon^2), \tag{B.10}$$

$$\Gamma(\varepsilon-n) = \frac{(-1)^n}{n!}\left[\frac{1}{\varepsilon} + \sum_{k=1}^{n}\frac{1}{k} - \gamma\right.$$

$$+\frac{\varepsilon}{2}\left\{\frac{\pi^2}{6}+\left(\sum_{k=1}^{n}\frac{1}{k}-\gamma\right)^2+\sum_{k=1}^{n}\frac{1}{k^2}\right\}+O(\varepsilon^2)\Bigg], \tag{B.11}$$

where γ is Euler constant. One may use following formulas in Feynman parameter integrals:

$$\begin{aligned}
\int dx\frac{Ax+B}{(x-p)^2+q^2} &= \frac{A}{2}\ln\{(x-p)^2+q^2\} \\
&\quad +(Ap+B)\int\frac{dx}{(x-p)^2+q^2}, && \text{(B.12)}\\
\int\frac{dx}{x^2+a^2} &= \frac{1}{a}\tan^{-1}\frac{x}{a}, && \text{(B.13)}\\
\int dx[\ln x]^2 &= x\{(\ln x)^2-2\ln x+2\}, && \text{(B.14)}\\
\int_0^1 dx\ln x\ln(1-x) &= 2-\frac{\pi^2}{6}, && \text{(B.15)}\\
\int_0^1 dx\frac{1}{x-1}\ln\frac{ax(x-1)+c}{c} &= \begin{cases} 2\left(\sin^{-1}\sqrt{\frac{a}{4C}}\right)^2 & \text{for} \quad a/c\geq 0, \\ 2\left(\frac{\pi}{2}+i\cosh^{-1}\sqrt{\frac{a}{4C}}\right)^2 & \text{for} \quad a/c\leq 0. \end{cases} && \text{(B.16)}
\end{aligned}$$

In real time formalism, we often use

$$\begin{aligned}
\delta(x^2-a^2) &= \frac{1}{2a}\{\delta(x-a)+\delta(x+a)\}, && \text{(B.17)}\\
\delta(f(x)) &= \frac{1}{|f'(a)|}\delta(x-a), && \text{(B.18)}\\
\frac{\varepsilon}{x^2+\varepsilon^2} &\stackrel{\varepsilon\to 0}{\longrightarrow} \pi\delta(x), && \text{(B.19)}\\
\frac{i}{x+i\varepsilon}\frac{\varepsilon}{x^2+\varepsilon^2} &= -\frac{i}{2}\frac{\partial}{\partial x}\left\{\frac{\varepsilon}{x^2+\varepsilon^2}\right\}+\left\{\frac{\varepsilon}{x^2+\varepsilon^2}\right\}^2 \\
&\stackrel{\varepsilon\to 0}{\longrightarrow} -\frac{i\pi}{2}\frac{\partial}{\partial x}\delta(x)+\pi^2\delta^2(x), && \text{(B.20)}
\end{aligned}$$

where $f(a)=0$.

Appendix C

2-loop effective potential in $\lambda\phi^4$-theory

Here, we calculate the physical effective potential in (2.10) in the real-time formalism, which is equivalent to the effective potential defined in the imaginary time formalism. According to Sec.3.1, we compute the tadpole functions $V^{(1,0)}$ and then it is integrated in terms of the classical field φ. Since the propagator in the $T=0$ part and $T\neq 0$ part decouples in the real time formalism, calculations of $T=0$ parts are completely equal to that in the ordinary $T=0$ perturbation theory. So, we can calculate T-dependent term and T-independent term separately.

The Feynman diagrams contributing to the φ_1 tadpole functions up to the two-loop level are shown in Fig.C.1 C.2 C.3. The vertex with number 1 (2) is indicated as the type 1 (2) field self-interaction. The type 2 field is necessary to cancel pathological pinch singularities.

Fig.C.1 contributes to the 1-loop effective potential in Fig.C.4, and reads

$$\begin{aligned} -iV^{(1,0)1} &= -i\frac{\lambda\varphi_1}{2}\kappa^{2\varepsilon}\int\frac{d^nk}{(2\pi)^n}iD^{11}_\beta + counter\ terms \\ &= -i\frac{\lambda\varphi_1}{2}\kappa^{2\varepsilon}\int\frac{d^nk}{(2\pi)^n}\frac{i}{k^2-M^2+i\varepsilon} + 2\pi n_B(|k_0|)\delta(k^2-M^2) \\ &\quad + counter\ terms, \end{aligned} \tag{C.1}$$

where,

$$M^2 = \mu^2+\frac{\lambda}{2}\varphi^2, \tag{C.2}$$

$$n_B(E) = (e^{\beta E}-1)^{-1}, \tag{C.3}$$

and κ is the renormalization point. The $(1,0)1$ in $V^{(1,0)1}$ means a function which has one-point type 1 external field and zero-point type 2 external field in one-loop level. Then, the integration over φ becomes

$$V^1 = \int d\varphi\ V^{(1,0)1}\Big|_{\varphi_1=\varphi}$$

$$
\begin{aligned}
&= -\frac{i}{2}\kappa^{2\varepsilon}\int\frac{d^nk}{(2\pi)^n}\ln(k^2-M^2)+\int_0^\infty\frac{dk}{(2\pi)^2}\frac{2}{\beta}k^2\ln(1-e^{-\beta E}) \\
&+counter\ terms \\
&= -\frac{1}{(4\pi)^2}\frac{M^4}{4}(\frac{3}{2}-\ln\frac{M^2}{\kappa^2})+\int_0^\infty\frac{dk}{(2\pi)^2}\frac{2}{\beta}k^2\ln(1-e^{-\beta E}), \qquad \text{(C.4)}
\end{aligned}
$$

where $E=\sqrt{k^2+M^2}$.

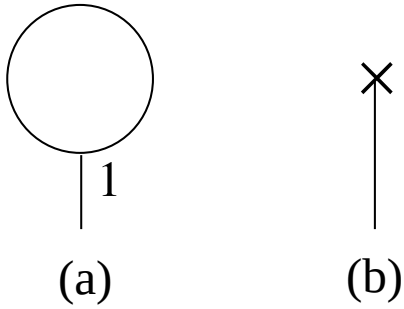

Figure C.1: (a):1-loop diagram contributing to the 1-point function. (b):Counter term contribution (which includes all $\hbar$-order contributions in principle). The index 1 (2) corresponds to the type 1 (2) vertex. The cross represents the counter terms.

According to the tadpole method, Fig.C.2 (a) (b) lead to the 2 bubble diagram Fig.C.5 (a):

$$
\begin{aligned}
-iV^{(1,0)2}_{2bubble} &= \frac{(-i\lambda)^2\varphi}{4}\kappa^{4\varepsilon}\left[\int\frac{d^nk_1}{(2\pi)^n}\{iD^{11}_\beta(k_1)\}^2\int\frac{d^nk_2}{(2\pi)^n}iD^{11}_\beta(k_2)\right. \qquad \text{(C.5)} \\
&\left.-\int\frac{d^nk_1}{(2\pi)^n}\{iD^{12}_\beta(k_1)\}^2\int\frac{d^nk_2}{(2\pi)^n}iD^{22}_\beta(k_2)\right]+counter\ terms,
\end{aligned}
$$

where $V^{(1,0)2}_{2bubble}$ shows contributions of φ_1 bubble diagram in two-loop level. Using the eq.(B.20), the integral of (C.5) reads

$$
\begin{aligned}
V^2_{2bubble} &= \frac{\lambda}{8}\left[\kappa^{2\varepsilon}\int\frac{d^nk}{(2\pi)^n}\frac{i}{k^2-M^2+i\varepsilon}+2\pi n_B(|k_0|)\delta(k^2-M^2)\right]^2 \\
&+counter\ terms \\
&= \frac{\lambda}{2}K_t^2-\frac{\lambda M^2}{4}C_f, \qquad \text{(C.6)}
\end{aligned}
$$

where,

$$
\begin{aligned}
K_t &= \frac{M^2}{2(4\pi)^2}(1-\ln\frac{M^2}{\kappa^2})-I_t \qquad \text{(C.7)} \\
C_f &= \frac{M^2}{(4\pi)^4}\{d-(\gamma-\ln 4\pi-1+\frac{1}{2}\ln\frac{M^2}{\kappa^2})\ln\frac{M^2}{\kappa^2}\}, \qquad \text{(C.8)} \\
I_t &= \int_0^\infty\frac{dk}{(2\pi)^2}\frac{k^2n_B(E)}{E}, \qquad \text{(C.9)} \\
d &= -\frac{1}{2}(\gamma^2-2\gamma+2+\frac{\pi^2}{6})+(\gamma-1-\frac{1}{2}\ln 4\pi)\ln 4\pi\simeq -5.68496, \qquad \text{(C.10)}
\end{aligned}
$$

and γ is the Euler constant.

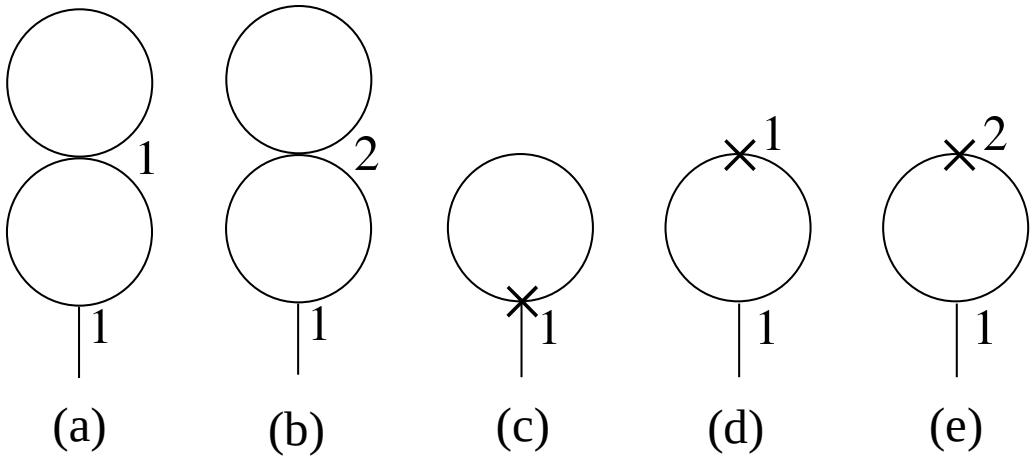

Figure C.2: (a) and (b):2 bubble diagrams. (c), (d) and (e): Tadpole diagrams including conter terms.

Also, Fig.C.5 (c) is the integral of Fig.C.2 (c) (d) (e), and the proper φ_1 tadpoles including counter term $V_c^{(1,0)2}$ read

$$\begin{aligned} -iV_c^{(1,0)2} &= -i\frac{\lambda}{2}(-iB_1\mu^2 - iC_1\varphi^2)\kappa^{2\varepsilon}\int\frac{d^nk}{(2\pi)^n}\{iD_\beta^{(11)}(k)\}^2 - \{iD_\beta^{(12)}(k)\}^2 \\ &\quad -i\frac{C_1\varphi^2}{2}\kappa^{2\varepsilon}\int\frac{d^nk}{(2\pi)^n}iD_\beta^{(11)}(k), \end{aligned} \tag{C.11}$$

where $B_1 = \lambda/2(4\pi)^2\bar{\varepsilon}$ and $C_1 = 3\lambda^2/2(4\pi)^2\bar{\varepsilon}$. The finite part V_c^2 reads

$$V_c^2 = \frac{\lambda}{4}(\mu^2 + \frac{3}{2}\lambda\varphi^2)C_f, \tag{C.12}$$

The setting sun diagram Fig.C.5 (b) is calculated from Fig.C.3. The φ_1 tadpoles which become setting sun ($V_s^{(1,0)2}$) read

$$\begin{aligned} -iV_s^{(1,0)2} &= \frac{(-i\lambda\varphi)^3}{4}\kappa^{6\varepsilon}\int\frac{d^nk_1}{(2\pi)^n}\frac{d^nk_2}{(2\pi)^n}[\{iD_\beta^{11}(k_1)\}^2 iD_\beta^{11}(k_2)iD_\beta^{11}(k_1+k_2) \\ &\quad -2iD_\beta^{11}(k_1)iD_\beta^{12}(k_1)iD_\beta^{12}(k_2)iD_\beta^{12}(k_1+k_2) \\ &\quad +\{iD_\beta^{12}(k_1)\}^2 iD_\beta^{22}(k_2)iD_\beta^{22}(k_1+k_2)] \\ &\quad +\frac{(-i\lambda\varphi)(-i\lambda)}{6}\kappa^{4\varepsilon}\int\frac{d^nk_1}{(2\pi)^n}\frac{d^nk_2}{(2\pi)^n}[iD_\beta^{11}(k_1)iD_\beta^{11}(k_2)iD_\beta^{11}(k_1+k_2) \\ &\quad -iD_\beta^{12}(k_1)iD_\beta^{12}(k_2)iD_\beta^{12}(k_1+k_2)] \\ &\quad +counter\ terms. \end{aligned} \tag{C.13}$$

Then, we find

$$V_s^2 = -i\frac{\lambda^2\varphi^2}{12}\kappa^{4\varepsilon}\int\frac{d^nk_1}{(2\pi)^n}\frac{d^nk_2}{(2\pi)^n}\left[\frac{i}{k_1^2 - M^2 + i\varepsilon}\frac{i}{k_2^2 - M^2 + i\varepsilon}\frac{i}{(k_1+k_2)^2 - M^2 + i\varepsilon}\right.$$

$$
\begin{aligned}
&+\frac{3i(2\pi)^2 n_B(|k_1^0|)n_B(|k_2^0|)\delta(k_1^2-M^2)\delta(k_2^2-M^2)}{(k_1+k_2)^2-M^2+i\varepsilon} \\
&+\frac{3i^2(2\pi)n_B(|k_1^0|)\delta(k_1^2-M^2)}{\{(k_1+k_2)^2-M^2+i\varepsilon\}\{k_1^2-M^2+i\varepsilon\}}\Big] + conter\ terms \\
= \quad & \frac{\lambda^2\varphi^2}{4}\frac{M^2}{(4\pi)^4}\{a+(\gamma-\ln 4\pi-3+\ln\frac{M^2}{\kappa^2})\ln\frac{M^2}{\kappa^2}\} \qquad \text{(C.14)} \\
&+\frac{1}{2(2\pi)^2}(\ln\frac{M^2}{\kappa^2}-2+\frac{\pi}{\sqrt{3}})I_t + I_l \\
\equiv \quad & \frac{\lambda^2\varphi^2}{4}S_s, \qquad \text{(C.15)}
\end{aligned}
$$

where

$$
\begin{aligned}
a &= \frac{\pi^2}{12}+\frac{9}{2}+\frac{1}{2}(\gamma-\ln 4\pi)(\gamma-\ln 4\pi-3) \\
&\quad +\int_0^1 dx\int_o^1 dy - \ln y(\ln\alpha-\frac{(1-y)\beta}{\alpha}) \qquad \text{(C.16)} \\
&\simeq 10.16186-2.17195=7.98891, \\
\alpha &= -(y-1+\frac{y}{x^2-x}), \qquad \text{(C.17)} \\
\beta &= -(1+\frac{1}{x^2-x}), \qquad \text{(C.18)}
\end{aligned}
$$

and

$$
I_l=\int_0^\infty \frac{dk_1dk_2}{(2\pi)^4}\frac{k_1k_2n_B(E_1)n_B(E_2)}{2E_1E_2}\ln\left|\frac{4E_1^2E_2^2-(M^2+2k_1k_2)^2}{4E_1^2E_2^2-(M^2-2k_1k_2)^2}\right|. \qquad \text{(C.19)}
$$

The sum of eq.(C.6), eq.(C.12) and eq.(C.14) leads to eq.(3.21).

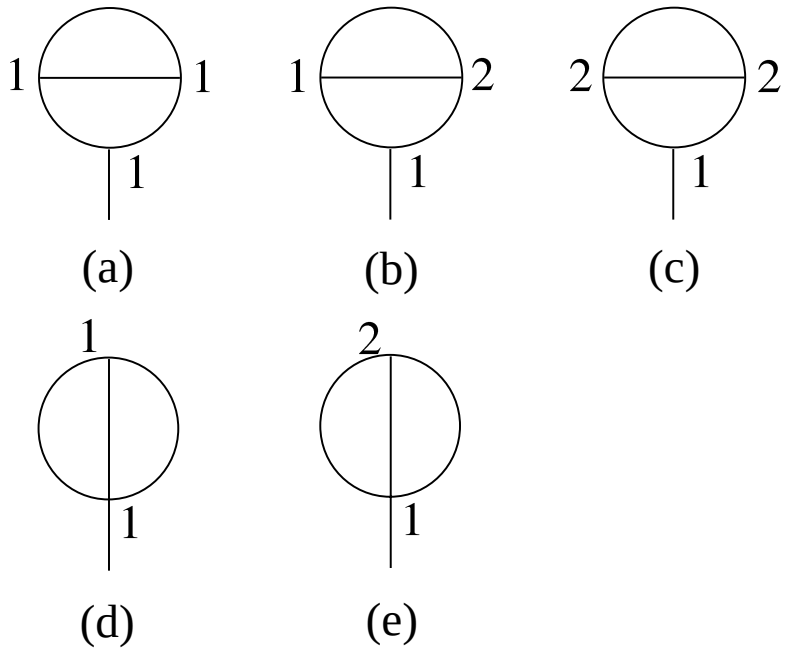

Figure C.3: Diagrams which contribute the setting sun diagram.

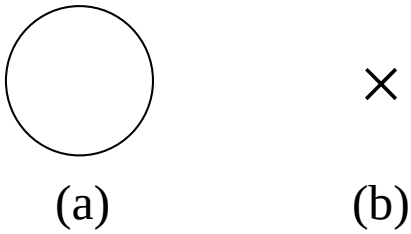

Figure C.4: One-loop effective potential diagrams.

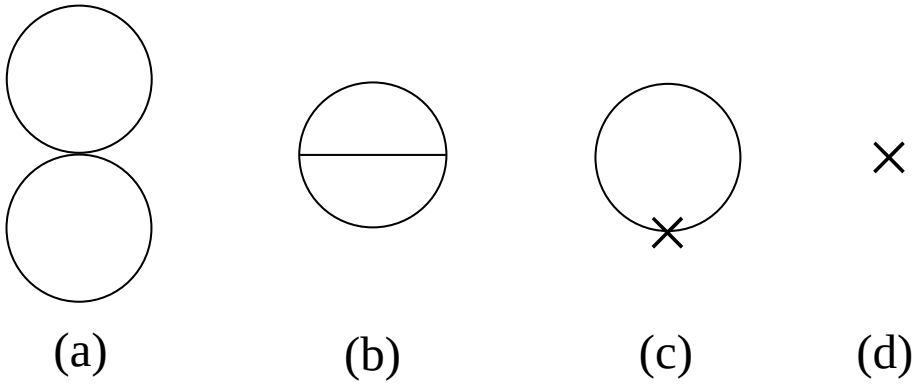

Figure C.5: Two-loop effective potential diagrams.

Appendix D

Full OPT equations

Here, we summarize the calculations of the effective potential and its derivatives in full OPT.

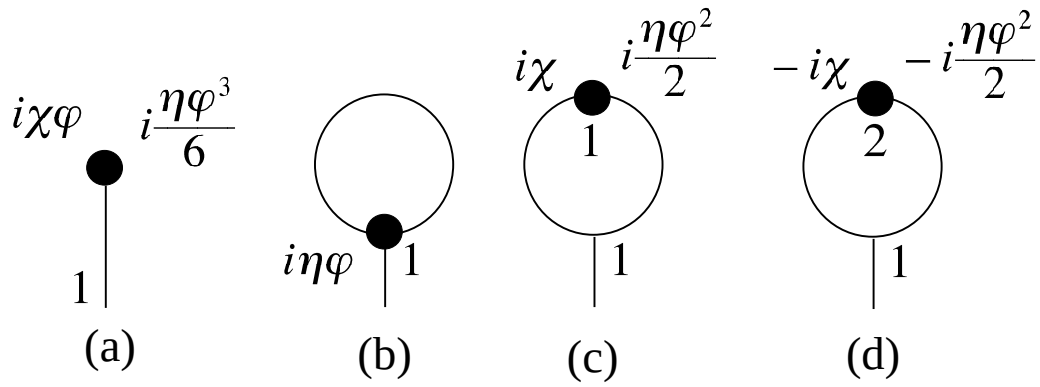

Figure D.1: (a): Additional $O(\delta)$ contributions to the 1-point function in full OPT. (b), (c) and (d): Additional $O(\delta^2)$ contributions to the 1-point function.

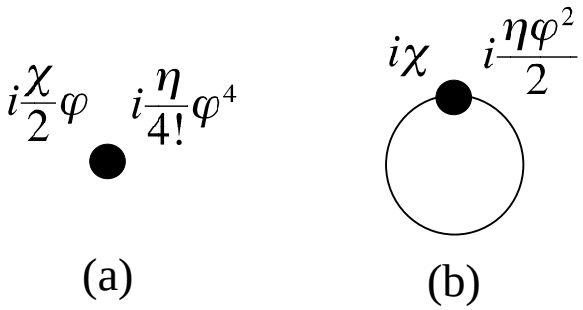

Figure D.2: (a): Additional $O(\delta)$ contributions to the effective potential in full OPT. (b): Additional $O(\delta^2)$ contributions.

The two-loop effective potential with the full optimized perturbation theory reads

$$V = V^0 + V^\delta + V^{\delta^2}, \tag{D.1}$$

$$
\begin{aligned}
V^0 &= \frac{1}{2}m^2\varphi^2 + \frac{g}{4!}\varphi^4, && \text{(D.2)}\\
V^\delta &= -\frac{1}{2}\chi\varphi^2 - \frac{\eta}{4!}\varphi^4 - \frac{1}{(4\pi)^2}\frac{M^4}{4}(\frac{3}{2} - \ln\frac{M^2}{\kappa^2}) \\
&\quad + \int_0^\infty \frac{dk}{(2\pi)^2}\frac{2}{\beta}k^2\ln(1-e^{-\beta E}), && \text{(D.3)}\\
V^{\delta^2} &= (\chi + \frac{\eta\varphi^2}{2} + \frac{g}{2}K_t)K_t + \frac{g^2\varphi^2}{4}T_f, && \text{(D.4)}
\end{aligned}
$$

where,

$$
\begin{array}{rclcl}
\mu^2 &=& m^2 - (m^2-\mu^2) &=& m^2 - \chi, \\
\lambda &=& g - (g-\lambda) &=& g - \eta,
\end{array}
\qquad \text{(D.5)}
$$

$$
\begin{aligned}
K_t &= \frac{M^2}{2(4\pi)^2}(1 - \ln\frac{M^2}{\kappa^2}) - I_t, && \text{(D.6)}\\
T_f &\equiv S_s + C_f \\
&= \frac{M^2}{(4\pi)^4}\{c + (-2 + \frac{1}{2}\ln\frac{M^2}{\kappa^2})\ln\frac{M^2}{\kappa^2}\} \\
&\quad + \frac{1}{2(2\pi)^2}(\ln\frac{M^2}{\kappa^2} - 2 + \frac{\pi}{\sqrt{3}})I_t + I_l, && \text{(D.7)}
\end{aligned}
$$

$$
\begin{aligned}
I_t &= \int_0^\infty \frac{dk}{(2\pi)^2}\frac{k^2 n_B(E)}{E}, && \text{(D.8)}\\
I_l &= \int_0^\infty \frac{dk_1 dk_2}{(2\pi)^4}\frac{k_1 k_2 n_B(E_1) n_B(E_2)}{2E_1E_2}\ln\left|\frac{4E_1^2E_2^2 - (M^2+2k_1k_2)^2}{4E_1^2E_2^2 - (M^2-2k_1k_2)^2}\right|, && \text{(D.9)}
\end{aligned}
$$

$$
\begin{aligned}
M^2 &= m^2 + \frac{g}{2}\varphi^2, && \text{(D.10)}\\
E &= \sqrt{k^2 + M^2}, && \text{(D.11)}\\
n_B(E) &= (e^{\beta E} - 1)^{-1}, && \text{(D.12)}
\end{aligned}
$$

$$
\begin{aligned}
c &= \frac{1}{2}(7 - \gamma - \ln 4\pi) - \int_0^1 dx \int_0^1 dy \ln y(\ln\alpha - \frac{(1-y)\beta}{\alpha}) \\
&\simeq 2.30495, && \text{(D.13)}\\
\alpha &= -(y - 1 + \frac{y}{x^2 - x}), && \text{(D.14)}\\
\beta &= -(1 + \frac{1}{x^2 - x}), && \text{(D.15)}
\end{aligned}
$$

and $\gamma = 0.5772\cdots$.

For PMS conditions

In the following, we will show equations to study the PMS conditions. For this purpose, we rewrite the arguments of the effective potential as $V(\varphi, M^2, m^2, g, \chi, \eta)$ for convenience. (When the arguments are written like this, the partial differentiation with respect to φ does not act on M^2, m^2, g, χ, η. On the other hand, if we write $V(\varphi, m^2, g)$, it act on $g\varphi/2$ in $M^2 = m^2 + g\varphi/2$.) Then, we can write the total derivative with respect to φ as

$$\frac{dV}{d\varphi} = \frac{\partial V}{\partial \varphi} + \frac{\partial M^2}{\partial \varphi}\frac{\partial V}{\partial M^2} = \frac{\partial V}{\partial \varphi} + g\varphi \frac{\partial V}{\partial M^2}, \tag{D.16}$$

$$\frac{\partial V}{\partial \varphi} = \varphi\left[m^2 + \frac{g}{6}\varphi^2\right] + \varphi\left[-\chi - \frac{\eta}{6}\varphi^2\right] + \varphi\left[\eta K_t + \frac{g^2}{2}T_f\right], \tag{D.17}$$

$$\frac{\partial V}{\partial M^2} = [-K_t] + \left[\frac{\partial K_t}{\partial M^2}(\chi + \frac{\eta\varphi^2}{2} + gK_t) + \frac{g^2\varphi^2}{4}\frac{\partial T_f}{\partial M^2}\right]. \tag{D.18}$$

The total derivative with respect to m^2 is found to be

$$\frac{dV}{dm^2} = \frac{\partial V}{\partial M^2} + \frac{\partial V}{\partial m^2} + \frac{\partial V}{\partial \chi}, \tag{D.19}$$

$$\frac{\partial V}{\partial m^2} = \frac{1}{2}\varphi^2, \tag{D.20}$$

$$\frac{\partial V}{\partial \chi} = -\frac{1}{2}\varphi^2 + K_t. \tag{D.21}$$

$$\tag{D.22}$$

The total derivative with respect to g reads

$$\frac{dV}{dg} = \frac{\partial V}{\partial g} + \frac{\partial V}{\partial \eta} + \frac{\partial M^2}{\partial g}\frac{\partial V}{\partial M^2} = \frac{\partial V}{\partial g} + \frac{\partial V}{\partial \eta} + \frac{\varphi^2}{2}\frac{\partial V}{\partial M^2}, \tag{D.23}$$

$$\frac{\partial V}{\partial g} = \frac{1}{4!}\varphi^4 + \left[\frac{1}{2}K_t^2 + \frac{g\varphi^2}{2}T_f\right], \tag{D.24}$$

$$\frac{\partial V}{\partial \eta} = -\frac{1}{4!}\varphi^4 + \left[\frac{\varphi^2}{2}K_t\right]. \tag{D.25}$$

Also, when $\varphi = 0$, (D.19), (D.23) read

$$\left.\frac{dV}{dm^2}\right|_{\varphi=0} = \frac{\partial K_t}{\partial M^2}(\chi + gK_t), \tag{D.26}$$

$$\left.\frac{dV}{dg}\right|_{\varphi=0} = \frac{1}{2}K_t^2. \tag{D.27}$$

For FAC conditions

Next, we list differentiations with respect to φ for FAC conditions. (Here, the arguments are written as $V(\varphi, m^2, g)$.) The first derivative of the effective potential

with respect to φ reads

$$\frac{\partial V}{\partial \varphi} = \frac{\partial V^0}{\partial \varphi} + \frac{\partial V^\delta}{\partial \varphi} + \frac{\partial V^{\delta^2}}{\partial \varphi}, \tag{D.28}$$

$$\frac{\partial V^0}{\partial \varphi} = \varphi\left[m^2 + \frac{g}{6}\varphi^2\right], \tag{D.29}$$

$$\frac{\partial V^\delta}{\partial \varphi} = \varphi\left[-\chi - \frac{\eta}{6}\varphi^2 - gK_t\right], \tag{D.30}$$

$$\frac{\partial V^{\delta^2}}{\partial \varphi} = \varphi\left[\eta K_t + g\frac{\partial K_t}{\partial M^2}(\chi + \frac{\eta\varphi^2}{2} + gK_t) + \frac{g^2}{2}(T_f + \frac{g\varphi^2}{2}\frac{\partial T_f}{\partial M^2})\right]. \tag{D.31}$$

The second derivative of the effective potential with respect to φ is found to be

$$\frac{\partial^2 V}{\partial \varphi^2} = \frac{\partial^2 V^0}{\partial \varphi^2} + \frac{\partial^2 V^\delta}{\partial \varphi^2} + \frac{\partial^2 V^{\delta^2}}{\partial \varphi^2}, \tag{D.32}$$

$$\frac{\partial^2 V^0}{\partial \varphi^2} = m^2 + \frac{g}{2}\varphi^2, \tag{D.33}$$

$$\frac{\partial^2 V^\delta}{\partial \varphi^2} = -\chi - \frac{\eta}{2}\varphi^2 - gK_t - g^2\varphi^2\frac{\partial K_t}{\partial M^2}, \tag{D.34}$$

$$\begin{aligned}\frac{\partial^2 V^{\delta^2}}{\partial \varphi^2} &= \eta K_t + g\frac{\partial K_t}{\partial M^2}(\chi + \frac{5}{2}\eta\varphi^2 + gK_t + g^2\varphi^2\frac{\partial K_t}{\partial M^2}) \\ &\quad + g^2\varphi^2\frac{\partial^2 K_t}{\partial (M^2)^2}(\chi + \frac{\eta\varphi^2}{2} + gK_t) \\ &\quad + \frac{g^2}{2}(T_f + \frac{5}{2}g\varphi^2\frac{\partial T_f}{\partial M^2} + \frac{1}{2}g^2\varphi^4\frac{\partial^2 T_f}{\partial (M^2)^2}),\end{aligned} \tag{D.35}$$

$$\begin{aligned}\Big[&= \left\{-\mu - \frac{\lambda}{6}\varphi^2 + gK_t\right\} \\ &\quad + g\varphi^2\left\{(2\eta + g^2\frac{\partial K_t}{\partial M^2})\frac{\partial K_t}{\partial M^2} + g\frac{\partial^2 K_t}{\partial (M^2)^2}(\chi + \frac{\eta\varphi^2}{2} + gK_t)\right. \\ &\quad \left. + g^2(\frac{\partial T_f}{\partial M^2} + \frac{g\varphi^2}{4}\frac{\partial^2 T_f}{\partial (M^2)^2})\right\} \quad (\text{ for } \varphi \neq 0)\Big].\end{aligned} \tag{D.36}$$

Finally, we find the forth derivative with respect to φ as

$$\frac{\partial^4 V}{\partial \varphi^4} = \frac{\partial^4 V^0}{\partial \varphi^4} + \frac{\partial^4 V^\delta}{\partial \varphi^4} + \frac{\partial^4 V^{\delta^2}}{\partial \varphi^4}, \tag{D.37}$$

$$\frac{\partial^4 V^0}{\partial \varphi^4} = g, \tag{D.38}$$

$$\frac{\partial^4 V^\delta}{\partial \varphi^4} = -\eta - 3g^2\frac{\partial K_t}{\partial M^2} - 6g^3\varphi^2\frac{\partial^2 K_t}{\partial (M^2)^2} - g^4\varphi^4\frac{\partial^3 K_t}{\partial (M^2)^3}, \tag{D.39}$$

$$\frac{\partial^4 V^0}{\partial \varphi^4} = 3g\frac{\partial K_t}{\partial M^2}(2\eta + g^2\frac{\partial K_t}{\partial M^2})$$

$$
\begin{aligned}
&+g^2\frac{\partial^2 K_t}{\partial(M^2)^2}(3\chi+\frac{39}{2}\eta\varphi^2+3gK_t+18g^2\varphi^2\frac{\partial K_t}{\partial M^2}+3g^3\varphi^4\frac{\partial^2 K_t}{\partial(M^2)^2})\\
&+g^3\varphi^2\frac{\partial^3 K_t}{\partial(M^2)^3}(6\chi+7\eta\varphi^2+6gK_t+4g^2\varphi^2\frac{\partial K_t}{\partial M^2})\\
&+g^4\varphi^4\frac{\partial^4 K_t}{\partial(M^2)^4}(\chi+\frac{\eta\varphi^2}{2}+gK_t) \qquad \text{(D.40)}\\
&+\frac{g^3}{2}(6\frac{\partial T_f}{\partial M^2}+\frac{39}{2}g\varphi^2\frac{\partial^2 T_f}{\partial(M^2)^2}+7g^2\varphi^4\frac{\partial^3 T_f}{\partial(M^2)^3}+\frac{1}{2}g^3\varphi^6\frac{\partial^4 T_f}{\partial(M^2)^4}).
\end{aligned}
$$

In the symmetric phase (namely, $\varphi=0$), eq.(D.32) eq.(D.37) can be simplified. Eq.(D.32) is reduced as

$$
\begin{aligned}
\left.\frac{\partial^2 V}{\partial\varphi^2}\right|_{\varphi=0} &= \left.\frac{\partial^2 V^0}{\partial\varphi^2}\right|_{\varphi=0}+\left.\frac{\partial^2 V^\delta}{\partial\varphi^2}\right|_{\varphi=0}+\left.\frac{\partial^2 V^{\delta^2}}{\partial\varphi^2}\right|_{\varphi=0}, && \text{(D.41)}\\
\left.\frac{\partial^2 V^0}{\partial\varphi^2}\right|_{\varphi=0} &= m^2, && \text{(D.42)}\\
\left.\frac{\partial^2 V^\delta}{\partial\varphi^2}\right|_{\varphi=0} &= -\chi-gK_t, && \text{(D.43)}\\
\left.\frac{\partial^2 V^{\delta^2}}{\partial\varphi^2}\right|_{\varphi=0} &= \eta K_t+g\frac{\partial K_t}{\partial M^2}(\chi+gK_t)+\frac{g^2}{2}T_f. && \text{(D.44)}
\end{aligned}
$$

Also, eq.(D.37) reads

$$
\begin{aligned}
\left.\frac{\partial^4 V}{\partial\varphi^4}\right|_{\varphi=0} &= \left.\frac{\partial^4 V^0}{\partial\varphi^4}\right|_{\varphi=0}+\left.\frac{\partial^4 V^\delta}{\partial\varphi^4}\right|_{\varphi=0}+\left.\frac{\partial^4 V^{\delta^2}}{\partial\varphi^4}\right|_{\varphi=0}, && \text{(D.45)}\\
\left.\frac{\partial^4 V^0}{\partial\varphi^4}\right|_{\varphi=0} &= g, && \text{(D.46)}\\
\left.\frac{\partial^4 V^\delta}{\partial\varphi^4}\right|_{\varphi=0} &= -\eta-3g^2\frac{\partial K_t}{\partial M^2}, && \text{(D.47)}\\
\left.\frac{\partial^4 V^{\delta^2}}{\partial\varphi^4}\right|_{\varphi=0} &= 3g\frac{\partial K_t}{\partial M^2}(2\eta+g^2\frac{\partial K_t}{\partial M^2})+3g^2\frac{\partial^2 K_t}{\partial(M^2)^2}(\chi+gK_t)\\
&\quad +3g^3\frac{\partial T_f}{\partial M^2}. && \text{(D.48)}
\end{aligned}
$$

The differentiations with respect to M^2 for eq.(D.8) are

$$
\begin{aligned}
\frac{\partial I_t}{\partial M^2} &= -\frac{1}{2}\int_0^\infty\frac{dk}{(2\pi)^2}R(E), && \text{(D.49)}\\
\frac{\partial^2 I_t}{\partial(M^2)^2} &= -\frac{1}{2}\int_0^\infty\frac{dk}{(2\pi)^2}\frac{\partial R(E)}{\partial M^2} && \text{(D.50)}\\
\frac{\partial^3 I_t}{\partial(M^2)^3} &= -\frac{1}{2}\int_0^\infty\frac{dk}{(2\pi)^2}\frac{\partial^2 R(E)}{\partial(M^2)^2} && \text{(D.51)}\\
\frac{\partial^4 I_t}{\partial(M^2)^4} &= -\frac{1}{2}\int_0^\infty\frac{dk}{(2\pi)^2}\frac{\partial^3 R(E)}{\partial(M^2)^3} && \text{(D.52)}
\end{aligned}
$$

where

$$
\begin{aligned}
R(E) &= \frac{n_B(E)}{E}, && \text{(D.53)}\\
\frac{\partial R(E)}{\partial M^2} &= -R(E)H(E), && \text{(D.54)}\\
\frac{\partial^2 R(E)}{\partial (M^2)^2} &= R(E)H^2(E) - R(E)\frac{\partial H(E)}{\partial M^2}, && \text{(D.55)}\\
\frac{\partial^3 R(E)}{\partial (M^2)^3} &= -R(E)H^3(E) + 3R(E)H(E)\frac{\partial H(E)}{\partial M^2} - R(E)\frac{\partial^2 H(E)}{\partial (M^2)^2}, && \text{(D.56)}\\
H(E) &= \frac{1}{2E}\left(\frac{1}{E} + f(E)\right), && \text{(D.57)}\\
\frac{\partial H(E)}{\partial M^2} &= -\frac{1}{4E^2}\left(\frac{2}{E^2} + \frac{f(E)}{E} + e^{-\beta E}f^2(E)\right), && \text{(D.58)}\\
\frac{\partial^2 H(E)}{\partial (M^2)^2} &= \frac{1}{8E^3}\left\{\frac{8}{E^3} + \frac{3}{E^2}f(E) + \left(\beta + \frac{3}{E}\right)e^{-\beta E}f^2(E) + 2e^{-2\beta E}f^3(E)\right\}, && \text{(D.59)}
\end{aligned}
$$

and $f(E) = \frac{\beta}{1-e^{-\beta E}}$.

The differentiations with respect to M^2 for eq.(D.9) are

$$
\begin{aligned}
\frac{\partial I_l}{\partial M^2} &= \int_0^\infty \frac{dk_1 dk_2}{(2\pi)^4}\left(R(E_1)\frac{\partial R(E_2)}{\partial M^2} + R(E_2)\frac{\partial R(E_1)}{\partial M^2}\right)L \\
&\quad + R(E_1)R(E_2)\frac{\partial L}{\partial M^2}, && \text{(D.60)}\\
\frac{\partial^2 I_l}{\partial^2 (M^2)^2} &= \int_0^\infty \frac{dk_1 dk_2}{(2\pi)^4}\frac{\partial^2 R(E_1)R(E_2)}{\partial (M^2)^2}L + R(E_1)R(E_2)\frac{\partial^2 L}{\partial (M^2)^2}, \\
&\quad + 2\left(R(E_1)\frac{\partial R(E_2)}{\partial M^2} + R(E_2)\frac{\partial R(E_1)}{\partial M^2}\right)\frac{\partial L}{\partial M^2} && \text{(D.61)}\\
\frac{\partial^3 I_l}{\partial^2 (M^2)^3} &= \int_0^\infty \frac{dk_1 dk_2}{(2\pi)^4}\frac{\partial^3 R(E_1)R(E_2)}{\partial (M^2)^3}L + 3\frac{\partial^2 R(E_1)R(E_2)}{\partial (M^2)^2}\frac{\partial L}{\partial M^2} \\
&\quad + 3\frac{\partial R(E_1)R(E_2)}{\partial M^2}\frac{\partial^2 L}{\partial (M^2)^2} + R(E_1)R(E_2)\frac{\partial^3 L}{\partial (M^2)^3}, && \text{(D.62)}\\
\frac{\partial^4 I_l}{\partial^2 (M^2)^4} &= \int_0^\infty \frac{dk_1 dk_2}{(2\pi)^4}\frac{\partial^4 R(E_1)R(E_2)}{\partial (M^2)^4}L + 4\frac{\partial^3 R(E_1)R(E_2)}{\partial (M^2)^3}\frac{\partial L}{\partial M^2} \\
&\quad + 6\frac{\partial^2 R(E_1)R(E_2)}{\partial (M^2)^2}\frac{\partial^2 L}{\partial (M^2)^2} + 4\frac{\partial R(E_1)R(E_2)}{\partial M^2}\frac{\partial^3 L}{\partial (M^2)^2} && \text{(D.63)}\\
&\quad + R(E_1)R(E_2)\frac{\partial^4 L}{\partial (M^2)^4},
\end{aligned}
$$

where

$$
\frac{\partial^2 R(E_1)R(E_2)}{\partial (M^2)^2} = R(E_1)\frac{\partial^2 R(E_2)}{\partial (M^2)^2} + 2\frac{\partial R(E_1)}{\partial M^2}\frac{\partial R(E_2)}{\partial M^2} + R(E_2)\frac{\partial^2 R(E_1)}{\partial (M^2)^2}, \quad \text{(D.64)}
$$

$$\frac{\partial^3 R(E_1)R(E_2)}{\partial(M^2)^3} = R(E_1)\frac{\partial^3 R(E_2)}{\partial(M^2)^3} + 3\frac{\partial R(E_1)}{\partial M^2}\frac{\partial^2 R(E_2)}{\partial(M^2)^2} + 3\frac{\partial^2 R(E_1)}{\partial(M^2)^2}\frac{\partial R(E_2)}{\partial M^2} + R(E_2)\frac{\partial^3 R(E_1)}{\partial(M^2)^3}, \quad \text{(D.65)}$$

$$\frac{\partial^4 R(E_1)R(E_2)}{\partial(M^2)^4} = R(E_1)\frac{\partial^4 R(E_2)}{\partial(M^2)^4} + 4\frac{\partial R(E_1)}{\partial M^2}\frac{\partial^3 R(E_2)}{\partial(M^2)^3} + 6\frac{\partial^2 R(E_1)}{\partial(M^2)^2}\frac{\partial^2 R(E_2)}{\partial(M^2)^2} + 4\frac{\partial^3 R(E_1)}{\partial(M^2)^3}\frac{\partial R(E_2)}{\partial M^2} + R(E_2)\frac{\partial^4 R(E_1)}{\partial(M^2)^4}, \quad \text{(D.66)}$$

$$\frac{\partial^4 R(E)}{\partial(M^2)^4} = R(E)H^4(E) - 6R(E)H^2(E)\frac{\partial H(E)}{\partial M^2} + 3R(E)\left(\frac{\partial H(E)}{\partial(M^2)}\right)^2 + 4R(E)H(E)\frac{\partial^2 H(E)}{\partial(M^2)^2} - R(E)\frac{\partial^3 H(E)}{\partial(M^2)^3}, \quad \text{(D.67)}$$

$$\frac{\partial^3 H(E)}{\partial(M^2)^3} = -\frac{1}{16E^4}\left\{\frac{48}{E^4} + \frac{15}{E^3}f(E) + \left(6\beta + \frac{15}{E}\right)\frac{e^{-\beta E}}{E}f^2(E) + \beta^2 e^{-\beta E}f^2(E) + 6\left(\beta + \frac{2}{E}\right)e^{-2\beta E}f^3(E) + 6e^{-3\beta E}f^4(E)\right\} \quad \text{(D.68)}$$

and

$$L = \ln\left|\frac{4E_1^2E_2^2 - (M^2 + 2k_1k_2)^2}{4E_1^2E_2^2 - (M^2 - 2k_1k_2)^2}\right|. \quad \text{(D.69)}$$

The derivatives with respect to M^2 for L can be found as

$$\frac{\partial L}{\partial M^2} = \frac{2\{2(k_1+k_2)^2 + 3M^2\}}{4E_1^2E_2^2 - (M^2 + 2k_1k_2)^2} - \frac{2\{2(k_1+k_2)^2 + 3M^2\}}{4E_1^2E_2^2 - (M^2 - 2k_1k_2)^2}, \quad \text{(D.70)}$$

$$\frac{\partial^2 L}{\partial(M^2)^2} = \frac{6}{4E_1^2E_2^2 - (M^2 + 2k_1k_2)^2} - 4\left\{\frac{2(k_1+k_2)^2 + 3M^2}{4E_1^2E_2^2 - (M^2 + 2k_1k_2)^2}\right\}^2 - \frac{6}{4E_1^2E_2^2 - (M^2 - 2k_1k_2)^2} + 4\left\{\frac{2(k_1+k_2)^2 + 3M^2}{4E_1^2E_2^2 - (M^2 - 2k_1k_2)^2}\right\}^2, \quad \text{(D.71)}$$

$$\frac{\partial^3 L}{\partial(M^2)^3} = -\frac{36\{2(k_1+k_2)^2 + 3M^2\}}{\{4E_1^2E_2^2 - (M^2 + 2k_1k_2)^2\}^2} + 16\left\{\frac{2(k_1+k_2)^2 + 3M^2}{4E_1^2E_2^2 - (M^2 + 2k_1k_2)^2\}}\right\}^3 + \frac{36\{2(k_1+k_2)^2 + 3M^2\}}{\{4E_1^2E_2^2 - (M^2 - 2k_1k_2)^2\}^2} - 16\left\{\frac{2(k_1+k_2)^2 + 3M^2}{4E_1^2E_2^2 - (M^2 - 2k_1k_2)^2}\right\}^3, \quad \text{(D.72)}$$

$$\frac{\partial^4 L}{\partial(M^2)^4} = -\frac{108}{\{4E_1^2E_2^2 - (M^2 + 2k_1k_2)^2\}^2} + \frac{288\{2(k_1+k_2)^2 + 3M^2\}^2}{\{4E_1^2E_2^2 - (M^2 + 2k_1k_2)^2\}^3} - 96\left\{\frac{2(k_1+k_2)^2 + 3M^2}{4E_1^2E_2^2 - (M^2 + 2k_1k_2)^2}\right\}^4 + \frac{108}{\{4E_1^2E_2^2 - (M^2 - 2k_1k_2)^2\}^2} + \frac{288\{2(k_1+k_2)^2 + 3M^2\}^2}{\{4E_1^2E_2^2 - (M^2 - 2k_1k_2)^2\}^3} + 96\left\{\frac{2(k_1+k_2)^2 + 3M^2}{4E_1^2E_2^2 - (M^2 - 2k_1k_2)^2}\right\}^4, \quad \text{(D.73)}$$

High T forms

Now, we give high temperature ($\beta M \to 0$) forms of eq.(D.6), eq.(D.8), eq.(D.9) and derivatives of eq.(D.6). We find

$$K_t \to -\frac{T^2}{24} + \frac{MT}{8\pi} + \frac{M^2}{2(4\pi)^2}(1 - \ln\frac{T^2}{\kappa^2}) - \frac{M^2}{(4\pi)^2}(\ln 4\pi - \gamma + \frac{1}{2}), \quad \text{(D.74)}$$

$$\frac{\partial K_t}{\partial M^2} \to \frac{T}{16\pi M} + \frac{1}{2(4\pi)^2}(1 - \ln\frac{T^2}{\kappa^2}) - \frac{1}{(4\pi)^2}(\ln 4\pi - \gamma + \frac{1}{2}), \quad \text{(D.75)}$$

$$\frac{\partial^2 K_t}{\partial (M^2)^2} \to -\frac{T}{32\pi M^3}, \quad \text{(D.76)}$$

$$\frac{\partial^3 K_t}{\partial (M^2)^3} \to \frac{3T}{64\pi M^5}, \quad \text{(D.77)}$$

$$\frac{\partial^4 K_t}{\partial (M^2)^4} \to -\frac{15T}{128\pi M^7}, \quad \text{(D.78)}$$

$$I_t \to \frac{T^2}{24} - \frac{MT}{8\pi} + \frac{M^2}{2(4\pi)^2}\ln\frac{T^2}{M^2} + \frac{M^2}{(4\pi)^2}(\ln 4\pi - \gamma + \frac{1}{2}), \quad \text{(D.79)}$$

$$I_l \to \frac{T^2}{12(4\pi)^2}(\ln\frac{M^2}{T^2} + 3.48871). \quad \text{(D.80)}$$

Appendix E

One loop formula for self-energy at $T \neq 0$

Formulas corresponding to Fig.4.2 read

$$\begin{aligned}
-i\Sigma^{11}_{\sigma}(\omega,\vec{k}) - i\Sigma^{11}_{\sigma}(\omega,\vec{k};T) &= -i\frac{\lambda}{2}[I^{(1)}_{\pi} + F^{(1)}_{\pi} + I^{(1)}_{\sigma} + F^{(1)}_{\sigma}] \\
&\quad + (-i\frac{\lambda\xi}{3})^2\frac{3}{2}[I^{(2)}_{\pi} + 2F^{(2)}_{\pi} + F^{(3)}_{\pi}] \\
&\quad + (-i\lambda\xi)^2\frac{1}{2}[I^{(2)}_{\sigma} + 2F^{(2)}_{\sigma} + F^{(3)}_{\sigma}] \qquad \text{(E.1)} \\
&\quad + i(m^2-\mu^2) + \text{counter terms} \\
-i\Sigma^{11}_{\pi}(\omega,\vec{k}) - i\Sigma^{11}_{\pi}(\omega,\vec{k};T) &= -i\frac{5\lambda}{6}[I^{(1)}_{\pi} + F^{(1)}_{\pi}] - i\frac{\lambda}{6}[I^{(1)}_{\sigma} + F^{(1)}_{\sigma}] \qquad \text{(E.2)} \\
&\quad + (-i\frac{\lambda\xi}{3})^2[I^{(3)} + F^{(4)} + F^{(5)}] \qquad \text{(E.3)} \\
&\quad + i(m^2-\mu^2) + \text{counter terms},
\end{aligned}$$

with

$$I^{(1)}_{\phi} = \kappa^{2\varepsilon}\int\frac{d^4p}{(2\pi)^4}\frac{i}{p^2 - m^2_{0\phi} + i\epsilon}, \qquad \text{(E.4)}$$

$$I^{(2)}_{\phi} = \kappa^{2\varepsilon}\int\frac{d^4p}{(2\pi)^4}\frac{i}{p^2 - m^2_{0\phi} + i\varepsilon}\frac{i}{(p+k)^2 - m^2_{0\phi} + i\epsilon}, \qquad \text{(E.5)}$$

$$I^{(3)} = \kappa^{2\varepsilon}\int\frac{d^4p}{(2\pi)^4}\frac{i}{p^2 - m^2_{0\sigma} + i\varepsilon}\frac{i}{(p+k)^2 - m^2_{0\pi} + i\epsilon}, \qquad \text{(E.6)}$$

$$F^{(1)}_{\phi} = \int\frac{d^4p}{(2\pi)^4}2\pi n_B(|p_0|)\delta(p^2 - m^2_{0\phi}), \qquad \text{(E.7)}$$

$$F^{(2)}_{\phi} = i\int\frac{d^4p}{(2\pi)^4}\frac{2\pi n_B(|p_0|)\delta(p^2 - m^2_{0\phi})}{(p+k)^2 - m^2_{0\phi} + i\epsilon}, \qquad \text{(E.8)}$$

$$F^{(3)}_{\phi} = \int\frac{d^4p}{(2\pi)^4}(2\pi)^2 n_B(|p_0|)n_B(|p_0+\omega|)\delta(p^2 - m^2_{0\phi})\delta((p+k)^2 - m^2_{0\phi}), \qquad \text{(E.9)}$$

$$F^{(4)} = i\int \frac{d^4p}{(2\pi)^4}\frac{2\pi n_B(|p_0|)\delta(p^2-m_{0\sigma}^2)}{(p+k)^2-m_{0\pi}^2+i\epsilon}+(m_{0\sigma}\leftrightarrow m_{0\pi}), \tag{E.10}$$

$$F^{(5)} = \int \frac{d^4p}{(2\pi)^4}(2\pi)^2 n_B(|p_0|)n_B(|p_0+\omega|)\delta(p^2-m_{0\sigma}^2)\delta((p+k)^2-m_{0\pi}^2). \tag{E.11}$$

Here $\varepsilon=(4-n)/2$, $p^2=p_0^2-\vec{p}^2$, $k^2=\omega^2-\vec{k}^2$ and $n_B(\omega)=[e^{\omega/T}-1]^{-1}$.

The explicit forms of eq.(E.4), (E.5), (E.6) for $k^2>0$ are

$$I_\phi^{(1)} = -\frac{m_{0\phi}^2}{16\pi^2}(\frac{1}{\bar{\varepsilon}}+1-\log\frac{m_{0\phi}^2}{\kappa^2}), \tag{E.12}$$

$$I_\phi^{(2)} = -i\frac{1}{16\pi^2}[\frac{1}{\bar{\varepsilon}}-\log\frac{m_{0\phi}^2}{\kappa^2}+2+\begin{cases} q_2(\log\frac{1-q_2}{1+q_2}+i\pi)] & \text{for} \quad k^2>4m_{0\phi}^2 \\ -2q_2\arctan\frac{1}{q_2}] & \text{for} \quad 0<k^2<4m_{0\phi}^2, \end{cases} \tag{E.13}$$

$$\begin{aligned} I^{(3)} = & -i\frac{1}{16\pi^2}[\frac{1}{\bar{\varepsilon}}-\log\frac{m_{0\pi}^2}{\kappa^2}+2+\frac{k^2+m_{0\sigma}^2-m_{0\pi}^2}{2k^2}\log\frac{m_{0\pi}^2}{m_{0\sigma}^2} \\ & -\begin{cases} q_3(\log\frac{(2k^2q_3+k^2-m_{0\sigma}^2+m_{0\pi}^2)(2k^2q_3+k^2+m_{0\sigma}^2-m_{0\pi}^2)}{(2k^2q_3-k^2+m_{0\sigma}^2-m_{0\pi}^2)(2k^2q_3-k^2-m_{0\sigma}^2+m_{0\pi}^2)}-2i\pi)] \\ \qquad\qquad \text{for} \quad (m_{0\sigma}+m_{0\pi})^2<k^2 \\ 2q_3(\arctan\frac{k^2-m_{0\sigma}^2+m_{0\pi}^2}{2k^2q_3}+\arctan\frac{k^2+m_{0\sigma}^2-m_{0\pi}^2}{2k^2q_3})] \\ \qquad\qquad \text{for} \quad (m_{0\sigma}-m_{0\pi})^2<k^2<(m_{0\sigma}+m_{0\pi})^2 \\ q_3\log\frac{(2k^2q_3+k^2-m_{0\sigma}^2+m_{0\pi}^2)(2k^2q_3+k^2+m_{0\sigma}^2-m_{0\pi}^2)}{(2k^2q_3-k^2+m_{0\sigma}^2-m_{0\pi}^2)(2k^2q_3-k^2-m_{0\sigma}^2+m_{0\pi}^2)}] \\ \qquad\qquad \text{for} \quad 0<k^2<(m_{0\sigma}-m_{0\pi})^2, \end{cases} \end{aligned} \tag{E.14}$$

with

$$q_2=\sqrt{\left|\frac{4m_{0\phi}^2}{k^2}-1\right|}, \qquad q_3=\frac{\sqrt{|(k^2+m_{0\sigma}^2-m_{0\pi}^2)^2-4k^2m_{0\sigma}^2|}}{2k^2}.$$

Eq.(E.7), (E.8), (E.9), (E.10) and (E.11) for $\vec{k}=0$ read

$$F_\phi^{(1)} = \int_0^\infty \frac{dp}{2\pi^2}\frac{p^2n_B(E(m_{0\phi}))}{E(m_{0\phi})}, \tag{E.15}$$

$$\begin{aligned} F_\phi^{(2)} = & \; i\int_0^\infty \frac{dp}{2\pi^2}\frac{p^2n_B(E(m_{0\phi}))}{E(m_{0\phi})}\frac{1}{\omega^2-4E^2(m_{0\phi})} \\ & +\theta(\omega^2-4m_{0\phi}^2)\frac{\sqrt{\omega^2-4m_{0\phi}^2}}{16\pi\omega}n_B(\frac{\omega}{2}), \end{aligned} \tag{E.16}$$

$$F_\phi^{(3)} = \theta(\omega^2-4m_{0\phi}^2)\frac{\sqrt{\omega^2-4m_{0\phi}^2}}{8\pi\omega}n_B^2(\frac{\omega}{2}), \tag{E.17}$$

$$\begin{aligned} F^{(4)} = & \; i\int_0^\infty \frac{dp}{(2\pi)^2}\frac{p^2n_B(E(m_{0\sigma}))}{E(m_{0\sigma})} \\ & \times\{\frac{1}{(\omega+E(m_{0\sigma}))^2-E(m_{0\pi})^2}+\frac{1}{(\omega-E(m_{0\sigma}))^2-E(m_{0\pi})^2}\} \end{aligned} \tag{E.18}$$

$$
\begin{aligned}
&+\begin{cases} \frac{1}{16\pi\omega^2}\sqrt{(\omega^2+m_{0\sigma}^2-m_{0\pi}^2)^2-4m_{0\sigma}^2\omega^2}\; n_B(\frac{|\omega^2+m_{0\sigma}^2-m_{0\pi}^2|}{2\omega}) \\ \qquad\qquad \text{for} \quad 0<\omega^2<(m_{0\sigma}-m_{0\pi})^2\ ,\ (m_{0\sigma}+m_{0\pi})^2<\omega^2 \\ 0 \qquad\qquad \text{for} \quad (m_{0\sigma}-m_{0\pi})^2<\omega^2<(m_{0\sigma}+m_{0\pi})^2, \end{cases} \\
&+(m_{0\sigma}\leftrightarrow m_{0\pi}) \\
F^{(5)} \;=\; &\begin{cases} \frac{1}{8\pi\omega^2}\sqrt{(\omega^2+m_{0\sigma}^2-m_{0\pi}^2)^2-4m_{0\sigma}^2\omega^2}\; n_B(\frac{|\omega^2+m_{0\sigma}^2-m_{0\pi}^2|}{2\omega})\; n_B(\frac{|\omega^2-m_{0\sigma}^2+m_{0\pi}^2|}{2\omega}) \\ \qquad\qquad \text{for} \quad 0<\omega^2<(m_{0\sigma}-m_{0\pi})^2\ ,\ (m_{0\sigma}+m_{0\pi})^2<\omega^2 \\ 0 \qquad\qquad \text{for} \quad (m_{0\sigma}-m_{0\pi})^2<\omega^2<(m_{0\sigma}+m_{0\pi})^2, \end{cases}
\end{aligned}
\tag{E.19}
$$

where $E(m)=\sqrt{\vec{p}^2+m^2}$.

Appendix F

Calculation of diphoton emission rates

Calculation of $g_{\sigma\to 2\pi\to\gamma\gamma}$

The loop integral of Fig.4.9 (a) reads

$$L^{\mu\nu}_{a\sigma} = \frac{1}{2}\int \frac{d^4p}{(2\pi)^4} \frac{i^3\mathrm{Tr}\{-ie_3(2p+k_2+q)^\mu\}\{-ie_3(2p+k_2)^\nu\}(-i\frac{\lambda}{3}\xi)}{(p^2-m^2_{0\pi}+i\varepsilon)\{(p+k_2)^2-m^2_{0\pi}+i\varepsilon\}\{(p+q)^2-m^2_{0\pi}+i\varepsilon\}}, \quad \text{(F.1)}$$

where the Tr is performed over the flavor index (e_3). The loop integral of Fig.4.9 (b), $L^{\mu\nu}_{b\sigma}$, is obtained by replacing k_2 with k_1 and exchanging μ and ν. The sum of these is

$$\begin{aligned} L^{\mu\nu}_{a\sigma} + L^{\mu\nu}_{b\sigma} &= \frac{ig_{\mu\nu}e^2\lambda\xi}{24\pi^2}\left\{\frac{1}{\bar{\varepsilon}} - \ln\frac{m^2_{0\pi}}{\kappa^2} + 2 - 2d\arctan\frac{1}{d}\right\} \\ &\quad + \frac{ie^2\lambda\xi}{24\pi^2}\left(g_{\mu\nu} - \frac{k_1^\mu k_2^\nu}{k_1\cdot k_2}\right)\left(1 - \frac{4m^2_{0\pi}}{2k_1\cdot k_2}\sin^{-1}\frac{\sqrt{2k_1\cdot k_2}}{2m_{0\pi}}\right), \quad \text{(F.2)} \end{aligned}$$

where $d = \sqrt{\frac{4m^2_{0\pi}}{2k_1\cdot k_2} - 1}$.

The Fig.4.9 (c) is given as

$$\begin{aligned} L^{\mu\nu}_{c\sigma} &= \frac{1}{2}\int \frac{d^4p}{(2\pi)^4} \frac{i^2\mathrm{Tr}2ie_3^2 g^{\mu\nu}\left(-i\frac{\lambda}{3}\xi\right)}{(p^2-m^2_{0\pi}+i\varepsilon)\{(p+q)^2-m^2_{0\pi}+i\varepsilon\}} \\ &= -\frac{ig_{\mu\nu}e^2\lambda\xi}{24\pi^2}\left\{\frac{1}{\bar{\varepsilon}} - \ln\frac{m^2_{0\pi}}{\kappa^2} + 2 - 2d\arctan\frac{1}{d}\right\}. \quad \text{(F.3)} \end{aligned}$$

The first line in eq.(F.2) and eq.(F.3) are canceled each other, thus $g_{\sigma\to 2\pi\to 2\gamma\gamma}$ reads

$$\begin{aligned} 4ig_{\sigma\to 2\pi\to\gamma\gamma}(k_1\cdot k_2 g^{\mu\nu} - k_1^\mu k_2^\nu) &= L^{\mu\nu}_{a\sigma} + L^{\mu\nu}_{b\sigma} + L^{\mu\nu}_{c\sigma} \\ g_{\sigma\to 2\pi\to\gamma\gamma} &= \frac{\alpha\lambda\xi}{12\pi}\left\{\frac{1}{q^2} - \frac{4m^2_{0\pi}}{(q^2)^2}\left(\sin^{-1}\frac{\sqrt{q^2}}{2m_{0\pi}}\right)^2\right\}, \quad \text{(F.4)} \end{aligned}$$

where $\alpha = e^2/(4\pi)$ and $q^2 = 2k_1\cdot k_2$.

Calculation of $g_{\sigma\to q\bar{q}\to\gamma\gamma}$

The loop integral of Fig.4.9 (d) reads

$$L^{\mu\nu}_{d\sigma} = -\int \frac{d^4p}{(2\pi)^2} \frac{i^3 \mathrm{Tr}(-ig)(\not{p}+m_q)(-ie_\tau\gamma^\nu)(\not{p}+\not{k}_2+m_q)(-ie_\tau\gamma^\mu)(\not{p}+\not{q}+m_q)}{(p^2-m_q^2+i\varepsilon)\{(p+k_2)^2-m_q^2+i\varepsilon\}\{(p+q)^2-m_q^2+i\varepsilon\}}. \quad \text{(F.5)}$$

Tr is performed over color, flavor and spinor indices. $L^{\mu\nu}_{d\sigma}$ is obtained by $k_2 \to k_1$ and $\gamma^\mu \leftrightarrow \gamma^\nu$. Thus, we get

$$\begin{aligned} 4ig_{\sigma\to q\bar{q}\to\gamma\gamma}(k_1\cdot k_2 g^{\mu\nu} - k_1^\mu k_2^\nu) &= L^{\mu\nu}_{d\sigma} + L^{\mu\nu}_{e\sigma} \\ g_{\sigma\to q\bar{q}\to\gamma\gamma} &= -\frac{5m_q^2\alpha}{3\pi f_\pi}\left\{\frac{1}{q^2} + \frac{q^2-4m_q^2}{(q^2)^2}\left(\sin^{-1}\frac{\sqrt{q^2}}{2m_q}\right)^2\right\}. \quad \text{(F.6)} \end{aligned}$$

Calculation of $g_{\pi^0\to\gamma\gamma}$

Contributions to $g_{\pi^0\to\gamma\gamma}$ are only from the quark-loops, and they are shown in Fig.4.9 (d) and (e). The loop integral of Fig.4.9 (d) is

$$\begin{aligned} L^{\mu\nu}_{d\pi^0} &= -\int \frac{d^4p}{(2\pi)^2} \frac{i^3 \mathrm{Tr}(-ig)i\gamma_5\tau_3(\not{p}+m_q)(-ie_\tau\gamma^\nu)(\not{p}+\not{k}_2+m_q)(-ie_\tau\gamma^\mu)(\not{p}+\not{q}+m_q)}{(p^2-m_q+i\varepsilon)\{(p+k_2)^2-m_q+i\varepsilon\}\{(p+q)^2-m_q+i\varepsilon\}} \\ &= 4ge^2 m_q \varepsilon^{\mu\nu\lambda\rho} q_\lambda k_{2\rho} I_3, \quad \text{(F.7)} \end{aligned}$$

where

$$\begin{aligned} I_3 &= \int \frac{d^4p}{(2\pi)^4} \frac{1}{(p^2-m_q+i\varepsilon)\{(p+k_2)^2-m_q+i\varepsilon\}\{(p+q)^2-m_q+i\varepsilon\}} \\ &= \frac{-i}{8\pi^2}\frac{1}{q^2}\left(\sin^{-1}\frac{\sqrt{q^2}}{2m_q}\right)^2. \quad \text{(F.8)} \end{aligned}$$

Thus,

$$\begin{aligned} 4ig_{\pi^0\gamma\gamma}\varepsilon^{\mu\nu\lambda\rho}k_{1\lambda}k_{1\rho} &= L^{\mu\nu}_{d\pi^0} + L^{\mu\nu}_{e\pi^0} \\ &= \frac{-ie^2 g m_q}{\pi^2 q^2}\varepsilon^{\mu\nu\lambda\rho}k_{1\lambda}k_{1\rho}\left(\sin^{-1}\frac{\sqrt{q^2}}{2m_q}\right)^2. \quad \text{(F.9)} \end{aligned}$$

Pair annihilation formula

The invariant amplitude of Fig.4.11 is given as

$$\begin{aligned} \mathcal{M}^{\mu\nu} &= \{-ie(2p_1-k_1)\cdot\varepsilon_1^*\}\frac{i}{(p_1-k_1)^2-m_\pi^2}\{-ie(-p_2+p_1-k_1)\cdot\varepsilon_2^*\} \\ &\quad \{-ie(2p_1-k_2)\cdot\varepsilon_2^*\}\frac{i}{(p_1-k_1)^2-m_\pi^2}\{-ie(-p_2+p_1-k_2)\cdot\varepsilon_1^*\} \quad \text{(F.10)} \\ &\quad +2ie^2 g^{\mu\nu}. \end{aligned}$$

Square of this with summing over all polarizations leads to

$$|\mathcal{M}|^2 = 4e^2 \left\{ 4 + \frac{m_\pi^4}{(p_1 k_1)^2} + \frac{m_\pi^4}{(p_1 k_2)^2} - \frac{2p_1 p_2}{p_1 k_1} - \frac{2p_1 p_2}{p_1 k_2} + \frac{2(p_1 p_2)^2}{(p_1 k_1)(p_1 k_2)} \right\}. \quad \text{(F.11)}$$

On the other hand, eq.(4.66) can be written as

$$\begin{aligned} \frac{dN}{d^4x} &= \int \frac{n_B(E_1)}{(2\pi)^3 2E_1} d^3p_1 \frac{n_B(E_2)}{(2\pi)^3 2E_2} d^3p_2 \int d^4q \delta^4(q - k_1 - k_2) \\ &\quad \times |\mathcal{M}|^2 (2\pi)^4 \delta^4(p_1 + p_2 - k_1 - k_2) \frac{d^3k_1}{(2\pi)^3 2k_1^0} \frac{d^3k_2}{(2\pi)^3 2k_2^0} \\ &= \int \left\{ \frac{n_B(E)}{(2\pi)^3 2E} \right\}^2 \delta(2E - \omega) \frac{|\mathcal{M}|^2}{4} p^2 dp d\cos\theta d^4q, \end{aligned} \quad \text{(F.12)}$$

where $E = \sqrt{p^2 + m_\pi^2}$ and we use the back to back kinematics ($\vec{q} = 0$). Substituting eq.(F.11), and performing angular integral, we get eq.(4.67).

Bibliography

[1] Y. Nambu, In Preludes in Theoretical Physics, in honor of V. F. Weisskopf, (North-Holland, Amsterdam, 1966).
T. Muta, *Foundations of Quantum Chromodynamics 2ed.*, (World Scientific, Singapore, 1987).

[2] D. Gross and F. Wilczek, Phys. Rev. Lett. **30** 1343 (1973); Phys. Rev. **D6** 3633 (1973).
H. D. Politzer, Phys. Rev. Lett. **30** 1346 (1973).

[3] Quark Matter '96, Nucl. Phys. **A610** (1996).
Quark Matter '97, Nucl. Phys. **A638** (1998).

[4] J. Stachel, Nucl. Phys. **A654** 119 (1999).

[5] LATTICE '98, Nucl. Phys. B (Proc. Suppl.) **73**, (1999).

[6] See, e.g. S. Weinberg, *GRAVITATION AND COSMOLOGY*, (John Wiley & Sons, Inc. 1972).
E. W. Kolb and M. S. Turner, *The Early Universe:Reprints*, (Addison-Wesley, 1988); *The Early Universe*, (Addison-Wesley, 1990).

[7] See examples quoted in *Basic Notion of Condensed Matter Physics*, P. W. Anderson, (Benjamin, California, 1984); *Phasenübergänge and Kritische Phänomene*, W. Gebhardt and U. Krey, (Friedr. Vieweg & Sohn, Wiesbaden, 1980).

[8] E. Braaten and R. D. Pisarski, Nucl. Phys. **B337**, 569 (1990); ibid. **B339**, 310 (1990).
J. Frenkel and J. C. Taylor, Nucl. Phys. **B334**, 199 (1990); ibid. **B374**, 156 (1992). J. C. Taylor and S. M. H. Wong, Nucl. Phys. **B346**, 115 (1990).

[9] A. Ukawa, Nucl. Phys. B (Proc. Suppl.) **53**, 106, (1997).

[10] Recently, the chiral symmetry on the lattice QCD is studied using domain wall fermions. See, e.g. ref.[5].

[11] However, recently, a method for handing it directly is studied in Y. Nakahara, M. Asakawa and T. Hatsuda, Phys. Rev. **D60**, 091503 (1999).

[12] S. Weinberg, Phys. Rev. **D9**, 3357 (1974).
L. Dolan and R. Jackiw, Phys. Rev. **D9**, 3320 (1974).

[13] D. A. Kirzhnits and A. D. Linde, Ann. Phys. **101**, 195 (1976).

[14] E. Braaten, R. D. Pisarski and T. C. Yuan, Phys. Rev. Lett. **64**, 2242 (1990).
S. M. H. Wong, Zeit. Phys. **C53**, 465 (1992). E. Braaten and R. D. Pisarski, Phys. Rev. Lett. **64**, 1338 (1990); Phys. Rev. **D42**, 2156 (1990); ibid. bf D46, 1829 (1992).
R. Kobes, G. Kunstatter and K. W. Mak, Phys. Rev. **D54**, 4632 (1992).

[15] H. Nakkagawa and H. Yokota, Mod. Phys. Lett. **A11**, 2259 (1996); Prog. Theor. Phys. Suppl. **129**, 209 (1997).
K. Ogure and J. Sato, Phys.Rev. **D58**, 085010 (1998).
Y. Nemoto, K. Naito and M. Oka, hep-ph/9911431 (1999) and references therein.

[16] T. Hatsuda and T. Kunihiro, Phys. Rep. **247**, 221 (1994).

[17] K. Rajagopal, in *Quark-Gluon Plasma 2*, ed. R. Hwa (World Scientific, Singapore, 1995).

[18] G. Baym and G. Grinstein, Phys. Rev. **D15**, 2897 (1977).
D. A. Kirzhnits and A. D. Linde, Ann. Phys. **101**, 195 (1976).
H. E. Haber and H. A. Weldon, Phys. Rev. **D25**, 502 (1982).
G. Amelino-Camelia and S-Y. Pi, Phys. Rev. **D47**, 2356 (1993).
G. Amelino-Camelia, Nucl. Phys. **B476**, 255 (1996); Phys. Lett. **B407**, 268 (1997).
H-S. Roh and T. Matsui, Eur. Phys. J. **A1**, 205 (1998).
See also, Y. Nemoto, K. Naito and M. Oka, hep-ph/9911431 (1999).

[19] R. E. Norton and J. M. Cornwall, Ann. Phys. **91**, 106 (1975).
M. B. Kislinger and P. D. Morley, Phys. Rev. **D13**, 2771 (1976).
H. Matsumoto, I. Ojima and H. Umezawa, Ann. Phys. **152**, 348 (1984).

[20] S. Chiku and T. Hatsuda, Phys. Rev. **D57**, R6 (1998).

[21] For applications of the mean-field method to field theories, see e.g. Y. Nambu and G. Jona-Lasinio, Phys. Rev. **122**, 345 (1961).
T. Kunihiro and T. Hatsuda, Prog. Theor. Phys. **71**, 1332 (1984).

[22] A. Okopińska, Phys. Rev. **D36**, 2415 (1987); Mod. Phys. Lett. **A12**, 1003 (1997). See also, G. A. Hajj and P. M. Stevenson, Phys. Rev. **D37**, 413 (1988).

[23] N. Banerjee and S. Mallik, Phys. Rev. **D43**, 3368 (1991).

[24] Since the number of works related to OPT is enormous, we quote only two books which contain the original references: G. A. Arteca, F. M. Fernández and E. A. Castro, *Large Order Perturbation Theory and Summation Methods in Quantum Mechanics*, (Springer-Verlag, Berlin, 1990).
H. Kleinert, *Path Integrals in Quantum Mechanics, Statistical and Polymer Physics*, 2nd. edition (World Scientific, Singapore, 1995), Section 5.
See also, T. Hatsuda, T. Kunihiro and T. Tanaka, Phys. Rev. Lett. **78**, 3229 (1997); T. Tanaka, Phys. Lett. **A238**, 79 (1998).

[25] P. M. Stevenson, Phys. Rev. **D23**, 2916 (1981).

[26] G. t'Hooft and M. Veltman, Nucl. Phys. **B44**, 189 (1972).

[27] P. Fendley, Phys. Lett. **B196**, 175 (1987).

[28] Y. Nambu, Phys. Lett. **B26** (1968).

[29] P. Arnold and C-X. Zhai, Phys. Rev. **D50**, 7603 (1994); ibid. **D51**, 1906 (1995).

[30] R. R. Parwani Phys. Rev. **D45**, 4695 (1992); erratum, ibid, **D48**, 5965 (1993).
See also, F. Karsch, A. Patkos and P. Petreczky, Phys. Lett. **B401**, 69 (1997).

[31] R. Kobes, G. Kunstatter and A. Rebhan, Phys. Rev. Lett. **64**, 2992 (1990).
R. Basier, G. Kunstatter, D. Schiff, Phys. Rev. **D45**, R4381 (1992).
A. Rebhan, Phys. Rev. **D46**, 4779 (1992).

[32] R. Jackiw, Phys. Rev. **D9**, 1686 (1974).
See e.g., J. Negele and H. Orland, *Quantum Many-Particle Systems*, (Addison-Wesley, New York, 1988).

[33] W. A. Bardeen, A. J. Buras, D. W. Duke and T. Muta, Phys. Rev. **D18**, 3998 (1978).

[34] B. W. Lee, Nucl. Phys. **B9**, 649 (1969).
B. W. Lee, *Chiral Dynamics*, (Gordon and Breach, New York, 1972).

[35] T. Kugo, Prog Theor. Phys. **57**, 593 (1977).

[36] This point was first recognized in [23].

[37] See the following papers and the references quoted therein for the breakdown of the NG theorem in self-consistent methods and for attempts to cure the problem: A. Okopińska, Phys. Lett. **B375**, 213 (1996). A. Dmitrašinović, J. A. McNeil and J. R. Shepard, Z. Phys. **C69**, 359 (1996). G. Amelino-Camelia, Phys. Lett. **B407**, 268 (1997).

[38] Y. Takahashi and H. Umezawa, Collective Phenom. **2**, 55 (1975).
N. P. Landsman and Ch. G. van Weert, Phys. Rep. **145**, 143 (1987).
M. Le Bellac, *Thermal Field Theory*, (Cambridge Univ. Press, Cambridge, 1996).

[39] A. J. Niemi and G. W. Semenoff, Ann. Phys. **152**, 105 (1984); Nucl. Phys. **B230** [FS10], 181 (1984).

[40] S. Weinberg, Phys. Rev. **D7**, 2887 (1973).

[41] See e.g., P. Ramond, *FIELD THEORY:A MODERN PRIMER 2ed.* (Addison-Wesley, New York, 1990).

[42] C. Ford and D. R. T. Jones, Phys. Lett. **B274**, 409 (1992) and references therein.
See, also 3-loop case, J. -M. Chung and B. K. Chung, Phys. Rev. **D56**, 6508 (1997); J.Korean Phys.Soc. **33**, 634 (1998).

[43] P. Arnold and O. Espinosa, Phys. Rev. **D47**, 3546 (1993).

[44] K. G. Wilson and J. Kogut, Phys. Rep. **12C**, 75 (1974).
See e.g. N. Goldenfeld, *Lectures on Phase Transitions and the Renormalization Group*, (Addison-Wesley, New York, 1992).)

[45] H. W. J. Blöte, A. Compagner, J. H. Croockewit, Y. T. J. C. Fonk, J. R. Heringa, A. Hoogland, T. S. Smit and A. L. van Villingen, Physica **A161**, 1 (1989).
K. Kanaya and S. Kaya, Phys. Rev. **D51**, 2404 (1995) and references therein.

[46] S. Mallik and K. Mukherjee, hep-th/9607087 (1996).

[47] W. A. Bardeen and M. Mosche, Phys. Rev. **D28**, 1372 (1983).

[48] M. Lüscher and P. Weisz, Nucl. Phys. **B290** [FS20], 25 (1987); ibid. **B290** [FS21], 65 (1988); ibid. **B318**, 705 (1989).

[49] T. Hatsuda and T. Kunihiro, Phys. Rev. Lett. **55**, 158 (1985); Phys. Lett. **B185**, 304 (1987).
Another interesting issue is the spectral change of vector mesons: R. D. Pisarski, Phys. Lett. **B110**, 155 (1982); G. E. Brown and M. Rho, Phys. Rev. Lett. **66**, 2720 (1991); T. Hatsuda and S. H. Lee, Phys. Rev. **C46** (1992) R34; T. Hatsuda, Y. Koike and S. H. Lee, Nucl. Phys. **B394**, 221 (1993).

[50] H. A. Weldon, Phys. Lett. **B274**, 133 (1992).
C. Song and V. Koch, Phys. Lett. **B404**, 1 (1997).

[51] S. Huang and M. Lissia, Phys. Rev. **D52**, 1134 (1995); Phys. Lett. **B348**, 571 (1995); Phys. Rev. **D53**, 7270 (1996).

[52] L. H. Chan and R. W. Haymaker, Phys. Rev. **D7**, 402 (1973); ibid. **D10**, 4170 (1974).

[53] R. D. Pisarski and F. Wilczek, Phys. Rev. **D29**, 338 (1984).
K. Rajagopal and F. Wilczek, Nucl. Phys. **B399**, 395 (1993).
See also, M. Asakawa, Z. Huang and X.-N. Wang, Phys. Rev. Lett. **74**, 3126 (1995); J. Randrup, Phys. Rev. **D55**, 1188 (1997) and references therein.

[54] C. Caso et all. (Particle Data Group), Eur. Phys. J. **C3**, 1 (1998).

[55] N. A. Törnqvist and M. Roos, Phys. Rev. Lett. **76**, 1575 (1996).
M. Harada, F. Sannino and J. Schechter, Phys. Rev. **D54**, 1991 (1996); Phys. Rev. Lett. **78**, 1603 (1997).
S. Ishida et al., Prog. Theor. Phys. **95**, 745 (1996); ibid. **98**, 1005 (1997).
J. A. Oller, E. Oset and J. R. Peláez, Phys. Rev. Lett. **80**, 3452 (1998).
K. Igi and K. Hikasa, Phys.Rev. **D59**, 034005 (1999).

[56] B. Kastening, Phys. Lett. **B283**, 287 (1992).
M. Bando, T. Kugo, N. Maekawa and H. Nakano, Phys. Lett. **B301**, 83 (1993); Prog. Theor. Phys. **90**, 405 (1993).

[57] M. Gell-Mann, R. J. Oakes and B. Renner, Phys. Rev. **175**, 2195 (1968).

[58] H. Itoyama and A. H. Mueller, Nucl. Phys. **B218**, 349 (1983).
E. V. Shuryak, Phys. Lett. **B207**, 345 (1988).
J. L. Goity and H. Leutwyler, Phys. Lett. **B228**, 517 (1989).
H. Leutwyler and A. V. Smilga, Nucl. Phys. **B342**, 302 (1990).
R. D. Pisarski and M. Tytgat, Phys. Rev. **D54**, 2989 (1996).

[59] J. W. Harris and B. Muller, Ann. Rev. Nucl. Part. Sci. **46**, 71 (1996).

[60] C. Gale and J. I. Kapusta, Nucl. Phys. **B 357**, 65 (1991).

[61] A preliminary version of this study has been reported in S. Chiku, Prog. Theor. Phys. Suppl. **129**, 91 (1998).

[62] S. Hafjitheodoridis and B. Moussallam, Phys. Rev. **D37**, 1331 (1988).

[63] S. P. Klevansky, Nucl. Phys. **A575**, 605 (1994)

[64] P. Rehberg, Yu. I. Kalinovskii and D. Blaschke, Nucl. Phys. **A622** (1997) 478. In this paper, the mode couplings are not taken into account. See also, M. K. Volkov, E. A. Kuraev, D. Blaschke, G. Roepke and S. Schmidt, Phys. Lett. **B424** 235 (1998).

[65] F. Bonutti et al. (CHAOS Collaboration), Phys. Rev. Lett. **77**, 603 (1996).
R. Rapp, J. W. Durso, Z. Aouissat, G. Chanfray, O. Krehl, P. Schuck, J. Speth and J. Wambach, Phys.Rev. **C59** R1237 (1999).
T. Hatsuda, T. Kunihiro and H. Shimizu, Phys. Rev. Lett. **82** 2840 (1999).

[66] A. D. Linde, Phys. Lett. **96B**, 289 (1980).
See also, T. Hatsuda, Phys. Rev. **D56**, 8111 (1997) and references therein.